



Title	Novel ferroelectric-semiconductor photovoltaics
Advisor(s)	Liu, F
Author(s)	Wang, Wentao; 王文韬
Citation	Wang, W. [王文韬]. (2014). Novel ferroelectric-semiconductor photovoltaics. (Thesis). University of Hong Kong, Pokfulam, Hong Kong SAR. Retrieved from http://dx.doi.org/10.5353/th_b5317031
Issued Date	2014
URL	http://hdl.handle.net/10722/206435
Rights	The author retains all proprietary rights, (such as patent rights) and the right to use in future works.

Novel Ferroelectric-Semiconductor Photovoltaics

by

Wentao WANG

王文韬

BEng Metal Material Engineering, Central South University

MEng Material Processing Engineering, Central South University

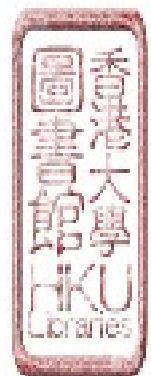
A thesis submitted in partial fulfillment of the requirements for
the degree of Doctor of Philosophy
at The University of Hong Kong

July 2014



Abstract of the thesis entitled
Novel Ferroelectric-Semiconductor Photovoltaics
submitted by
Wentao WANG
for the degree of Doctor of Philosophy
at The University of Hong Kong
in July 2014

Solar cells have been traditionally developed for optimizing three key steps for charge carriers: generation, separation, and transport. Conventional solar cells are essentially PN junction based, and utilize the internal electric field near the junction interface for realizing charge carrier separation. However, this kind of structure limits material choices and device fabrication to form a working junction due to issues such as lattice mismatch, doping, and band alignment. Ferroelectric photovoltaic devices with typical capacitor structure have been developed to overcome the junction caused disadvantage but suffer from the poor charge transport issue. In this work, novel ferroelectric-semiconductor photovoltaic devices were developed and investigated in detail with experimental results and theoretical simulation. This type of solar cell is fundamentally different with traditional PN junction based solar cells, utilizing ferroelectric polarization for charge separation in semiconductor layer. Systematical works have been conducted on: (1) device working principle and mechanism study; (2) effect of electrode; (3) influence of device key dimension parameters. The new cells showed the rectifying behavior and effective photovoltaic effect after specific asymmetric



polarization. Furthermore, the device performance has been improved through adjusting electrode design and semiconductor layer thickness, which is mainly due to the optimized electric field strength and distribution resulting from polarization.

As low cost commercial semiconductor, the multicrystalline silicon (mc-Si) has great potential application in the novel ferroelectric-semiconductor photovoltaic devices. However, the grain boundaries with high density of defects limit the material electric properties. In order to improve the multicrystalline silicon transport property, a polar molecules system was developed to play the role in grain boundaries passivation. The small polar molecule composition and solution passivation process were carried out to optimize the passivation effect. The result showed the developed ZK series solutions reduced the R_{sheet} across large-angle grain boundaries by up to more than one order to be close to the bulk R_{sheet} . Also, the correlation between the grain misorientation and passivation effectiveness was built up.



Declaration

I hereby declare that this thesis, entitled “Novel Ferroelectric-Semiconductor Photovoltaics”, represents my own work, except where due acknowledgement is made, and that it has not been previously included in a thesis, dissertation or report submitted to this University or any other institution for application of a degree, diploma or other qualifications.

Signed: _____

Wentao WANG

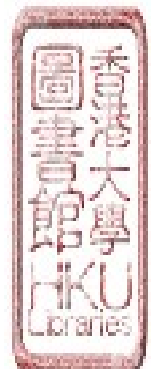


Acknowledgement

I would like to express my most grateful thanks to my supervisor, Dr. Fude Liu, for his kindness, patience, and constant support to my research work and life throughout the four years. I really appreciate the opportunity to study in Dr. Liu's group. His rigorous mind and enthusiasm into science set an example of a classical scientist. His creativity and brilliant insight in solving scientific problem map the path, inspiring me to be no fear to devote my research in developing photovoltaic devices. He always unreservedly gives me a helping hand and sharing his research and life experience with me. I learnt from him not only the in depth knowledge of semiconductor and renewable energy, restrict attitude to work, but also an open mindset of thinking.

I would like to thank my group mates Wang Lei and Zheng Dawei for their constant encourage and support whenever I faced any difficulties. I would like to thank Yang Guandong, Lau Chor Man for great help in my research. I also would like to thank my friends Ren Xiaochen, Ma Jiaoni, Zhai Peng, Lee W. C., Boris, Liu Haipei, Kou Shuting, Wang Xiaoxue, Gu Rui, Zhang Di, Li Xuanhua, Peng Boyu, Wang Zongrong, Zhou Zhuolong, Wang Shuo, Wang Chong, Xie Qing and others for sharing my life.

Last but not least, I would like to express my greatest thanks to my wife Qin Yaohua and my mother Lu Fenglian for their consistent understanding, trust and great support. This thesis would not have been possible without their love and encouragement. I would like to thank my angle daughter Wang Jinghan for bring my happiness, courage and faith to overcome any difficulties in life. Mostly, I would like to thank my father Wang Guoqing for everything he brings to me.



Content

List of Figures..... vi

List of Tables..... x

1. Introduction..... 1

 1.1 Motivation and objective..... 1

 1.2 Structure of the thesis 3

 References 5

2. Literature Review 7

 2.1 Development of solar cells 7

 2.2 Development of ferroelectric photovoltaic devices.....11

 2.2.1 Ferroelectric material and applications 12

 2.2.2 Ferroelectric photovoltaic devices 15

 2.3 Development of grain boundaries passivation technique for photovoltaic 23

 References 27

3. Non-PN Junction Based Ferroelectric-Semiconductor Solar Cells: Concept

Proof..... 35

 3.1 Introduction 37



3.2 Experimental	38
3.3 Results and discussion.....	41
3.4 Conclusions	48
References	49

4. Effect of Electrodes on Non-PN Junction Based Ferroelectric-Semiconductor

Solar Cells	52
4.1 Introduction	55
4.2 Experimental	56
4.3 Results and discussion.....	59
4.4 Conclusions	66
References	68

5. Effect of Absorber Layer Thickness and Device Dimension on Non-PN Junction

Based Ferroelectric-Semiconductor Solar Cells.....	72
5.1 Introduction	74
5.2 Experimental	76
5.3 Results and discussion.....	77
5.4 Conclusions	84
References	86



6. Preliminary Passivation Study for Non-PN Junction Based Ferroelectric-Semiconductor Solar Cells: Passivating Silicon Grain Boundaries with Small Polar Molecules.....	88
6.1 Introduction	91
6.2 Experimental	93
6.3 Results and discussion.....	94
6.4 Conclusions	102
References	104
7. Conclusions.....	109
Overall References	112
Appendix	123
Publications	129



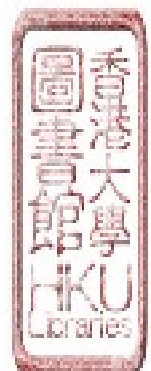
List of Figures

2. Literature Review

Fig. 1. Schematic of solar cell working principle.....	8
Fig. 2. Best research solar cell efficiencies, NREL.....	9
Fig. 3. Microscopic origins of the electric polarization.....	13
Fig. 4. Ionic displacements in BaTiO ₃	14
Fig. 5. Crystal structures of BaTiO ₃ : Higher than Tc (left) and lower than Tc (right).....	15
Fig. 6. Schematic illustration of ferroelectric photovoltaic device.....	16
Fig. 7. Schematic illustrations of two types of ferroelectric polymer hybrid OPV cells... <td>22</td>	22
Fig. 8. Schematic of the energy band diagram in the “Two-Diode Model” for grain boundaries of n-type and p-type mc-Si.....	24

3. Ferroelectric-Semiconductor Photovoltaics: Non-PN Junction Solar Cells

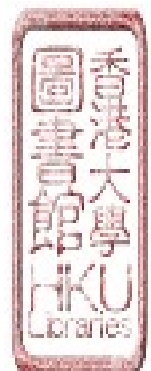
Fig. 1. Schematic of device structure and real cell. (a) Schematic of device structure (cross-section view; not drawn to scale). (b) Real cell (top-down view from the ferroelectric side).....	40
Fig. 2. I-V curves of the before-polarization and reverse-polarization states, respectively, under dark condition.....	41
Fig. 3. Rectifying behavior and photovoltaic effect of the forward-polarization state. (a) IV curves under dark and illumination conditions, respectively. (b) Time-	



dependent I_{sc} when the illumination is switched on or off.....	43
Fig. 4. Effect of the electric field on the band diagram of a semiconductor (intrinsic). (a) Under dark condition. (b) Under sunlight illumination.....	45
Fig. 5. Simulation of the electric field distribution in the real cell. (a) Model geometry (not drawn to scale). (b) Simulated electric field distribution in the real cell. Also included is the electric field legend that is color-coded.....	46
Fig. 6. Simulation of the electric field distribution in a possible optimized cell. (a) Model geometry (not drawn to scale). (b) Electric field distribution in the optimized cell. Also included is the electric field legend that is color-coded.....	47

4. Effect of Electrodes on Non-PN Junction Ferroelectric-Semiconductor Solar Cells

Fig. 1. Device structure and working principles. (a) Schematic of cross-sectional view. (b) Schematic of 3D view.....	59
Fig. 2. J-V curves of three typical cells under illumination before polarization (blue curve) and after forward polarization (red curve), respectively. (a) Cell #1 with Al/Al contacts. (b) Cell #2 with Ti/Al contacts. (c) Cell #3 with Ti/Au contacts.....	61
Fig. 3. Schematic of the energy-band diagram of silicon and the work function of each metal.....	63
Fig. 4. Characterization of the BaTiO_3 layer. (a) SEM image (top-down view). (b) SEM image (cross-sectional view). (c) XRD spectrum. (d) Hysteresis loop.....	64
Fig. 5. Simulation of the electric field distribution in the real device. (a) Model geometry.	



(b) Electric field distribution in the device. Also included is the electric field legend that is color coded.....	66
--	----

5. Enhanced Photovoltaic Properties in Non-PN Junction BaTiO₃/Ultra-thin Si Solar Cells

Fig. 1. Schematic of device structure and working principle.....	75
Fig. 2. Simulation of the electric field distribution in the device. (a) Model geometry. (b) Electric field distribution in the device. Also included is the electric field legend that is color coded.....	79
Fig. 3. J-V curves of the device at before-polarization, forward-polarization and reverse-polarization states, respectively. (a) Under dark condition. (b) Under illumination condition.....	80
Fig. 4. Schematic of Ag/Si/Al energy band diagrams at different polarization states. (a) Forward polarization. (b) Reverse polarization.....	83

6. Passivating Silicon Grain Boundaries with Small Polar Molecules for Ferroelectric-Semiconductor Photovoltaics

Fig. 1. Sheet resistance (R_{sheet}) across GBs vs. passivation time of acetonitrile, methanol, and formic acid under dark (D) and illuminated (L) conditions, respectively. (a) Large-angle random GBs. (b) $\Sigma 3$ GBs.....	95
Fig. 2. Sheet resistance (R_{sheet}) across GBs vs. passivation time of ZK-24, ZK-22, and ZK-42 under dark (D) and illuminated (L) conditions, respectively. (a) Large-angle random GBs. (b) $\Sigma 3$ GBs.....	97

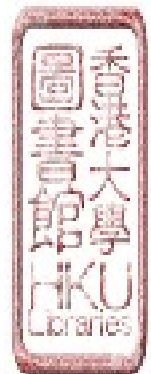


Fig. 3. Sample passivated with ZK-42. (a) PL image of a sample passivated for 30 hours. The insets are the corresponding PL intensity profiles across GBs #1–3. (b) Sheet resistance (R_{sheet}) across GBs #1–3 *vs.* passivation time under dark condition. (c) Plan-view EBSD maps at GBs #1–3. EBSD maps are color-coded with the IPF coloring in the sample normal direction Z_0 . The inset is the color-coding legend.....98

Fig. 4. Random GB model. (a) Before passivation. (b) After passivation.....101



List of Tables

4. Effect of Electrodes on Non-PN Junction Ferroelectric-Semiconductor Solar Cells

Table I. Performance summary of three cells.....	60
---	----

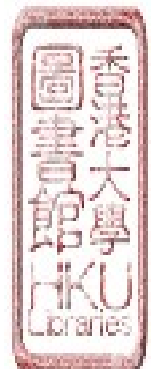


1. Introduction

1.1 Motivation and objective

Solar energy is the original source for all kinds of energy on the earth. By far the solar cell is regarded as the only clean technique to generate electricity without pollution. Solar cells have been traditionally developed for optimizing three key steps for charge carriers: generation, separation, and transport[1]. In particular, how to realize charge carrier separation usually dictates the basic device structure. Conventional solar cells are essentially PN junction based, and utilize the internal electric field near the junction interface for realizing charge carrier separation. However, the junction-based structure is just one way to realize the functions of solar cells. In addition, this kind of structure limits material choices and device fabrication to form a working junction due to issues such as lattice mismatch, doping, and band alignment.

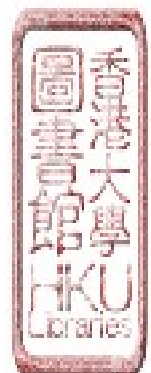
In order to overcome the issues that occur with PN junctions, ferroelectric photovoltaic devices have been developed. The typical structure is a ferroelectric layer sandwiched between the top and bottom electrodes [2]. The devices utilize the ferroelectric layer for both light absorption and charge separation with its internal electric field due to polarization. However, ferroelectric are in general large band gap materials [3], which limits the absorption of sunlight. Different efforts have been made to enhance the light responsibility, such as incorporation of narrow band-gap nanoparticles of Ag_2O [4] or exploring the narrow band gap ferroelectric of



BiFeO_3 [5]. Unfortunately, the ferroelectric material is usually high insulating, which result in the poor charge transport properties and therefore the low power conversion efficiency.

It has been shown recently that a large, permanent, internal electric field can be achieved for enhancing charge separation by incorporating a ferroelectric polymer layer into organic solar cells, which eliminates the need for an external bias[6]. One issue with this approach is that the ferroelectric layer has to be made extremely thin (a few monolayers) for charge carriers to tunnel through it, which make it very challenging to fabricate large-area solar cells. Furthermore, the nature of the enhanced photovoltaic effect by ferroelectric is far from fully understand. Therefore, it is worth exploring other possibilities and systematically studies the mechanisms behind. The objective of this work is to develop novel ferroelectric semiconductor solar cells with non-PN junction structure.

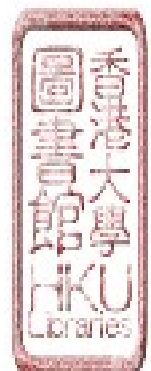
On the other hand, the performance of solar cells, especially the ferroelectric-semiconductor photovoltaic cell, depends on the charge carrier transport property, which is correlated to the semiconductor quality. Multicrystalline and polycrystalline silicon have been widely used for commercial solar cells due to their low cost. However, grain boundaries are a significant concern because they play a major role in determining the device performance of these solar cells [7-9]. The high density defects in GBs act as recombination centers to trap the minority flow carriers. Hydrogen has traditionally been applied to passivate the defects at GBs. However, hydrogenated films are subject to the low thermal stability [10, 11]. Furthermore, excessive hydrogenation leads to new defect creation and results in the increase of



GB electrical activity in poly-Si[12, 13]. Consequently, alternative passivation agents and simplified method should be developed. This work is to investigate a new grain boundaries passivation method with small polar molecules to improve the multi-crystalline silicon transport property for novel ferroelectric-semiconductor photovoltaics applications.

1.2 Structure of the thesis

The following chapters begin with an introduction of the motivation and objective of the research, and the structure outline of the thesis. Then chapter 2 presents a literature review of the development of solar cells, development ferroelectric photovoltaic devices, and development of grain boundaries passivation techniques for photovoltaic. Chapter 3 describes the concept of the novel ferroelectric semiconductor solar cells. The cells utilize the ferroelectric polarization to realize charge separation in semiconductor layer, avoiding the PN junction caused interface issue. The new cell shows photovoltaic effect and rectifying behavior, reifying the feasibility of the new concept. Chapter 4 studies the effect of electrodes on the BaTiO₃-Si solar cells performance. The positions of contacts are carefully designed to avoid potential screening effect at the ferroelectric/semiconductor interface. Different metal materials are selected to optimize the photovoltaic effect as well as for mechanism study. Chapter 5 investigates the effect of semiconductor film thickness, electrodes space length on the novel ferroelectric-semiconductor cell property. The finite element simulation indicates the optimized device dimension and the real cell shows significantly improved photovoltaic output comparing with the previous result.

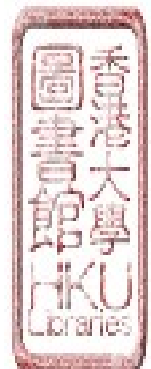


Chapter 6 presents a new passivation method for grain boundaries with small polar molecules for potential ferroelectric-semiconductor photovoltaics application. An excellent correlation between the multi-crystalline silicon grain misorientation, electrical resistance across grain boundaries, and passivation effectiveness is build up. The charge transport across grain boundaries is greatly enhanced after the wafers are properly treated in the polar molecule solutions. Chapter 7 draws the conclusion of the thesis and outlooks the future research directions.



References

1. Nelson, J., *The physics of solar cells*. 2003: Imperial College Press.
2. Qin, M., K. Yao, and Y. Liang, *High efficiency photovoltaics in nanoscaled ferroelectric thin films*. Applied Physics Letters, 2008. **93**: p. 122904.
3. Dawber, M., K.M. Rabe, and J.F. Scott, *Physics of thin-film ferroelectric oxides*. Reviews of Modern Physics, 2005. **77**(4): p. 1083-1130.
4. Yang, X.L., et al., *Enhancement of Photocurrent in Ferroelectric Films Via the Incorporation of Narrow Bandgap Nanoparticles*. Advanced Materials, 2012. **24**(9): p. 1202-1208.
5. Choi, T., et al., *Switchable Ferroelectric Diode and Photovoltaic Effect in $BiFeO_3$* . Science, 2009. **324**(5923): p. 63-66.
6. Yuan, Y.B., et al., *Efficiency enhancement in organic solar cells with ferroelectric polymers*. Nature Materials, 2011. **10**(4): p. 296-302.
7. Chen, J., et al., *Recombination activity of $\Sigma 3$ boundaries in boron-doped multicrystalline silicon: Influence of iron contamination*. Journal of Applied Physics, 2005. **97**(3): p. 033701.
8. Bertoni, M.I., et al., *Influence of defect type on hydrogen passivation efficacy in multicrystalline silicon solar cells*. Progress in Photovoltaics: Research and Applications, 2011. **19**(2): p. 187-191.
9. Dimassi, W., et al., *Two-dimensional LBIC and Internal-Quantum-Efficiency investigations of grooved grain boundaries in multicrystalline silicon solar cells*. Solar Energy, 2011. **85**(2): p. 350-355.
10. Banerjee, S., et al., *Hot-electron degradation of n-channel polysilicon*



- MOSFETs*, IEEE Transactions on Electron Devices, 1988. **35**(2): p. 152-157.
11. Nickel, N.H., W.B. Jackson, and N.M. Johnson, *Light-induced creation of metastable paramagnetic defects in hydrogenated polycrystalline silicon*. Physical Review Letters, 1993. **71**(17): p. 2733-2736.
 12. Saad, A., et al., *Influence of low-energy ion-beam treatment by hydrogen on electrical activity of grain boundaries in polycrystalline silicon*. Vacuum, 2005. **78**(2-4): p. 269-272.
 13. Honda, S., et al., *Defects generation by hydrogen passivation of polycrystalline silicon thin films*. Solar Energy, 2006. **80**(6): p. 653-657.

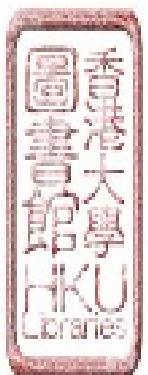


2. Literature Review

2.1 Development of solar cells

Solar energy is the original source for all kinds of energy on the earth. By far the solar cell is regarded as the only clean technique to generate electrical energy without pollution.

Generally, the solar cell is one step device that directly converts the solar energy into electricity. A solar cell consists of a semiconductor material for light absorption, which is connected to an external circuit in an asymmetric manner. After absorbing photons of light, electron-hole pairs are generated in the semiconductor, and then are driven towards different electrodes by the build-in spatial asymmetry. This light induced charge separation generates a photovoltage at open circuit condition (V_{oc}), and establishes a photocurrent at short circuit condition (I_{sc}). When a load is applied to external circuit, the device generates electric power to do electrical work [1]. Fig. 1 shows the working principle of energy band diagram for a solar cell [2].



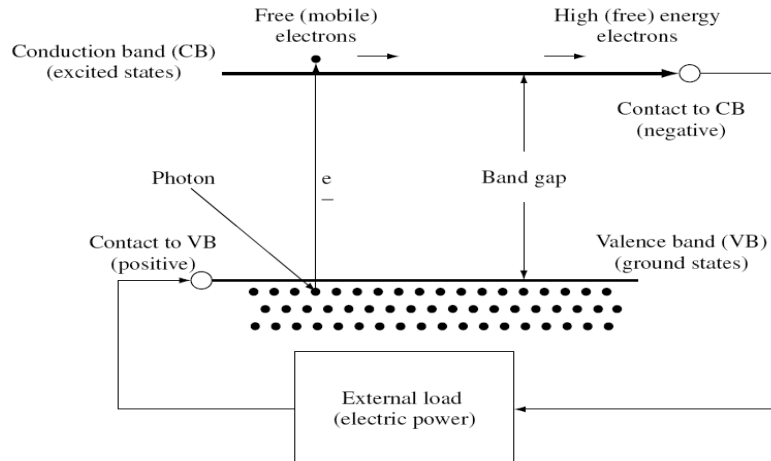


Fig. 1. Schematic of solar cell working principle.

(Source: reference [2])

The three key steps of conversion of photovoltaic energy in a solar cell are charge generation, charge separation and charge transport. The charge generation and transport are mostly depends on the materials properties [1]. Normally, semiconductors are suitable materials for photovoltaic due to the appropriate band gap between valence and conduction bands which can response to visible photons. Also the conductivity is considerable good for charge transport there. While light induced charge carrier separation is related to the build in driving force, which mainly arises from the structure spatial variations in the electronic environment. Spatial variation in band gap, electron affinity, and density of states or work function can provide charge separation. From the electrical picture point of view, the driving force provides different resistance paths: one path has much lower resistance for positive than negative charge, and the other path is easier for negative charge pass through than positive one. With such a purpose, all kinds of



efforts have been made to achieve high performance solar cell devices. The Fig. 2 indicated the best research solar cell efficiencies of the latest achievement, edited by National Renewable Energy Laboratory (NREL).

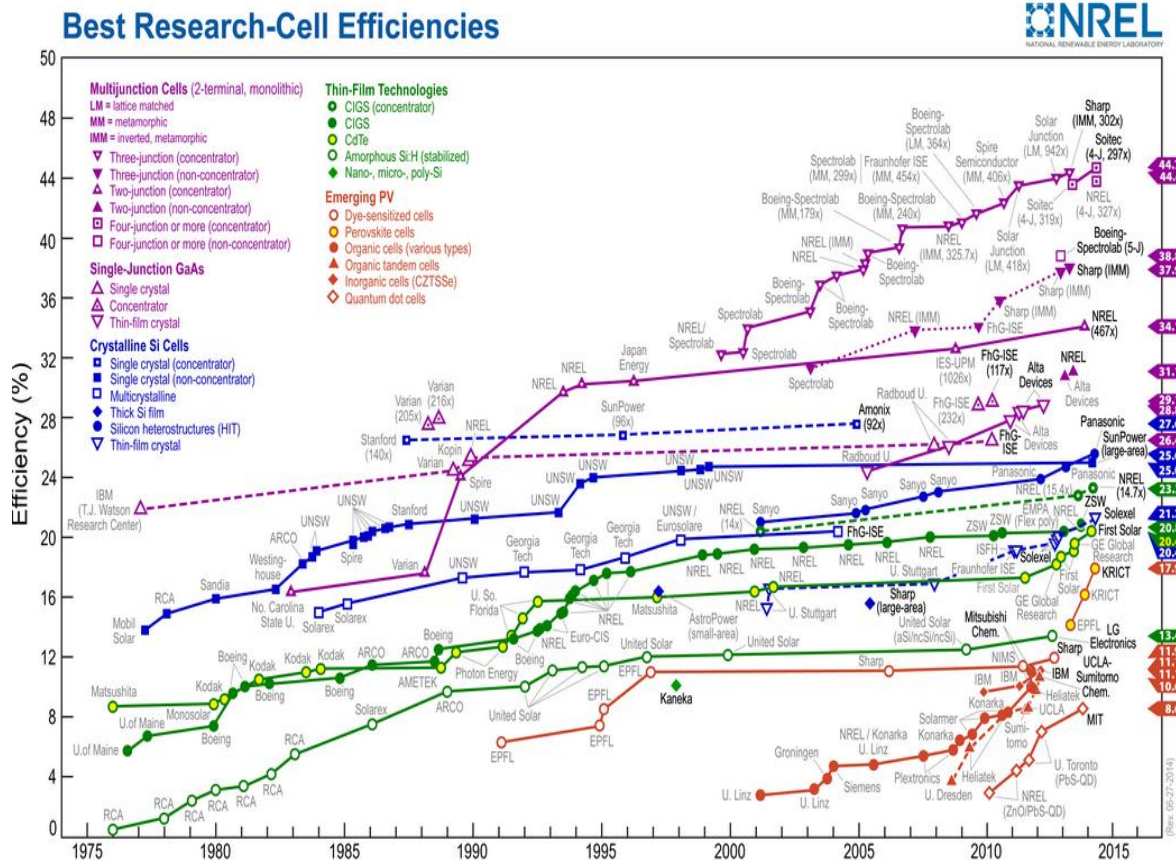
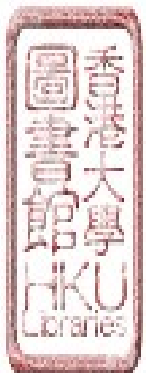


Fig. 2. Best research solar cell efficiencies.

(Source: NREL)

Most of the current solar cells are based on the structure of junction, which between two electronically different materials provides an electrostatic force. The junction is an effective structure for electron-hole pair separation due to the depletion region there playing the role of blocking majority carriers' across.



Charge carriers' exchange can establish a potential step at the interface between two materials with different electronic properties. The induced potential can be represented by the bands bending [1]. The height of the potential step and maximum charge separation determine the photovoltage. The formation of an inversion layer at the junction indicates a rectifying action. If the semiconductor is enriched with charge the junction is Ohmic. A Schottky contact can be formed between a metal and semiconductor. When the device is illuminated, electron and holes are separated by the electric field at the junction, and accumulate on opposite sides[1].

During different types of junctions, the p-n junction is the classic model of a solar cell and is the most widely used devices structure in photovoltaics. Selective doping of the different sides of a semiconductor wafer of p-type and n-type leads to a depletion region for both electrons and holes, which realizes a selective path to the carrier with different electric charges. The p-n junction drives the collection of minority carriers which are photo-generated throughout the p and n layers, and reach the junction by diffusion. The junction generates a barrier of potential to charge carrier flow. Consequently, the resistance for electrons to the n contact is low, and the same situation for holes to the p contact. This structure provides the asymmetry in resistance, which is the key part for photovoltaic energy conversion.

However, defects at the interface introduce states in the semiconductor band gap which can trap charges and influence the potential distribution at the



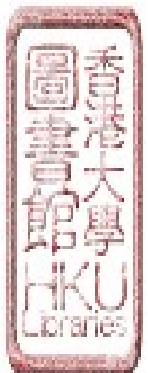
junction. A high density of interface states reduces the photovoltage and degrades the photovoltaic performance of the device [1].

In order to address this issue, novel concept of non-pn junction based solar cells have been proposed and investigated. Regan et al. recently reported a type of solar cell with the name of “screening-engineered field effect solar cell”. This architecture made use of the electric field effect to control the charge flow through careful design of the top metal contacts [3]. It mainly provides a benefit of non-doping related crystal damage to the interface. Similar efforts were also targeted to overcome the p-n junction drawbacks. Wadhwa et al. introduced electrolyte to generate inversion layer in the n-Si/carbon nanotube solar cell [4, 5]. A junction interface dipole and a field developed across the depletion layer modified the built in potential and boosted up the power conversion efficiency up to 12%.

Alternatively, another fascinating type of non-pn junction solar cell is ferroelectric photovoltaic cell, which fundamentally different with traditional solar cell, and attracting considerable attentions.

2.2 Development of ferroelectric photovoltaic devices

Ferroelectric material based photovoltaic device is a novel type of solar cell. This cell mainly makes use of the unique ferroelectric polarization property to accomplish light absorption and charge separation for the photovoltaic generation. In conventional Si solar cells, electron-hole pairs are created by light



absorption and separated by the electric field across a pn junction, with a maximum photovoltage equal to the electronic band gap. By contrast, ferroelectric material based photovoltaic devices avoid junction caused issue, and exhibits many unique features such as extremely large photovoltage higher than the band gap, and photocurrent proportional to the polarization magnitude interest [6]. The photovoltaic effect in ferroelectric photovoltaic is deeply correlated to the physics of ferroelectricity and has potential application in solar cells to satisfy the increasing demands for clean and sustainable powers.

2.2.1 Ferroelectric material and applications

Ferroelectric is considered a very promising materials for wide applications such as high-permitivity dielectrics, ferroelectric memories, pyroelectric sensors, resistivity component containing positive temperature coefficient (PTC), and electroptical devices [7].

The ferroelectric belongs to dielectric materials. The constituent atoms are partially ionized, and are either negatively or positively charged. In such ionic crystals, when an electric field is applied, cations are attracted to the cathode and anions to the anode due to electrostatic interaction. The electron clouds also deform, causing electric dipoles [7]. This phenomenon is known as electric polarization, and the polarization is expressed quantitatively as the sum of the electric dipoles per unit volume (C/m^2). The dielectric polarization P, the electric displacement D (the stored electric charge per unit area), and the electric field E follows the



expression [7]:

$$D = \epsilon_0 E + P = \epsilon \epsilon_0 E$$

Here, ϵ_0 is the vacuum permittivity (8.854×10^{-12}), and ϵ is the material's relative permittivity (dielectric constant).

Fig. 3 indicates the schematic of the electric polarization the origination [7]. There are three major contributions: electronic, ionic, and dipole reorientation-related. The frequency of the applied field determines the contribution to the overall polarization from the above three mechanisms.

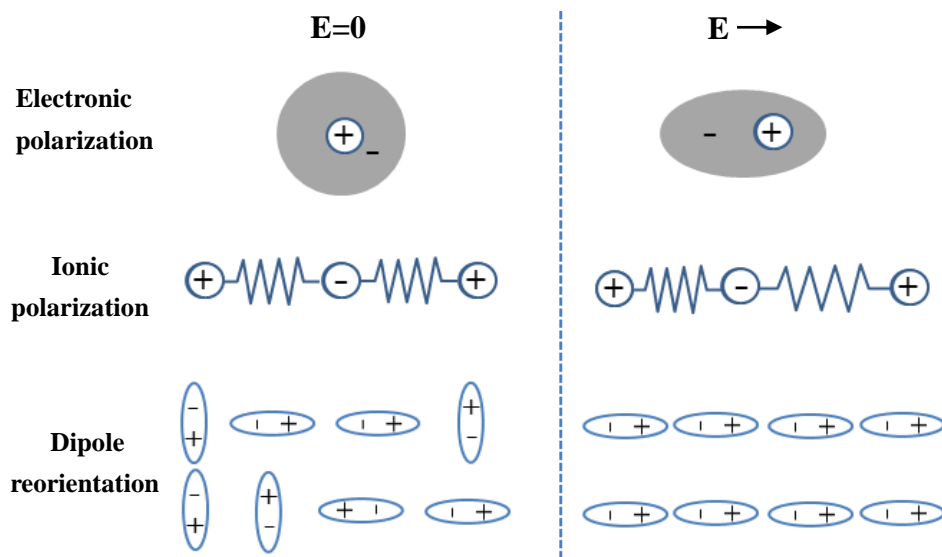


Fig. 3. Microscopic origins of the electric polarization.

(Source: reference [7])

BaTiO_3 is a typical ferroelectric material, exhibiting ionic displacements as illustrated in Fig. 4 at room temperature [7]. The lattice constants are $c = 0.4036$ nm and $a = 0.3992$ nm.



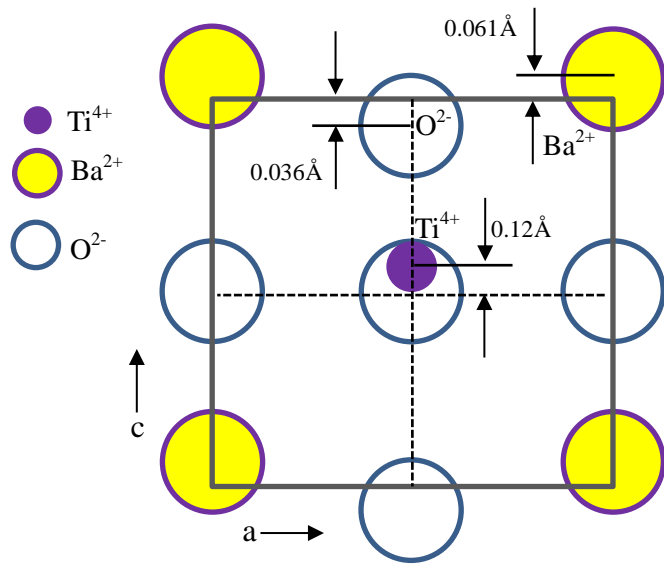


Fig. 4. Ionic displacements in BaTiO_3 .

(Source: reference [7])

BaTiO_3 has a peroskite crystal structure as shown in Fig. 5 [7]. Under high temperature conditions, there is no spontaneous polarization for the crystal. Below the Curie temperature (T_c about 130°C), the transition temperature, the spontaneous polarization generates, and the lattice structure turns to tetragonal with slight elongation, which shows the polarization property.

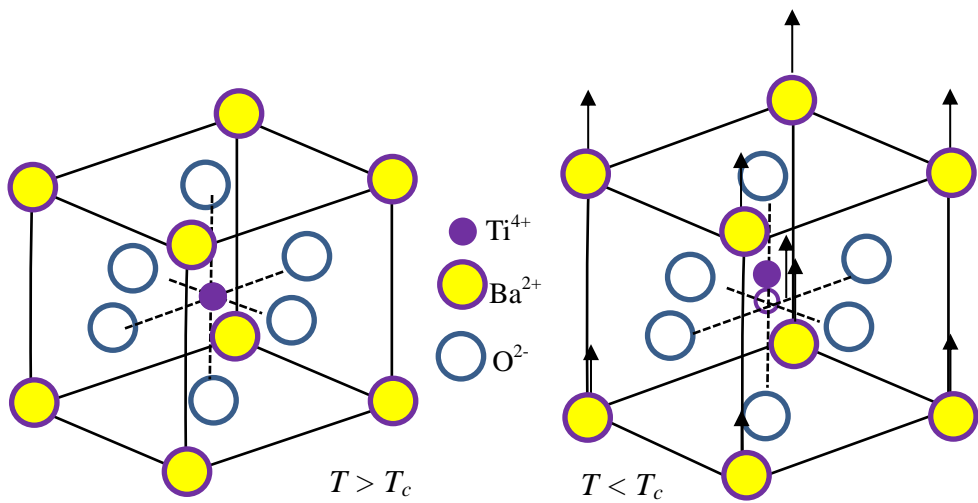


Fig. 5. Crystal structures of BaTiO₃: Higher than T_c (left) and lower than T_c

(right).

(Source: reference [7])

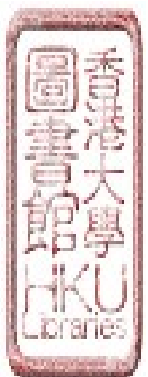
The thin film ferroelectric has widely applied in the semiconductor devices.

The ferroelectric thin film techniques for fabrication usually include chemical and physical process. The chemical process includes Chemical vapor deposition (CVD), metal-oxide CVD (MOCVD), dipping/spin coating based sol-gel method, and diverse epitaxy methods. The RF/DC or ion beam sputtering, electron beam evaporation, and ion plating methods are common physical deposition process.

According to the ferroelectric polarization properties and thin film techniques, the ferroelectric have been applied to the photovoltaic field.

2.2.2 Ferroelectric photovoltaic devices

Base on the unique ferroelectric properties, the ferroelectric photovoltaic devices (Ferro-PV) have been developed. Since 1960s, the anomalous



photovoltaic effect has been observed in a number of ferroelectric materials [8].

A typical Ferro-PV is shown in Fig. 6 [9], with capacitor like structure. A layer of ferroelectric is sandwiched between top and bottom electrodes, with internal electrical field throughout the bulk region [10]. Different from the p-n junction build in electric field, Ferro-PV is utilizing the ferroelectric remnant polarization field to realize control of charge carrier flow.

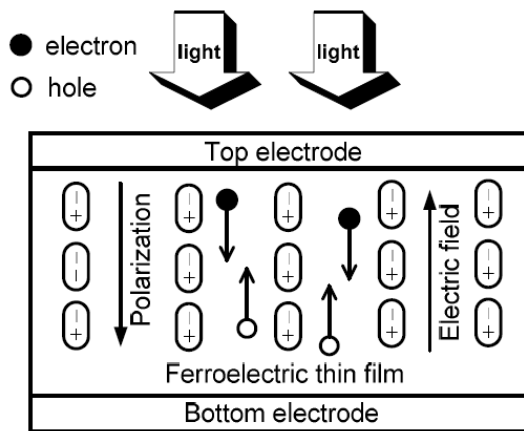
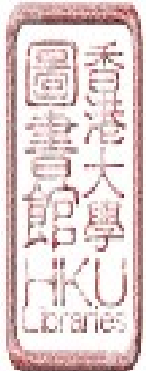


Fig. 6. Schematic illustration of ferroelectric photovoltaic device.

(Source: reference [9])

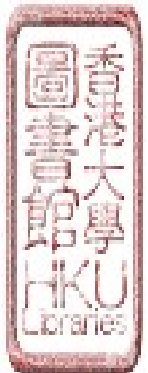
This Ferro-PV exhibits advantages such as extremely large photo voltage, a photocurrent proportional to the polarization magnitude. The photovoltaic effect is fundamentally different from that based on Si solar cells, with a fascinating charge separation mechanism. A steady-state photovoltaic current can be generated by uniform illumination of ferroelectrics with polarization field. Furthermore, attributing to the non-pn junction structure, the V_{oc} is not subjected to the material band gap limitation. The phenomenon of the light induced V_{oc}



greater than the band gap had been previously observed in ferroelectric BaTiO₃ single crystals [11] as well as the photovoltaic effect was discovered in lithium niobate and several other ferroelectric niobates [12-15].

The electronic transport properties and a diode effect associated with the direction of bulk electric polarization had been discovered in BiFeO₃ (BFO) Ferro-PV [16]. It is indicated that substantial currents were observed, having nonlinear relation with the applied external electric field. The current strongly depended on the electric field direction in BFO device. The polarization switching didn't occur during the J-V test because of the much lower magnitude of electric field than ferroelectric coercivity. But at 300 and 350 K, BFO showed linear scale J-V curves, which exhibited diode like behavior. The external pulses induced polarization would switch the rectification direction. Also, the diode forward direction was parallel with the ferroelectric polarization direction. The observed diode like dc conduction behavior implied a potential of zero-bias photovoltaic effect. The result showed a substantial PV effect had been found when the BFO device with semitransparent metal electrodes illuminated by visible light with a total power density lower than 20m W/cm².

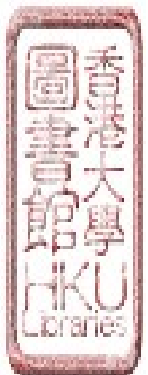
This investigation of photovoltaic effect and switchable diode in BFO reveals unusual behavior of charge conduction by ferroelectrics. Although, the bulk photovoltaic effect in ferroelectric BFO materials have been mainly studied in research activities, the mechanisms behind for the effect was not very clear. It was generally believed that the effect was associated with the loss of inversion



symmetry in the distribution of defects, impurities, space charges and polarizations in ferroelectrics [17]. Previously, the ferroelectric PV effect is proposed to be associated with the photorefractive effect and a change in the spontaneous polarization due to illumination. However, the nature of the photovoltaic effect in ferroelectric is far from fully understand and only the first steps have been taken in developing the theory of the PV effect [18-21].

Recently, Yang et al. indicated the ferroelectric domain wall played an important role on PV effect [22]. Through careful design of the experiments by using BFO thin film of varying thicknesses and domain types, they convinced that the photovoltaic effect in BFO thin films of the 71° and/or 109° domain walls, resulting from the polarization asymmetry, instead of bulk photovoltaic effect. They observed a very high photovoltaic voltage resulted from the ferroelectric domain walls in the BFO thin films Ferro-PV. The polarization divergence at the domain walls is non-zero and the imbalance charge accumulates at the domain walls, inducing an electrostatic potential offset. The potential step raises a band bending across the domain wall, which is similar to the band situation in the depletion region of a typical p-n junction. Therefore, the stronger electric field and efficient charge separation occurs at domain wall (2nm) in films.

New carrier transport mechanisms allowing for the explanation for the photovoltaic current should be hypothesized and systematically studied. There is no doubt that the investigation of the photovoltaic effect will make an important contribution to the physics of ferroelectricity, which is of intrinsic interest. A

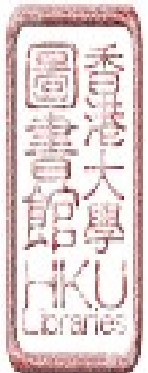


number of investigations have been conducted on the studies of Ferro-PV electrode [23-25], ferroelectric material quality [26], ferroelectric film thickness [27], device structure [28], and mechanisms [19, 29-31].

Qin et al. investigated the photovoltaic effect on the epitaxial fabricated PLZT Ferro-PV [9]. LSMO and Nb: STO were selected as the contact electrodes. Through control of the PLZT thin film thickness below 100nm, power conversion efficiency of around 0.28% was obtained. Their theoretical analysis indicated that the cell performance can be significantly upgraded by decreasing the film ferroelectric film thickness in nanoscale. Rather than epitaxial ferroelectric films, polycrystalline thin films seem more suitable for practical applications due to their simple deposition process and low price. Chemical solution derived polycrystalline PLZT thin film was applied to Ferro-PV [23]. The linear illuminated J-V curves showed the photovoltaic responses.

Shen et al. systematically studied the effect of the ferroelectric/electrode contact interface on photovoltaic output [31-33]. The result suggested the Schottky barrier height of ferroelectric/metal interface and the layer thickness directly determine the photocurrent of Pt/PZT/Pt Ferro-PV. Furthermore, they inserted an n-type Cu₂O layer in the ITO/PZT/Pt cell to generate a favorable energy alignment of the PZT/Pt interface. The short-circuit current was dramatically increased about 120-fold [28].

Actually, the type of electrodes played a crucial role on the device performance. It is theoretically discovered that use of high dielectric constant



electrodes can substantially increase the photocurrent of PLZT ferroelectric PV device [29]. Zhang et al. reported an enhanced photovoltaic effect in the PLZT using low work function metal as contacts [30]. The white light illuminated J_{sc} and V_{oc} of Mg/PLZT/ITO were about 150 and 2 folders of those of Pt/PLZT/ITO, respectively. The expanded spectra response was attributed to the possible photo-emitted electrons from low function metal to ferroelectric. Harsham et al. also studied the effect of the top electrodes on the PLZT ferroelectric capacitor [25]. It is confirmed the low work function metal was more appropriate to be the top contacts. The result showed that Al top electrode enhanced the photovoltaic efficiency of the cell by one order magnitude than Pt.

However, ferroelectric are in general large band gap materials [34], which limits the absorption of sunlight. To address this issue, narrow band-gap nanoparticles, such as Ag_2O , were implanted to enhance the visible light absorption in Pt/PZT/Pt ferro-PV device [35]. On the other hand, exploring the narrow band gap ferroelectric material is effective alternative to enhance the light absorption. BiFeO_3 , with a large polarization and a direct band gap of 2.67 eV (465 nm) [22] within the visible range of 2.5-2.9 eV, has prompted renaissance in research on ferroelectric photovoltaics. Ji et al. sputtered epitaxial BFO thin film for photovoltaic effect study, and observed enhanced visible light response property [26]. This discovery seems to be encouraged for increasing significantly the energy conversion efficiency in ferroelectric photovoltaic cells.

Unfortunately, the power conversion efficiency of Ferro-PV is still poor



and lower than that of commercially solar cells. A main reason is that the ferroelectric material is usually high insulating, leading to an intrinsically low conductivity for charge carrier transport. In addition, the physical origin and mechanism of the photovoltaic effect in ferroelectrics remains unclear and controversial. These could be the major obstacles in achieving high power conversion efficiency in Ferro-PV, and the recently observed efficiency in such ferroelectric photovoltaic cells is still poor. To solve these problems is one of the most significance tasks in the future development of ferroelectric solar cells.

Consequently, capacitor like Ferro-PV structure is not ideal to achieve high efficiency solar cells. Recently, notable studies were conducted on the application of the ferroelectric material into hybrid solar cells by Huang's research group. The P(VDF-TrFE), an organic ferroelectric, has been applied to OPV device, and significantly improved the power conversion efficiency after polarization [36-39]. Two typical structures are schematically indicated in Fig. 7 [36] [39].



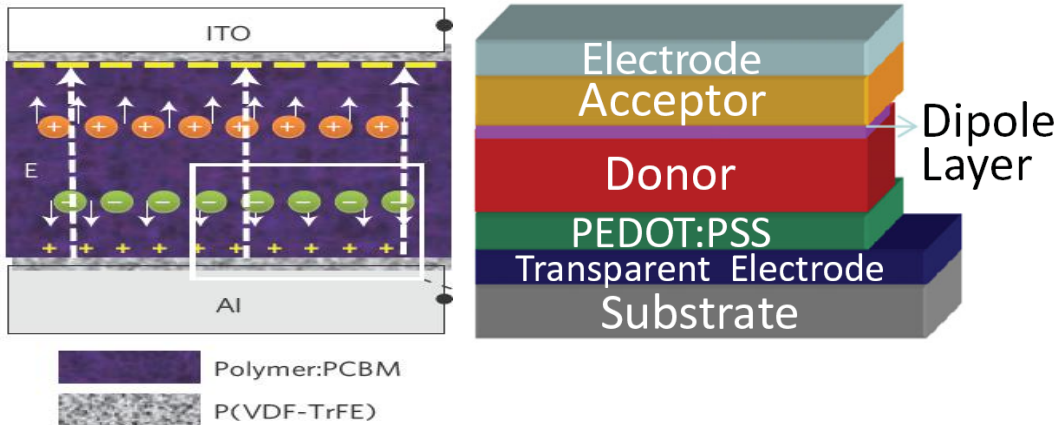


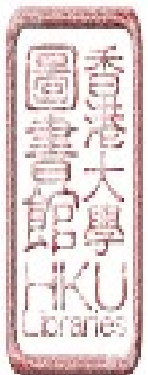
Fig. 7. Schematic illustrations of two types of ferroelectric polymer hybrid OPV

cells.

(Source: reference [36] [39])

A similar study was also conducted by incorporating the ferroelectric polymer, P(VDF-TrFE), at the crystalline silicon/PEDOT:PSS Schottky solar cell [40]. Poling of the ferroelectric layer resulted in the power conversion efficiency improvement from 10.2% to 12.3%, which further confirmed the effect of the spontaneous polarization of the ferroelectric material.

Another novel design is focused on the ferroelectric/semiconductor materials formed hetero-junction devices, which mainly makes use of the ferroelectric spontaneous polarization property to control optical electric performance. Various type of device, such as BFO/Nb-SrTiO₃ [41], BTO/Si [42], BFO/grapheme [24], BFO/BVO [43] were demonstrated. Remarkable rectifying property and white light photovoltaic effect were obtained. These experimental results indicate that a system combination with semiconductor and ferroelectric



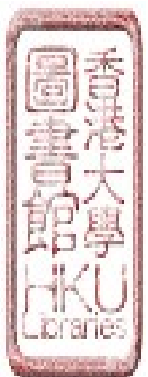
materials can provide a considerably high photovoltaic effect.

Despite nowadays the development of photovoltaic cells based on silicon and other functional materials has been greatly achieved, the use of ferroelectric into photovoltaic cell seems to provide another potential pathway for further boosting conversion efficiency and lowing cost, and may lead to a new future trend for solar energy research [17].

2.3 Development of grain boundaries passivation technique for photovoltaic

In solar cell the charge carrier transport property is correlated to the semiconductor materials property. Till now, silicon based materials still dominate the photovoltaic market share, especially for multicrystalline silicon (mc-Si), due to the low cost and comparable high efficiency. Also, as the new generation solar cell, polycrystalline silicon (pc-Si) thin film material is considered has a promising future. However, grain boundaries, exist in multicrystalline and polycrystalline silicon, and intensively limit the performances of solar cells. The two-diode mode illustrates the potential barrier raised from grain boundaries in p-type and n-type materials. (Fig. 8 [44])

Generally, defects density along grain boundaries (GBs) is considered higher than bulk due to the different orientation neighboring crystal grains give rise to dangling bonds, dislocations, misplaced atoms, vacancies, distorted bond angles and bond distances at the interfaces. In addition, intrinsic impurities are



likely to exist along loose GBs [1]. These defects introduce extra electronic states, localized within silicon band gap. According to their energetic position, shallow states, act as trap state, increase the potential barrier and offer substantial impedance for majority charge carriers' transportation. While the deep states tend to act as the recombination center for minority carriers, accordingly shorten their life time and reduce the V_{oc} of junction. Especially, the presence of dangling bonds is thought to give rise to the most effective recombination site, and plays a key role in effecting the electrical properties of multicrystalline and polycrystalline silicon [45, 46].

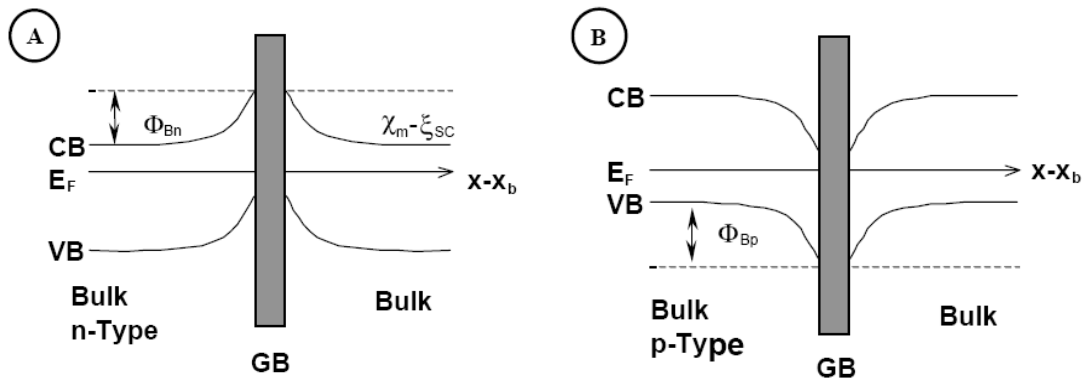
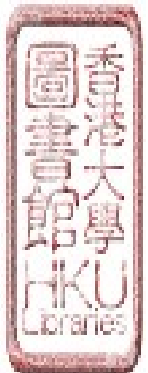


Fig. 8. Schematic of the energy band diagram in the “Two-Diode Model” for grain boundaries of n-type and p-type mc-Si.

(Source: reference [44])

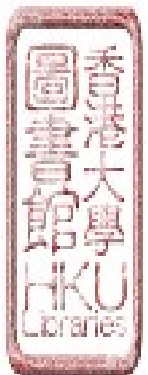
To limit the effect of GBs, the key is to either to eliminate GBs or to eliminate their electrical activity [47]. Comparably, the later method, passivation GBs, is considered effectively and economically, which attract a lot of studies.



The milestone is using hydrogen for the passivation.

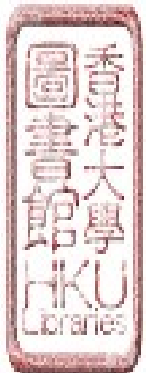
Considering Hydrogen's high mobility in solids, Seager and Ginley attempted exposing large-grained silicon to atomic hydrogen, and observed very definite decrease in the impedance of individual grain boundary barriers at sample temperature of around 400 [47, 48]. Their study indicated the low potential barrier of GBs is due to the reduction of trap-state densities caused by hydrogen. However, the character of hydrogen is either to tie up the dangling bonds or to reduce native Si-O bond is unknown. It is interesting that they indicated the stability of Si-H bonds through annealing at 320 for periods excess of 50h, which didn't observed in amorphous Si [48]. In virtue of the application of electron spin resonance (ESR), hydrogen is verified to reduce the dangling bonds spin density by forming Si-H bonds, and the excess hydrogen accumulated as clusters, which strong depends on temperature [49]. Actually, later studies indicated the diffusion of hydrogen is rather complex because hydrogen can exist in several charge sites. In addition, hydrogen can be present in a number of forms such as atomic and molecular forms and bound to a defect or an impurity, and the probability depends on the hydrogenation condition (temperature, time, concentration and power) [50]. Excessive hydrogen passivation led to surface damage and defects creation, such as Si-H₂ bonds and H₂, which evidenced by Raman spectroscopy and X-ray diffraction [51].

The main problem of hydrogen plasma treatment is it will loss the passivation effect when subjected to high temperature annealing (>500°C).



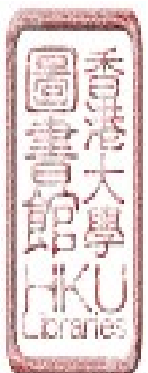
Furthermore, it needs long hydrogenation time, thereby increase the process complication, as well as cost. Consequently, it is necessary to find alternative chemistry agents. Recently, Honda et al. had searched for a new effective and low-cost method for passivation polycrystalline silicon grain boundaries by annealing in water vapor [52, 53]. The measurement of Hall mobility reflected the performance of poly Si after water vapor treatment was almost the same as the value through hydrogenation. However, differ from the hydrogen, water vapor didn't introduce crystalline disorder, and thereby decreased the potential at grain boundaries. Confirmed by Kelvin force microscopy and microscopic Raman spectroscopy, potential changes at grain boundaries strongly related to the lattice disorder and grain boundary type.

It is worth pointing out the mechanism of passivation by water vapor is different compare with hydrogen. The authors considered water molecules in defects might be chemically dissociated by heat energy, and then passivated the dangling bonds by forming Si-H, Si-O or Si-OH bonds. Beside, this treatment might only work on the defects without creation of defects or disorder in process. Water molecule is a polar molecule. However, there has been few studies on passivation grain boundaries by polar molecule, as well as the corresponding passivation procedure. Consequently, systematical investigations of polar molecule for passivating grain boundaries is of great value to provide effective and low cost approach, and this method can be applied to the novel solar cell design.



References

1. Nelson, J., *The physics of solar cells*. 2003: Imperial College Press.
2. Luque, A.H., Steven, *Handbook of Photovoltaic Science and Engineering*. 2003: Wiley.
3. Regan, W., et al., *Screening-Engineered Field-Effect Solar Cells*. Nano Letters, 2012. **12**(8): p. 4300-4304.
4. Wadhwa, P., et al., *Electronic Junction Control in a Nanotube-Semiconductor Schottky Junction Solar Cell*. Nano Letters, 2010. **10**(12): p. 5001-5005.
5. Wadhwa, P., et al., *Electrolyte-Induced Inversion Layer Schottky Junction Solar Cells*. Nano Letters, 2011. **11**(6): p. 2419-2423.
6. Yao, K., et al., *Large photo-induced voltage in a ferroelectric thin film with in-plane polarization*. Applied Physics Letters, 2005. **87**(21): p. 212906.
7. Uchino, K., *Ferroelectric devices*, ed. second. 2010: CRC Press.
8. Fridkin, V.M., *Bulk photovoltaic effect in noncentrosymmetric crystals*. Crystallography Reports, 2001. **46**(4): p. 654-658.



9. Qin, M., K. Yao, and Y.C. Liang, *High efficient photovoltaics in nanoscaled ferroelectric thin films*. Applied Physics Letters, 2008. **93**(12): p. 122904.
10. Qin, M., K. Yao, and Y.C. Liang, *High efficient photovoltaics in nanoscaled ferroelectric thin films*. Applied Physics Letters, 2008. **93**(12): p. 112904.
11. Volk, T.R., et al., *Effect of Illumination on Domain-Structure and Curie Temperature in BaTiO₃*. Fizika Tverdogo Tela, 1972. **14**(11): p. 3214.
12. Ionov, P.V., *Photosensitivity of Ferroelectric Niobates*. Fizika Tverdogo Tela, 1973. **15**(9): p. 2827-2828.
13. Glass, A.M. and D. Vonderlinde, *Photovoltaic, Photoconductive and Excited-State Dipole Mechanisms for Optical Storage in Pyroelectrics*. Ferroelectrics, 1976. **10**(1-4): p. 163-166.
14. Micheron, F., *Sensitivity of Photorefractive Processes*. Ferroelectrics, 1978. **18**(1-3): p. 153-159.
15. Gabrielyan, V.T., et al., *Influence of K, Mg and Fe impurities on the composition, absorption spectra and photovoltaic properties of LiNbO₃ crystals*. Ferroelectrics, 2002. **281**: p. 151-161.



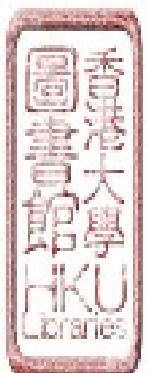
16. Choi, T., et al., *Switchable Ferroelectric Diode and Photovoltaic Effect in BiFeO₃*. Science, 2009. **324**(5923): p. 63-66.
17. Huang, X.L.M., Su Lyn, *Ferroelectrics New Research: Electrical Engineering Developments*. 2012: NOVA.
18. Ji, W., K. Yao, and Y.C. Liang, *Evidence of bulk photovoltaic effect and large tensor coefficient in ferroelectric BiFeO₃ thin films*. Physical Review B, 2011. **84**(9): p. 094115.
19. Cao, D.W., et al., *Understanding the nature of remnant polarization enhancement, coercive voltage offset and time-dependent photocurrent in ferroelectric films irradiated by ultraviolet light*. Journal of Materials Chemistry, 2012. **22**(25): p. 12592-12598.
20. Zheng, F., et al., *Separation of the Schottky barrier and polarization effects on the photocurrent of Pt sandwiched Pb(Zr 0.20Ti 0.80)O₃ films*. Applied Physics Letters, 2008. **93**(17): p. 172101.
21. Cao, D.W., et al., *Polarization effect on the photocurrent of Pt sandwiched multi-crystalline ferroelectric films*. Materials Chemistry and Physics, 2011. **129**(3): p. 783-786.
22. Yang, S.Y., et al., *Above-bandgap voltages from ferroelectric photovoltaic devices*. Nature Nanotechnology, 2010. **5**(2): p. 143-147.



23. Qin, M., K. Yao, and Y.C. Liang, *Photovoltaic characteristics in polycrystalline and epitaxial (Pb_{0.97}La_{0.03})(Zr_{0.52}Ti_{0.48})O₃ ferroelectric thin films sandwiched between different top and bottom electrodes*. Journal of Applied Physics, 2009. **105**(6): p. 061624.
24. Zang, Y.Y., et al., *Enhanced photovoltaic properties in graphene/polycrystalline BiFeO₃/Pt heterojunction structure*. Applied Physics Letters, 2011. **99**(13): p. 132904.
25. Harshan, V.N. and S. Kotru, *Influence of work-function of top electrodes on the photovoltaic characteristics of Pb_{0.95}La_{0.05}Zr_{0.54}Ti_{0.46}O₃ thin film capacitors*. Applied Physics Letters, 2012. **100**(17): p. 173901.
26. Ji, W., K. Yao, and Y.C. Liang, *Bulk Photovoltaic Effect at Visible Wavelength in Epitaxial Ferroelectric BiFeO₃ Thin Films*. Advanced Materials, 2010. **22**(15): p. 1763-1766.
27. Qin, M., et al., *Thickness effects on photoinduced current in ferroelectric (Pb_{0.97}La_{0.03})(Zr_{0.52}Ti_{0.48})O₃ thin films*. Journal of Applied Physics, 2009. **105**(12): p. 014104.
28. Cao, D.W., et al., *High-Efficiency Ferroelectric-Film Solar Cells with an n-type Cu₂O Cathode Buffer Layer*. Nano Letters, 2012. **12**(6): p. 2803-2809.



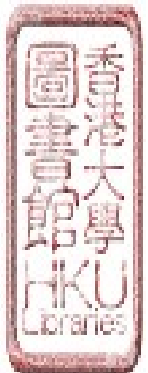
29. Qin, M., K. Yao, and Y.C. Liang, *Photovoltaic mechanisms in ferroelectric thin films with the effects of the electrodes and interfaces*. Applied Physics Letters, 2009. **95**(2): p. 022912.
30. Zhang, J.J., et al., *Enlarging photovoltaic effect: combination of classic photoelectric and ferroelectric photovoltaic effects*. Scientific Reports, 2013. **3**: p. 2109.
31. Cao, D.W., et al., *Interface layer thickness effect on the photocurrent of Pt sandwiched polycrystalline ferroelectric Pb(Zr, Ti)O₃ films*. Applied Physics Letters, 2010. **97**(10): p. 102104.
32. Zhang, P., et al., *Enhanced photocurrent in Pb(Zr0.2Ti0.8)O₃ ferroelectric film by artificially introducing asymmetrical interface Schottky barriers*. Materials Chemistry and Physics, 2012. **135**(2-3): p. 304-308.
33. Cao, D., et al., *Interface effect on the photocurrent: A comparative study on Pt sandwiched (Bi_{3.7}Nd_{0.3})Ti₃O₁₂ and Pb(Zr_{0.2}Ti_{0.8})O₃ films*. Applied Physics Letters, 2010. **96**(19): p. 192101.
34. Dawber, M., K.M. Rabe, and J.F. Scott, *Physics of thin-film ferroelectric oxides*. Reviews of Modern Physics, 2005. **77**(4): p. 1083-1130.



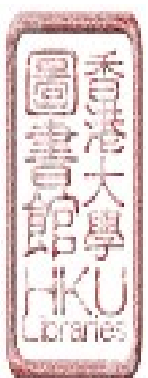
35. Yang, X.L., et al., *Enhancement of Photocurrent in Ferroelectric Films Via the Incorporation of Narrow Bandgap Nanoparticles*. Advanced Materials, 2012. **24**(9): p. 1202-1208.
36. Yuan, Y.B., et al., *Efficiency enhancement in organic solar cells with ferroelectric polymers*. Nature Materials, 2011. **10**(4): p. 296-302.
37. Xiao, Z.G., et al., *Synthesis and Application of Ferroelectric P(VDF-TrFE) Nanoparticles in Organic Photovoltaic Devices for High Efficiency*. Advanced Energy Materials, 2013. **3**(12): p. 1581-1588.
38. Yuan, Y.B., et al., *Understanding the effect of ferroelectric polarization on power conversion efficiency of organic photovoltaic devices*. Energy & Environmental Science, 2012. **5**(9): p. 8558-8563.
39. Yang, B., et al., *Tuning the Energy Level Offset between Donor and Acceptor with Ferroelectric Dipole Layers for Increased Efficiency in Bilayer Organic Photovoltaic Cells*. Advanced Materials, 2012. **24**(11): p. 1455-1460.
40. Liu, Q., et al., *Improved photovoltaic performance of crystalline-Si/organic Schottky junction solar cells using ferroelectric polymers*. Applied Physics Letters, 2013. **103**(16): p. 163503.



41. Qu, T.L., et al., *Resistance switching and white-light photovoltaic effects in BiFeO₃/Nb-SrTiO₃ heterojunctions*. Applied Physics Letters, 2011. **98**(17): p. 173507.
42. Xing, J., et al., *Photovoltaic effects and its oxygen content dependence in BaTiO(3-delta)/Si heterojunctions*. Applied Physics Letters, 2008. **92**(7): p. 071113.
43. Dong, W., et al., *Enhanced Photovoltaic Effect in BiVO₄ Semiconductor by Incorporation with an Ultrathin BiFeO₃ Ferroelectric Layer*. Acs Applied Materials & Interfaces, 2013. **5**(15): p. 6925-6929.
44. Diaz, M.B., et al., *Resistivity topography: a grain boundary characterisation method*. Solar Energy Materials and Solar Cells, 2002. **72**(1-4): p. 473-486.
45. Mataré H.F., *Defect Electronics in Semiconductors*. 1971, New York: Wiley-interscience.
46. Johnson, N.M., D.K. Biegelsen, and M.D. Moyer, *Deuterium Passivation of Grain-Boundary Dangling Bonds in Silicon Thin-Films*. Applied Physics Letters, 1982. **40**(10): p. 882-884.
47. Seager, C.H. and D.S. Ginley, *Studies of the Hydrogen Passivation of Silicon Grain-Boundaries*. Journal of Applied Physics, 1981. **52**(2): p. 1050-1055.



48. Seager, C.H. and D.S. Ginley, *Passivation of Grain-Boundaries in Polycrystalline Silicon*. Applied Physics Letters, 1979. **34**(5): p. 337-340.
49. Nickel, N.H., N.M. Johnson, and W.B. Jackson, *Hydrogen Passivation of Grain-Boundary Defects in Polycrystalline Silicon Thin-Films*. Applied Physics Letters, 1993. **62**(25): p. 3285-3287.
50. Darwiche, S., et al., *Effects of hydrogen plasma on passivation and generation of defects in multicrystalline silicon*. Solar Energy Materials and Solar Cells, 2007. **91**(2-3): p. 195-200.
51. Honda, S., et al., *Hydrogenation of polycrystalline silicon thin films*. Thin Solid Films, 2006. **501**(1-2): p. 144-148.
52. Honda, S., et al., *Microscopic study of the H₂O vapor treatment of the silicon grain boundaries*. Journal of Non-Crystalline Solids, 2008. **354**(19-25): p. 2310-2313.
53. Honda, S., et al., *Annealing in water vapor as a new method for improvement of silicon thin film properties*. Journal of Non-Crystalline Solids, 2006. **352**(9-20): p. 955-958.



3. Non-PN Based Ferroelectric-Semiconductor Solar Cells: Concept Proof

In this chapter, we mainly focus on the concept proof of the novel non-PN junction based ferroelectric-semiconductor solar cells. In the following chapters 4 to 6, different factors affecting the device performance are studied separately in detail.

This part was adapted from two papers published in *Applied Physics Letter*:

1. Wentao Wang, Fude Liu^{a)}, Chor Man Lau, Lei Wang, Guandong Yang, Dawei Zheng and Zhigang Li, Field-effect BaTiO₃-Si solar cells. *Applied Physics Letters*, 2014. 104 (12): p. 123901.
2. Fude Liu ^{a)}, Wentao Wang, Lei Wang, Guandong Yang, Ferroelectric-semiconductor photovoltaics: Non-PN junction solar cells. *Applied Physics Letters*, 2014. 104 (10): p. 103907.



Abstract

Conventional solar cells make use of the spatial variation in electronic environment due to junctions for charge separation. We investigated field-effect BaTiO₃-Si solar cells that utilize the bound surface charges of BaTiO₃ to separate charge carriers in silicon. Rectifying behavior and photovoltaic effect were observed on cells that were forward polarized. Theoretical simulation indicated that the induced electric field due to BaTiO₃ polarization could extend into the silicon layer, which is consistent with experimental observations. In addition, adjusting relevant parameters may optimize the electric field distribution. The new cells are promising in terms of material selection, device design and fabrication.

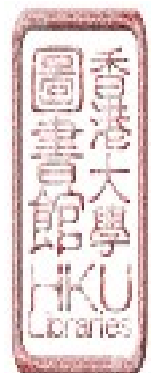
Keywords: Photovoltaics; BaTiO₃; silicon; field effect; solar cells.



3.1 Introduction

Photovoltaic devices are generally developed for optimizing three key steps: charge carrier generation, separation, and transport. In particular, how to realize charge carrier separation usually dictates the basic device structure. Conventional solar cells make use of the spatial variation in electronic environment due to junctions for charge separation, and the PN junction structure is a classic model of this concept. However, this kind of structure has limitations on materials selection and device fabrication to form a working junction due to issues such as lattice mismatch, doping, and band alignment. Moreover, either homo-junctions or hetero-junctions inevitably introduce defect states that act as recombination or trapping centers for charge carriers [1]. In contrast, ferroelectric-based photovoltaic cells, which usually consist of a ferroelectric layer sandwiched between two electrode plates, can avoid aforementioned issues, and thus have attracted considerable attention recently [2-4]. These cells have an internal electric field throughout the bulk region originating from electrical polarizations that are not completely compensated by screening charges [5]. Consequently, a fascinating charge separation mechanism exists in these cells, and even the light-induced open circuit voltage (V_{oc}) can be greater than the band gap [6, 7]. However, ferroelectric materials are in general highly insulating because of their large band gaps [8], which limits the absorption of sunlight. Thus, ferroelectrics should be coupled with semiconductors in order to achieve photovoltaic devices with good performance.

In this work, we investigated a new type of solar cells that combine a ferroelectric and a semiconductor. The new photovoltaic cells, like traditional



counterparts, still use semiconductor materials with suitable energy bandgaps and excellent carrier transport as the light-absorbing layer. In addition, ferroelectric materials are introduced to provide an external electric field on the semiconductor layer for realizing the charge carrier separation therein. Unlike the case in traditional ferroelectric solar cells though, the ferroelectric layer herein is not used for light absorption. Therefore, the new cells can overcome the aforementioned problems with conventional photovoltaic cells. BaTiO₃ and P-Si were selected to demonstrate this new concept cell. Actually, this unique structure can be adapted for other ferroelectric-semiconductor combinations in principle, and is promising in preparing novel solar cells because it provides us more flexibility in material selection, device design and fabrication.

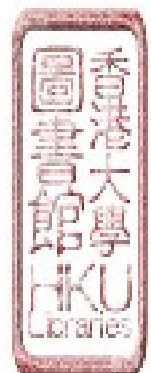
3.2 Experimental

The schematic of device structure and a real cell are shown in Fig. 1, respectively. As illustrated in Fig. 1a, the cell consists of a ferroelectric layer, a semiconductor layer, a pair of poling electrodes (*P*-electrodes), and a pair of working electrodes (anode and cathode). The *P*-electrodes patterns are aligned well with those of anode and cathode, respectively. Note that neighboring regions in the ferroelectric layer are polarized in opposite directions such that negative and positive bound surface charges are accumulated to different electrodes in a fashion as shown in the figure. After polarization, external electric fields are removed and then remnant polarizations exist. Anode and cathode thus collect electrons and holes, respectively, in the semiconductor layer under the influence of the external field due to



ferroelectric polarizations; electrons then flow through the external circuit to do work on the load (R) and finally recombine with holes at the cathode.

To fabricate a real cell (Fig. 1b), silicon and BaTiO_3 were chosen as the semiconductor absorber and ferroelectric layer, respectively, because of mature technologies. A piece of *p*-type single crystalline Si wafer with thickness of 280 μm and size of $20 \times 20 \text{ mm}^2$ was cleaned with the RCA (= Radio Corporation of America) clean. Ti and Au were chosen for anode and cathode, respectively, that were deposited on Si with sputtering using a shadow mask. BaTiO_3 was then spin coated on Si with the sol-gel method using a precursor solution (0.40 mol/L) based on $\text{Ba}(\text{CH}_3\text{COO})_2$, $\text{Ti}(\text{OC}_2\text{H}_5)_4$, polyvinylpyrrolidone (PVP)-360000, H_2O , CH_3COOH and $\text{C}_2\text{H}_5\text{OH}$ [9]. After each spin coating step, the sample was dried at 350°C for 10 minutes before proceeding to next step; the coating may be repeated several times depending on the film thickness required. Then, the sample was stepwise heated at 300°C and 500°C for 10 minutes, respectively, and finally at 700°C for 15 minutes to achieve full crystallization of BaTiO_3 [10]. *P*-electrodes of Ag were deposited on BaTiO_3 with thermal evaporation. Post annealing at 450°C for 15 minutes was then conducted to form good metal contacts. Finally, the sample was wired out with Ag paste and metal wire, and was then packaged with epoxy and glass for insulating. The poling was conducted at 180°C and then at room temperature for 10 minutes, respectively. During the poling process, the silver *P*-electrodes were grounded, and 18V was applied on the Au cathode and -18V on the Ti anode simultaneously, which is defined as forward polarization; it is called reverse polarization when the external poling voltage are swapped between anode and cathode. The electrical



characterization was carried out with a standard solar simulator (ABET Sun 2000 coupled with Keithley 2602A). All current-voltage (I-V) measurements were conducted by sweeping the voltage from the negative to positive. The distribution of the induced electric field in Si due to the bound surface charges of BaTiO₃ was simulated with the finite-element method using the AC/DC Module of COMSOL®.

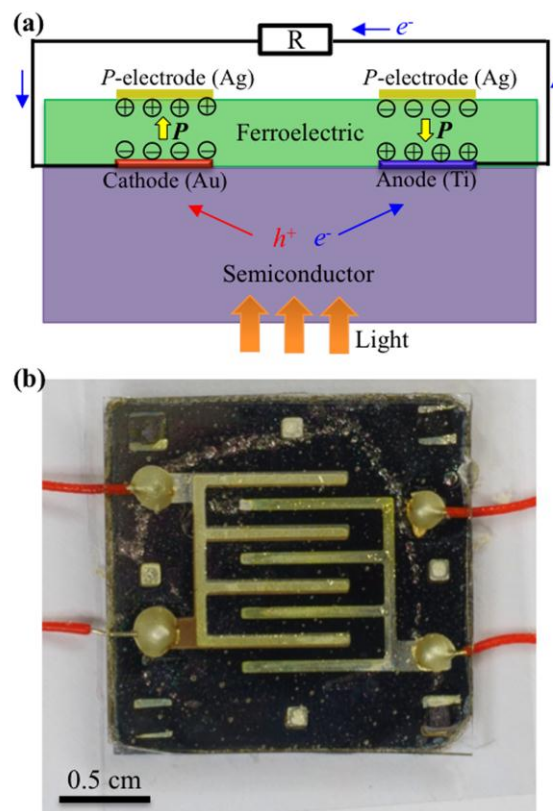
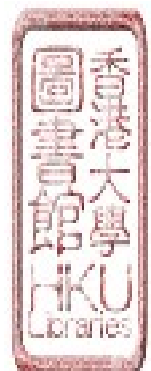


Fig. 1. Schematic of device structure and real cell. (a) Schematic of device structure (cross-section view; not drawn to scale). (b) Real cell (top-down view from the ferroelectric side).



3.3 Results and discussion

The way of poling on the ferroelectric plays an important role in device performance. Fig. 2 depicts the I-V curves of the before-polarization and reverse-polarization states, respectively, under dark condition. Before polarization, the I-V curve is a straight line with high resistivity. After reverse polarization, the I-V curve in general is still linear but with lower resistivity. So the cell shows Ohmic behaviors for both cases. However, after forward polarization, the conduction behavior under dark condition is changed dramatically; a substantial diode rectifying behavior is evident in the corresponding I-V curve (black curve in Fig. 3a). The rectification ratio is ~ 220 at $V = \pm 0.5$ V. The diode-like behavior of dc conduction has been constantly observed in all our cells (>20 cells). Therefore, the polarization of BaTiO_3 can greatly affect the transport of charge carriers in Si.

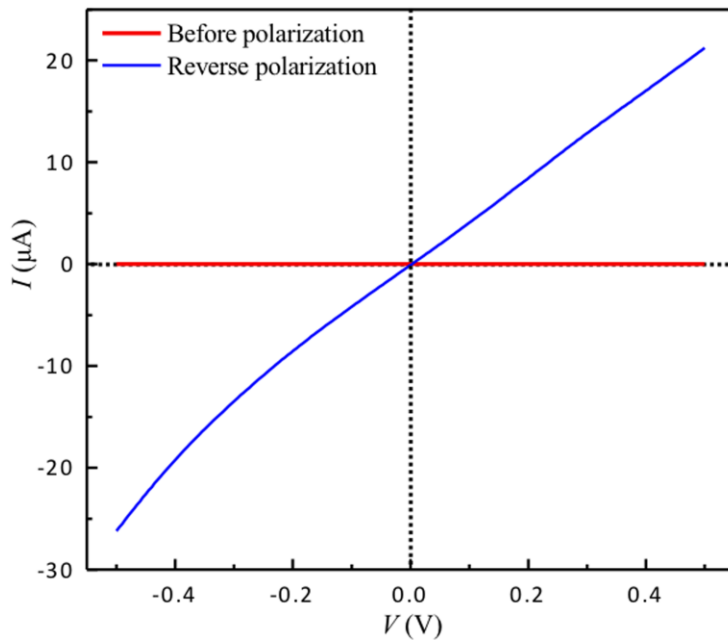


Fig. 2. I-V curves of the before-polarization and reverse-polarization states, respectively, under dark condition.



Under sunlight illumination at 100 mW/cm^2 , the I-V curve shifts downward for the forward-polarization state, exhibiting the photovoltaic effect (brown curve in Fig. 3a). The corresponding V_{oc} and I_{sc} are $\sim 170 \text{ mV}$ and $0.035 \mu\text{A}$, respectively. We also studied the time-dependent I_{sc} when the illumination was switched on or off under short-circuit condition (Fig. 3b). We see that the photocurrent is generated whenever the cell is exposed to sunlight, and it disappears whenever the illumination is off. Therefore, photon-generated charge carriers in Si can be separated and then collected by anode or cathode. Because the band gap of BaTiO_3 is 3.2 eV and the light is shot from the thick Si side, it is reasonable to assume that photon-generated charge carriers in Si mainly contribute to the photovoltaic effect. In addition, there is no initial small spikes of photocurrent, which rules out the pyroelectric effect as well [11].



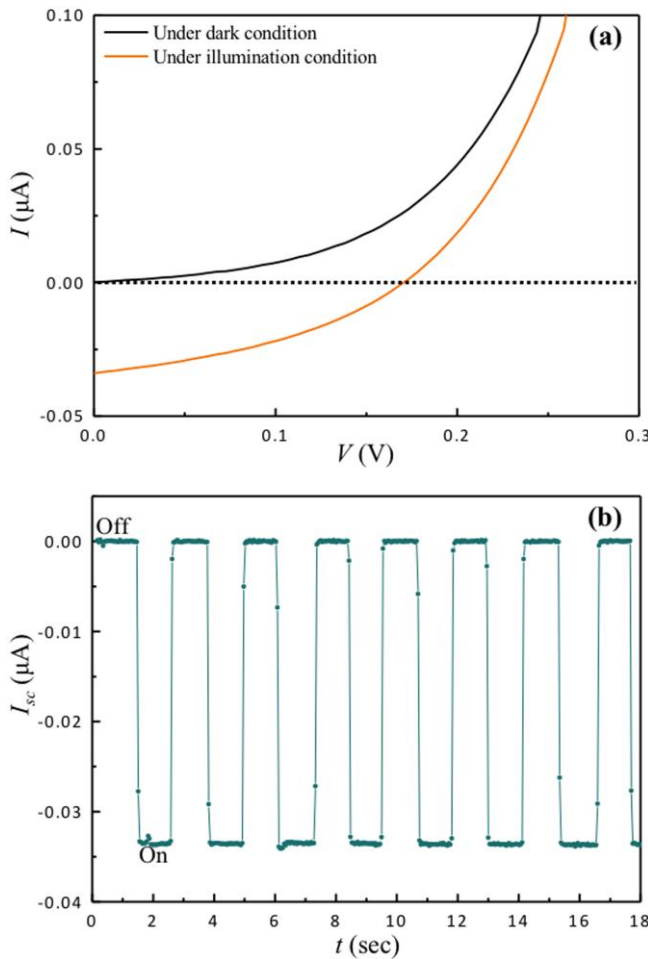


Fig. 3. Rectifying behavior and photovoltaic effect of the forward-polarization state.

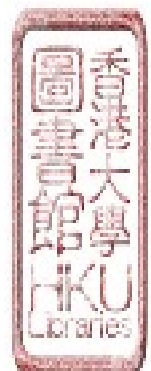
(a) I-V curves under dark and illumination conditions, respectively. (b) Time-dependent I_{sc} when the illumination is switched on or off.

The result successfully confirmed the effectiveness of the novel cell works. We then check in principle the device feasibility by considering the induced electric field in the semiconductor due to the ferroelectric bound surface charges. First of all, it is important to know the influence of an external electric field (or voltage) on the band diagram of an intrinsic semiconductor (Fig. 4). Under dark condition (Fig. 4a), the



external electric field will tilt the semiconductor band diagram, and then electrons and holes will accumulate to the anode and cathode, respectively, until the Fermi level lines up to reach the equilibrium state. If we shoot sunlight on the semiconductor under open-circuit condition (Fig. 4b), the Fermi levels in the semiconductor split and more free carriers are accumulated on the electrodes; differences in the Fermi energies (i.e., $V_{oc} = EF_{left} - EF_{right}$) and carrier concentrations occur between two surfaces with strong surface recombination [12]. Overall, we see that the band diagrams shown here are similar to that of a p-i-n solar cell. Therefore, it is expected that the new solar cells in principle work.

We now understand the crucial role played by the external electric field in the semiconductor as well as by the forward polarization in the rectifying behavior and photovoltaic effect. To further understand this, it is necessary to know the distribution of the induced electric field in Si due to the bound surface charges of BaTiO₃. Fig. 5a represents the simulation model whose geometry parameters are from real cells. The relative permittivity of Si, BaTiO₃ and Au is 11.9 [13], 290 [14] and 6.9 [15], respectively. The relative permittivity of Ti and Ag is unknown in the literature; we simply took the same value of 6.9 for them too (which is not expected to greatly affect the over picture on electric field distribution). Next, the bound surface charge density was set to be $\pm 0.10 \text{ C/m}^2$ (typical value) for the polarized BaTiO₃ layer. The simulated electric field distribution in the cell is shown in Fig. 5b. Also included is the electric field legend that is color-coded for easy viewing. Because the BaTiO₃ layer is very thin compared to the Si layer, it is barely seen in the figure. It is obvious that the induced electric field extends into the Si layer. Overall, the electric field



points toward the cathode and points away from the anode, as indicated by black arrows. Thus photon-generated electrons and holes would drift to the anode and cathode, respectively, under the influence of the induced electric field. The current flow direction is then consistent with our experimental results shown in Fig. 3. Note that the electric field is in the order of 10^0 V/cm, which is much weaker than that of a typical PN junction (in the order of $10^3 - 10^4$ V/cm) [16]. In addition, the electric field distribution in the Si layer is not uniform. In particular, the field is relatively stronger in regions (in red) near the electrodes and is relatively weaker in regions (in blue) between cathode and anode. The weak and non-uniform electric field may be one major reason for the poor device performance.

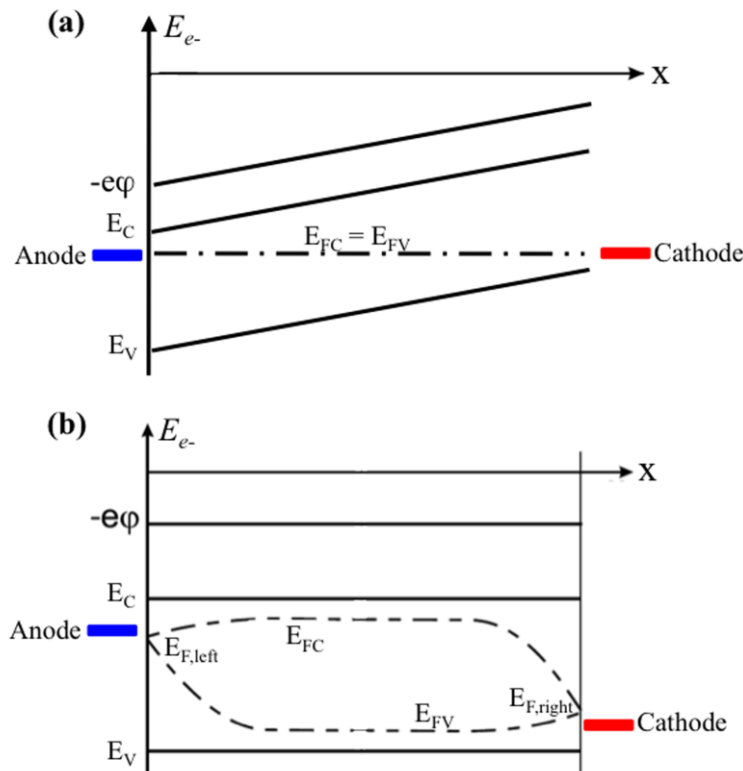


Fig. 4. Effect of the electric field on the band diagram of a semiconductor (intrinsic).

(a) Under dark condition. (b) Under sunlight illumination.



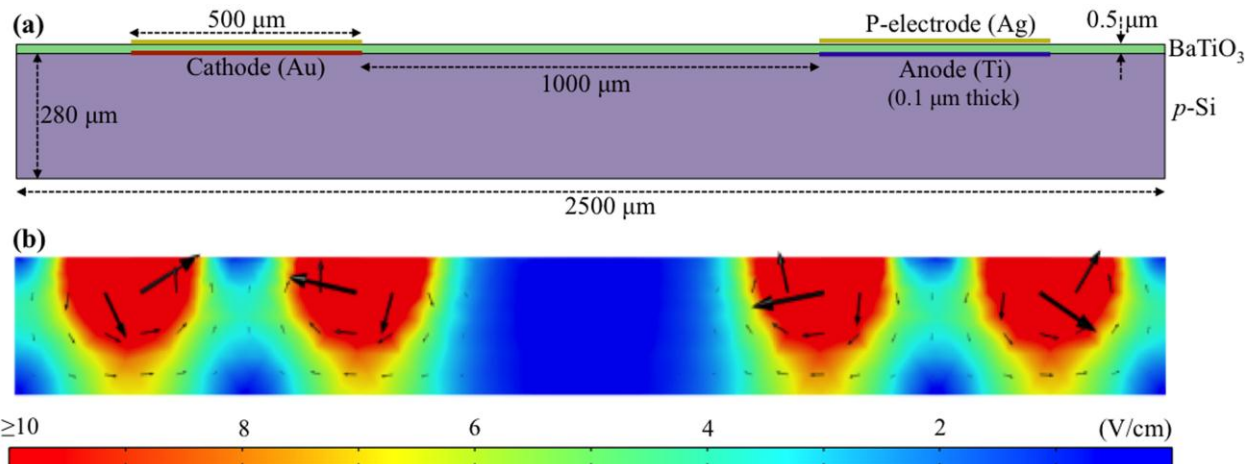


Fig. 5. Simulation of the electric field distribution in the real cell. (a) Model geometry (not drawn to scale). (b) Simulated electric field distribution in the real cell. Also included is the electric field legend that is color-coded.

The device performance can be improved through geometry optimization. Fig. 6 shows the simulation of the electric field distribution in a possible optimized cell after adjusting the dimension parameters. We see that in the optimized cell, the electric field in Si is now increased to be in the order of 10^3 V/cm, which is comparable to that in a typical PN junction. In addition, its electric field distribution is more uniform. It is then expected that real cells based on the optimized model will have better performance.



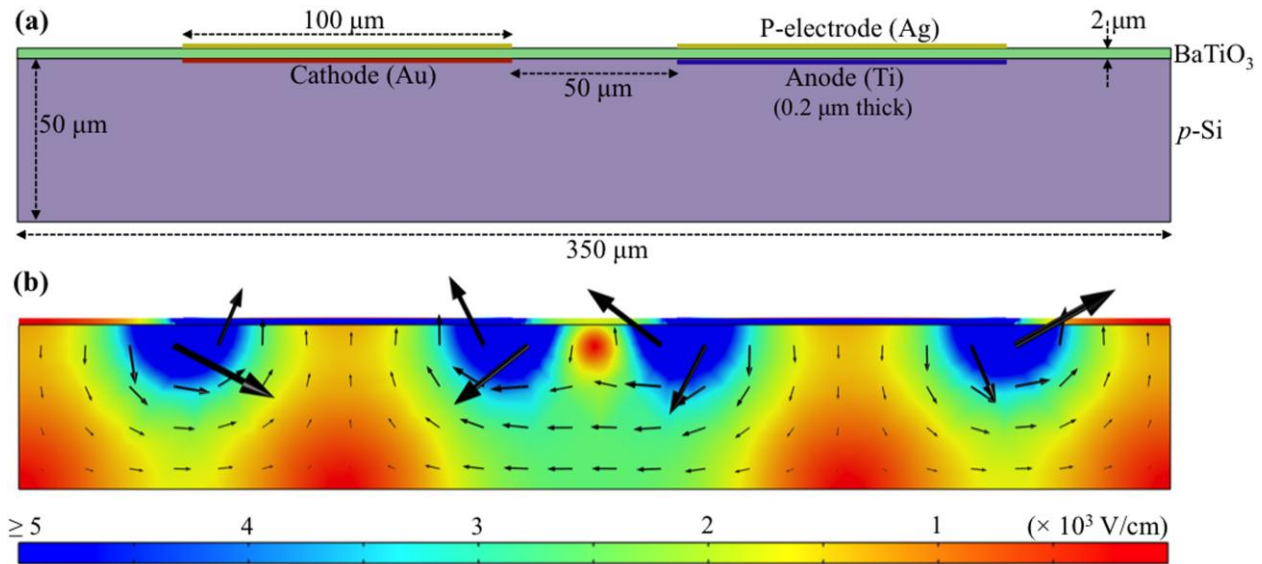


Fig. 6. Simulation of the electric field distribution in a possible optimized cell. (a) Model geometry (not drawn to scale). (b) Electric field distribution in the optimized cell. Also included is the electric field legend that is color-coded.

It should be pointed out that in our simulation we have not considered the screening effect of metal electrodes on the bound surface charges of the ferroelectric, which may weaken the induced electric field in the semiconductor [17, 18]. Transparent conducting oxides (TCO) with less carrier density and longer screening length may be used as electrodes instead to mitigate this problem. In real cells, besides the weak and non-uniform electric field, poor metal contacts with high resistance are another major reason for the low device performance, in particular, low current, as indicated in Figs 2 and 3. In addition, we may need to consider other issues such as surface passivation, ionic defects in the ferroelectric [19] and possible carrier injection between the semiconductor and ferroelectric. All the aforementioned



issues are good points to address in the future work. In this study, however, we focus mainly on the concept demonstration of BaTiO₃-Si cells.

3.4 Conclusions

In summary, we investigated field-effect BaTiO₃-Si solar cells in detail with both experimental and theoretical approaches. Real solar cells showed the rectifying behavior and photovoltaic effect after forward polarization only. Theoretical simulation indicated that the induced electric field due to the BaTiO₃ polarization could extend into the Si layer and then photon-generated carries in Si could be separated and collected for electricity generation. Adjusting relevant parameters such as dimension, materials and polarization charge density can optimize the electric field distribution for improving device performance. Although we have focused only on BaTiO₃ and Si, the concept introduced herein may be applied to other material systems because of its flexibility in material selection, device design and fabrication.

Acknowledgements

The authors acknowledge the financial support of the Seed Funding Programme for Basic Research at HKU (Project Code 201211159091), the HKU Initiative on Clean Energy & Environment (HKU-ICEE), and the University Development Fund (UDF) 2009-2010 (Second Round).



References

1. Nelson, J., *The physics of solar cells*. 2003: Imperial College Press.
2. Ji, W., K. Yao, and Y.C. Liang, *Bulk Photovoltaic Effect at Visible Wavelength in Epitaxial Ferroelectric BiFeO₃ Thin Films*. Advanced Materials, 2010. **22**(15): p. 1763-1766.
3. Cao, D.W., et al., *Polarization effect on the photocurrent of Pt sandwiched multi-crystalline ferroelectric films*. Materials Chemistry and Physics, 2011. **129**(3): p. 783-786.
4. Xu, J., et al., *Space charge effect on the photocurrent of Pt-sandwiched Pb(Zr0.20Ti0.80)O-3 film capacitors*. Journal of Applied Physics, 2009. **106**(11): p. 113705.
5. Qin, M., K. Yao, and Y.C. Liang, *High efficient photovoltaics in nanoscaled ferroelectric thin films*. Applied Physics Letters, 2008. **93**(12): p. 112904.
6. Yang, S.Y., et al., *Above-bandgap voltages from ferroelectric photovoltaic devices*. Nature Nanotechnology, 2010. **5**(2): p. 143-147.
7. Yao, K., et al., *Large photo-induced voltage in a ferroelectric thin film with in-plane polarization*. Applied Physics Letters, 2005. **87**(21): p. 212906.
8. Dawber, M., K.M. Rabe, and J.F. Scott, *Physics of thin-film ferroelectric oxides*. Reviews of Modern Physics, 2005. **77**(4): p. 1083-1130.
9. Kozuka, H., et al., *PVP-assisted sol-gel deposition of single layer ferroelectric thin films over submicron or micron in thickness*. Journal of the European Ceramic Society, 2004. **24**(6): p. 1585-1588.



10. Kozuka, H. and M. Kajimura, *Single-step dip coating of crack-free BaTiO₃ films > 1 μm thick: Effect of poly(vinylpyrrolidone) on critical thickness*. Journal of the American Ceramic Society, 2000. **83**(5): p. 1056-1062.
11. Choi, T., et al., *Switchable Ferroelectric Diode and Photovoltaic Effect in BiFeO₃*. Science, 2009. **324**(5923): p. 63-66.
12. Würfel, P., *Physics of Solar Cells: From Basic Principles to Advanced Concepts*. 2 ed. 2009: Wiley-VCH.
13. Tabib-Azar, M., N.S. Shoemaker, and S. Harris, *Non-destructive characterization of materials by evanescent microwaves*. Measurement Science and Technology, 1993. **4**(5): p. 583.
14. Kozuka, H. and A. Higuchi, *Stabilization of Poly(vinylpyrrolidone)-containing Alkoxide Solutions for Thick Sol-Gel Barium Titanate Films*. Journal of the American Ceramic Society, 2003. **86**(1): p. 33-38.
15. Shklyarevskii, I.N. and P.L. Pakhmov, *Separation of the contribution of free and bound electrons into real and imaginary parts of the dielectric constant of gold*. Optika i Spektroskopiya, 1973. **34**(1): p. 163-6.
16. Streetman, B. and S. Banerjee, *Solid State Electronic Devices*. 2000: Prentice Hall.
17. Qin, M., K. Yao, and Y.C. Liang, *Photovoltaic mechanisms in ferroelectric thin films with the effects of the electrodes and interfaces*. Applied Physics Letters, 2009. **95**(2): p. 022912.
18. Regan, W., et al., *Screening-Engineered Field-Effect Solar Cells*. Nano Letters, 2012. **12**(8): p. 4300-4304.



19. Yi, H.T., et al., *Mechanism of the Switchable Photovoltaic Effect in Ferroelectric BiFeO₃*. Advanced Materials, 2011. **23**(30): p. 3403-3407.



4. Effect of Electrodes on Non-PN Junction Based Ferroelectric-Semiconductor Solar Cells

In chapter 3 we have proved the feasibility of the novel non-PN junction based ferroelectric-semiconductor solar cells. In order to improve the device performance and investigate the unique charge separation mechanisms, in this chapter, we studied the effect of electrodes with different metal materials on the photovoltaic effect of the novel structure solar cells.

This part was adapted from a paper under review.

Wentao Wang, Fude Liu,^{a)} Chor Man Lau, Lei Wang, Guandong Yang, Dawei

Zheng

Department of Mechanical Engineering, The University of Hong Kong, Hong

Kong, China

Huanpo Ning

School of Engineering and Materials Science, Queen Mary University of London,

London E1 4NS, UK

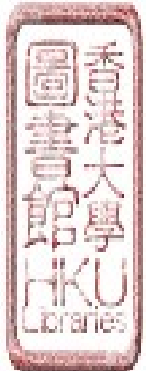
Zhuangchun Wu

School of Materials Science and Engineering, Nanjing University of Science and
Technology, Nanjing 210094, China



*Author to whom correspondence should be addressed. Tel.: (+852) 2859-2631.

FAX: 2858-5415. Electronic mail: fordliu@hku.hk. Department of Mechanical Engineering, The University of Hong Kong, Hong Kong, China.



Abstract

Conventional solar cells make use of the spatial variation in electronic environment due to junctions for carrier separation. We investigated a new type of solar cell that utilizes the bound surface charges of BaTiO₃ to separate charge carriers in silicon. Real solar cells showed dramatically enhanced photovoltaic effect in all cells with either symmetric Al electrodes or asymmetric electrodes (Al/Ti or Au/Ti electrodes) after forward polarization. Theoretical simulation indicated that the induced electric field due to the BaTiO₃ polarization could extend into the Si layer and then photon-generated carriers in Si could be separated and collected for electricity generation. The new cell structure is promising in terms of material selection, device design and fabrication.

Keywords: Photovoltaics, BaTiO₃, silicon, polarization, solar cells.



4.1 Introduction

One key step in photovoltaics is the charge carrier separation, i.e., free electron and holes are physically separated from each other once they are photon-generated in the absorber layer. In general, how to realize the carrier separation dictates the device structure. So far almost all solar cells have been essentially junction based: positive-negative (PN) junctions for inorganic cells, e^- -donor/ e^- -acceptor junctions for organic cells, or hybrid junctions for hybrid cells (for example, dye sensitized solar cells) [1]. From energy point of view, the three types of junctions actually function in a similar fashion, i.e., they provide the spatial variation in electronic environment for carrier separation. However, it is usually challenging to form a workable junction due to issues such as lattice mismatch, doping, and band alignment [2]. In principle, besides the junction-based structure, there ought to be other device structures for realizing carrier separation in solar cells. Ferroelectric material based photovoltaic cells have attracted a lot of interests recently [3-5]. An anomalous photovoltaic effect has been observed in a number of ferroelectric materials since 1960s [6]. A typical ferroelectric cell is of an electrode/ferroelectric/electrode sandwich structure [3, 7-15]. Because the ferroelectric cells make use of the ferroelectric remnant polarization field for carrier separation [16] a, carrier separation mechanism exists in these cells, and high open circuit voltage (V_{oc}) can be achieved [17, 18]. However, almost all ferroelectrics have large band gaps [19], which limits the sunlight absorption. It has been shown recently that a strong internal electric field



can be achieved for enhancing carrier separation by incorporating a ferroelectric polymer layer into organic solar cells [20]. One issue with this approach is that the ferroelectric layer has to be made extremely thin (a few monolayers) for charge carriers to tunnel through it. Therefore, it is worth exploring other possibilities for introducing ferroelectrics to solar cells.

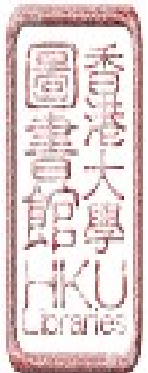
In this work, we investigated a new type of solar cells that combine a ferroelectric (BaTiO_3) and a semiconductor (Si). The cells avoid the traditional junction structure and utilize the bound surface charges of BaTiO_3 to separate the photon-generated charge carriers in Si. Three groups of solar cells with different electrode materials were tested to prove this concept. This unique structure can be adapted for other ferroelectric-semiconductor combinations in principle, and is promising in preparing novel solar cells because it provides us more flexibility in material selection, device design and fabrication.

4.2 Experimental

Three groups of solar cells with different metal contacts were prepared according to Fig. 1. As illustrated in Fig. 1a, a cell consists of a ferroelectric layer, a semiconductor layer, a pair of poling electrodes (*P*-electrodes), and a pair of anode and cathode. The *P*-electrodes patterns are aligned well with those of anode and cathode, respectively, with identical shadow masks during top and bottom electrodes preparation. Note that no electrodes are deposited at the interface between the semiconductor and ferroelectric to avoid possible screening effect

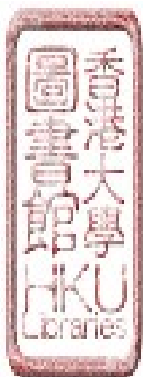


[21-23]. Anode and cathode collect photon-generated electrons and holes, respectively, in the semiconductor layer, under the influence of the external field due to ferroelectric polarizations; electrons then flow through the external circuit to do work on the load (R) and finally recombine with holes at the cathode to close the electron flow loop. Note that neighboring regions in the ferroelectric layer are polarized in opposite directions. When the ferroelectric is polarized as that shown in Fig. 1a, it is defined as forward polarization; if the polarization directions are reversed, it is called reverse polarization. The 3D view is shown in Fig. 1b. To fabricate a real cell, silicon and BaTiO_3 were chosen as the semiconductor absorber and ferroelectric layer, respectively. A 280- μm -thick *p*-type single crystalline Si wafer of $20 \times 20 \text{ mm}^2$ was cleaned with the RCA (= Radio Corporation of America) clean. BaTiO_3 was then spin coated on Si with the sol-gel method using a 0.40 M precursor solution based on $\text{Ba}(\text{CH}_3\text{COO})_2$, $\text{Ti}(\text{OC}_2\text{H}_5)_4$, polyvinylpyrrolidone (PVP)-360000, H_2O , CH_3COOH and $\text{C}_2\text{H}_5\text{OH}$ [24]. After each spin coating step, the cell was dried at 350°C for 10 minutes before proceeding to next step; the coating was repeated for several times until the thickness reached $\sim 500 \text{ nm}$. Then the cell was stepwise heated at 300, 500 and 700°C for 10, 10 and 15 minutes, respectively, to achieve full crystallization of BaTiO_3 [25]. We focused on three typical cells that were prepared following the above steps. For cell #1, Al was chosen for both anode and cathode (prepared with thermal evaporation); for cell #2, Ti and Al were for anode and cathode, respectively (prepared with sputtering and thermal evaporation, respectively); for



cell #3, Ti and Au were for anode and cathode, respectively (both were prepared with sputtering). For all cells, Ag was selected for *P*-electrodes and was deposited with thermal evaporation. Post annealing at 450°C for 15 minutes was then carried out to form good metal contacts. Finally, the cells were wired out with Ag paste and Al wire, and then the entire surface of the ferroelectric layer was covered with epoxy and glass for insulating.

The polarization was conducted at 180°C and subsequently at room temperature for 10 minutes, respectively. During the poling process, the silver *P*-electrodes were grounded, and +25V was applied on the cathode and -25V on the anode simultaneously. All current-voltage (I-V) measurements were carried out with a standard solar simulator (ABET Sun 2000 coupled with Keithley 2602A) by sweeping the voltage from the negative to positive. The BaTiO₃ layer was characterized with scanning electron microscopy (SEM) (Leo 1530), X-ray Diffraction (XRD) (Bruker D8 Advance), and hysteresis measurement (Radiant Precision LC). The distribution of the induced electric field in Si due to the bound surface charges of BaTiO₃ was simulated with the AC/DC Module of COMSOL®.



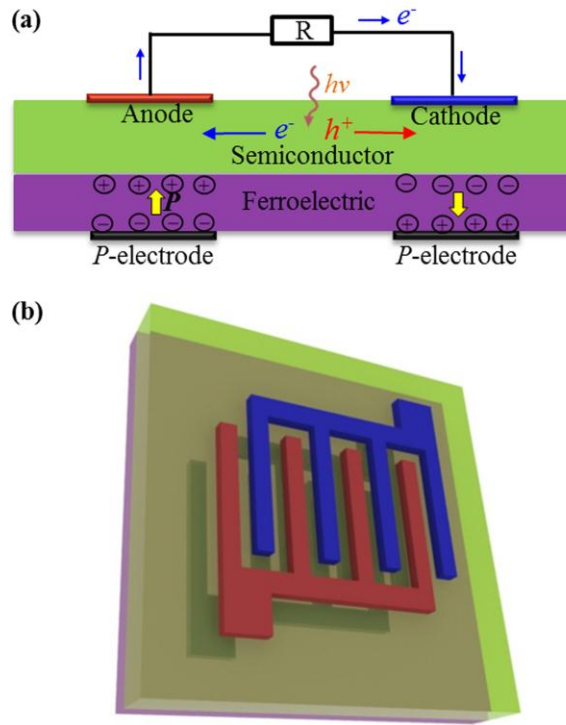


Fig. 1. Device structure and working principles. (a) Schematic of cross-sectional view. (b) Schematic of 3D view.

4.3 Results and discussion

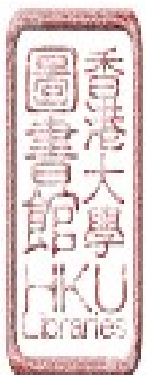
Fig. 2 depicts the electric characteristic of three cells before-polarization and after-polarization, respectively, under illumination condition. As to cell #1 with Al/Al contacts, there is almost no photovoltaic output before polarization (see the blue curve in Fig. 2a), which is expected because the device is symmetrical. After forward polarization, however, the current density-voltage (J-V) curve shifts downward (see the red curve in Fig. 2a), indicating the photovoltaic effect. So the driving force to separate electron-hole pairs in Si is due to BaTiO_3 polarization. For cell #2 with Ti/Al contacts, the J-V curve shifts downward



slightly before polarization (see the blue cure in Fig. 2b), and the shift is enhanced greatly after forward polarization (see the red cure in Fig. 2b). To cell #3, similar phenomena can be found as cell #2 (Fig. 3c). Table 1 summarizes the performance of the three cells under illumination before polarization and after forward polarization, respectively, in terms of V_{oc} and short-circuit current density (J_{sc}). As indicated by the improvement ratios in the brackets in Table 1, the asymmetric polarization of BaTiO₃ can greatly enhance the carrier separation in Si so that improved photovoltaic effect is achieved.

Table I. Performance summary of three cells.

Cell	Polarization status	V_{oc} (mV)	J_{sc} ($\mu\text{A}/\text{cm}^2$)
Cell #1 with Al/Al contacts	Before polarization	2.0	1.8
	After forward polarization	31.2	28.5
Cell #2 with Ti/Al contacts	Before polarization	19.1	3.3
	After forward polarization	54.3	16.8
Cell #3 with Ti/Au contacts	Before polarization	113.2	0.6
	After forward polarization	234.6	12.5



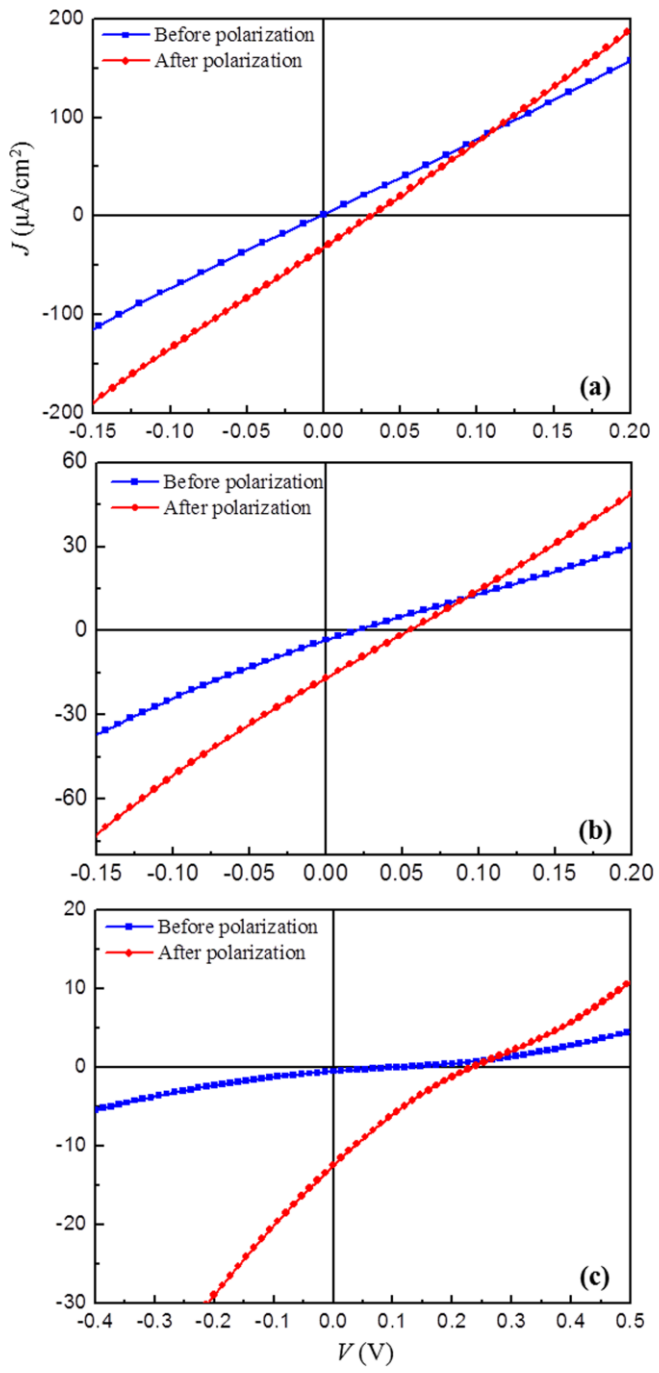
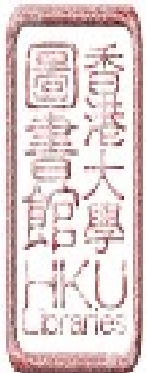
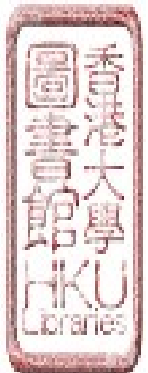


Fig. 2. J-V curves of three typical cells under illumination before polarization (blue curve) and after forward polarization (red curve), respectively. (a) Cell #1 with Al/Al contacts. (b) Cell #2 with Ti/Al contacts. (c) Cell #3 with Ti/Au contacts.



The above observations are consistent with the band diagram alignment between silicon and metal electrodes before contact (Fig. 3). The work function of Al, Ti and Au is 4.28, 4.33 and 5.1 eV, respectively [26]. Note that Al can heavily dope Si to form p^+ -Si after post annealing so that a tunneling junction is formed between Al and Si, and then the effective work function of Al is adjusted as indicated by the arrow in Fig. 3. Cell #1 has Al as both cathode and anode. So there is no photovoltaic effect before polarization because the device is symmetric. After polarization, however, the external electric field induced by the forward polarization of underlying BaTiO₃ will tilt the silicon band diagram, which is responsible for the photovoltaic effect in this cell [22]. In contrast, cell #2 (Al/Ti contacts) and cell #3 (Ti/Au contacts) have different metal contacts as anodes and cathodes. So even before polarization, slight photovoltaic effect was observed on the two cells; with forward polarization, the silicon band diagram can be further tilted to facilitate the carrier separation so that the photovoltaic effect can be enhanced.



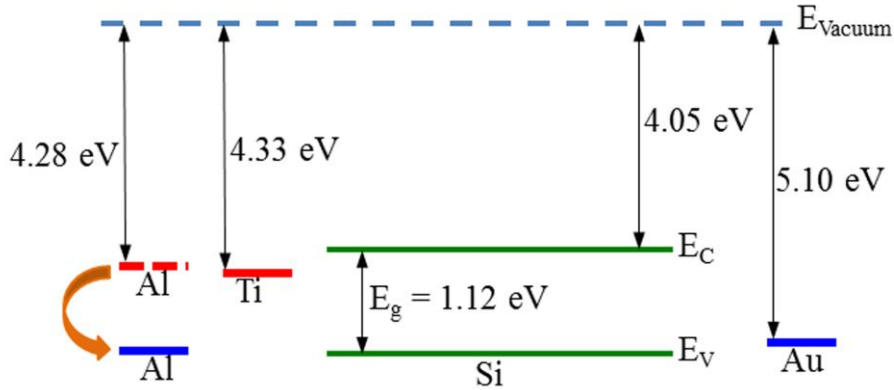


Fig. 3. Schematic of the energy-band diagram of silicon and the work function of each metal.

The device performance at present is still very poor compared with traditional solar cells. Besides other reasons such as poor metal contacts and non-optimized device geometry [22], one major reason is related to the low quality of BaTiO₃. Figs. 4a and 4b display the top-down and cross-sectional SEM images, respectively, of a polycrystalline BaTiO₃ layer spin coated on Si. The thickness of BaTiO₃ layer is around 500 nm and the average grain size is about 100 nm. In addition, the BaTiO₃ layer is porous, which indicates its poor material quality. The XRD pattern shown in Fig. 4c confirms that the BaTiO₃ layer is polycrystalline and possesses a tetragonal lattice structure that has lattice constants of $a = b = 0.3994$ nm and $c = 0.4038$ nm. The ferroelectric property of BaTiO₃ is characterized with the hysteresis loop (Fig. 4d); the remnant polarization is $0.243 \mu\text{C}/\text{cm}^2$ and the coercive electric field is 136.4 kV/cm, which are much smaller than those values reported for high quality BaTiO₃ [27].



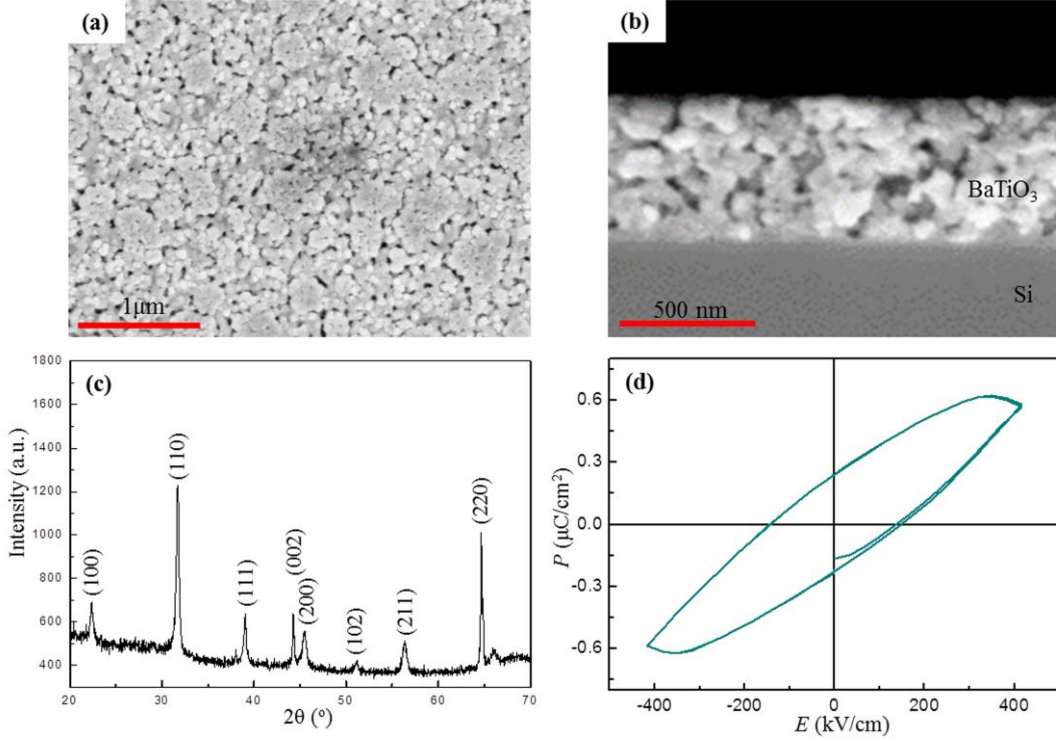
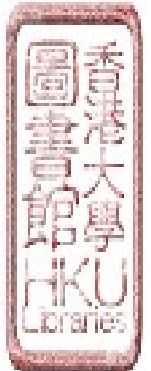


Fig. 4. Characterization of the BaTiO_3 layer. (a) SEM image (top-down view). (b) SEM image (cross-sectional view). (c) XRD spectrum. (d) Hysteresis loop.

We now know the crucial role played by the asymmetric polarization of BaTiO_3 in the device performance. To further understand this, it is necessary to know the distribution of the induced electric field in Si due to the bound surface charges along BaTiO_3/Si interface. We simulated the electric field distribution with the AC/DC module of COMSOL®. Fig. 5a represents the model setup whose geometry parameters are from real cells, where Au is chosen for all electrodes. The relative permittivity of Si, BaTiO_3 and Au is set to be 11.9 [28], 290 [29], and 6.9 [30], respectively. The bound surface charge density of $\pm 0.243 \mu\text{C}/\text{cm}^2$ (experimental value) is chosen for the polarized BaTiO_3 layer. The simulated electric field distribution in the Si layer is shown in Fig. 5b. Also included is the



electric field legend that is color-coded for easy viewing. It is obvious that the induced electric field extends into the Si layer. Overall, the electric field points toward the cathode and points away from the anode in the horizontal direction, as indicated by black arrows. Thus in general photon-generated electrons and holes would drift to the anode and cathode, respectively, under the influence of the induced electric field. The current flow direction is then consistent with our experimental results. Note that the overall electric field is in the order of 10^{-2} V/cm, which is several orders of magnitude weaker compared to that in a typical PN junction (in the order of $10^3 - 10^4$ V/cm) [31]. In addition, the electric field distribution in the Si layer is not uniform. In particular, the field is relatively stronger directly above the region (in red) near the Si/ BaTiO₃ interfaces and is relatively weaker in regions (in blue) between cathode and anode. The weak and non-uniform electric field contributes to poor device performance. The device performance may be improved through geometry optimization and material quality improvement [1].



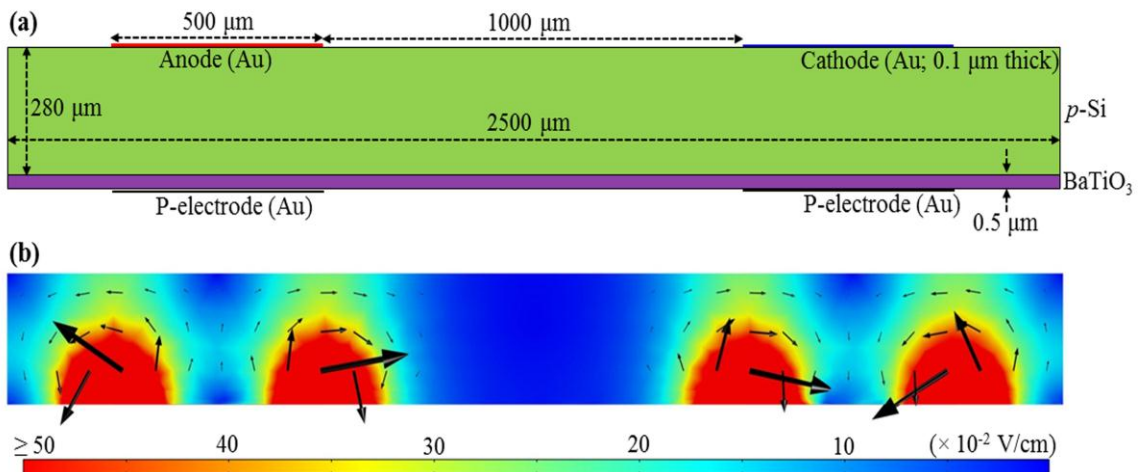
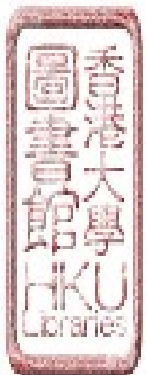


Fig. 5. Simulation of the electric field distribution in the real device. (a) Model geometry. (b) Electric field distribution in the device. Also included is the electric field legend that is color coded.

4.4 Conclusions

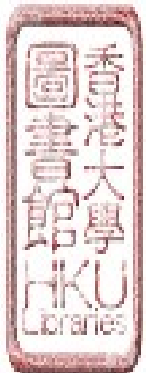
In summary, we investigated a new device structure for photovoltaics in detail with both experimental and theoretical approaches. Real solar cells showed enhanced photovoltaic effect in all cells with either symmetric Al electrodes or asymmetric electrodes (Al/Ti or Au/Ti electrodes). Theoretical simulation indicated that the induced electric field due to the BaTiO₃ polarization could extend into the Si layer and then photon-generated carriers in Si could be separated and collected for electricity generation. It is expected that the device performance can be improved through geometry optimization and material quality improvement. Although we have focused only on BaTiO₃ and Si, the concept introduced herein may be applied to other ferroelectric-semiconductor systems



because of its flexibility in material selection, device design and fabrication.

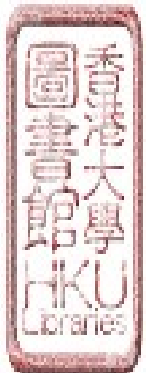
Acknowledgements

The authors acknowledge the financial support of the Seed Funding Programme for Basic Research at HKU (Project Code 201211159091), the HKU Initiative on Clean Energy & Environment (HKU-ICEE), and the University Development Fund (UDF) 2009-2010 (Second Round). Also, great thanks go to Xiaochen Ren at HKU for helping with the device 3D drawing.



References

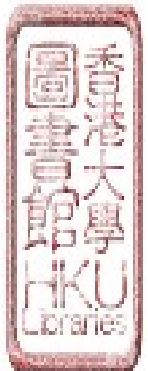
1. Liu, F., et al., *Working principles of solar and other energy conversion cells*. Nanomaterials and Energy, 2012. **2**(1): p. 3 –10.
2. Nelson, J., *The Physics of Solar Cells*. 2003: Imperial College Press.
3. Ji, W., K. Yao, and Y.C. Liang, *Bulk Photovoltaic Effect at Visible Wavelength in Epitaxial Ferroelectric BiFeO₃ Thin Films*. Advanced Materials, 2010. **22**(15): p. 1763-1766.
4. Cao, D.W., et al., *Polarization effect on the photocurrent of Pt sandwiched multi-crystalline ferroelectric films*. Materials Chemistry and Physics, 2011. **129**(3): p. 783-786.
5. Xu, J., et al., *Space charge effect on the photocurrent of Pt-sandwiched Pb(Zr0.20Ti0.80)O-3 film capacitors*. Journal of Applied Physics, 2009. **106**(11): p. 113705.
6. Fridkin, V.M., *Bulk photovoltaic effect in noncentrosymmetric crystals*. Crystallography Reports, 2001. **46**(4): p. 654-658.
7. Qin, M., K. Yao, and Y.C. Liang, *Photovoltaic characteristics in polycrystalline and epitaxial (Pb0.97La0.03)(Zr0.52Ti0.48)O-3 ferroelectric thin films sandwiched between different top and bottom electrodes*. Journal of Applied Physics, 2009. **105**(6): p. 061624.
8. Zang, Y.Y., et al., *Enhanced photovoltaic properties in graphene/polycrystalline BiFeO₃/Pt heterojunction structure*. Applied Physics Letters, 2011. **99**(13): p. 132904.



9. Harshan, V.N. and S. Kotru, *Influence of work-function of top electrodes on the photovoltaic characteristics of Pb_{0.95}La_{0.05}Zr_{0.54}Ti_{0.46}O₃ thin film capacitors*. Applied Physics Letters, 2012. **100**(17): p. 173901.
10. Qin, M., et al., *Thickness effects on photoinduced current in ferroelectric (Pb_{0.97}La_{0.03})(Zr_{0.52}Ti_{0.48})O₃ thin films*. Journal of Applied Physics, 2009. **105**(12): p. 014104.
11. Cao, D.W., et al., *High-Efficiency Ferroelectric-Film Solar Cells with an n-type Cu₂O Cathode Buffer Layer*. Nano Letters, 2012. **12**(6): p. 2803-2809.
12. Cao, D.W., et al., *Understanding the nature of remnant polarization enhancement, coercive voltage offset and time-dependent photocurrent in ferroelectric films irradiated by ultraviolet light*. Journal of Materials Chemistry, 2012. **22**(25): p. 12592-12598.
13. Qin, M., K. Yao, and Y.C. Liang, *Photovoltaic mechanisms in ferroelectric thin films with the effects of the electrodes and interfaces*. Applied Physics Letters, 2009. **95**(2): p. 022912.
14. Zhang, J.J., et al., *Enlarging photovoltaic effect: combination of classic photoelectric and ferroelectric photovoltaic effects*. Scientific Reports, 2013. **3**: p. 2109.
15. Cao, D.W., et al., *Interface layer thickness effect on the photocurrent of Pt sandwiched polycrystalline ferroelectric Pb(Zr, Ti)O₃ films*. Applied Physics Letters, 2010. **97**(10): p. 102104.



16. Qin, M., K. Yao, and Y.C. Liang, *High efficient photovoltaics in nanoscaled ferroelectric thin films*. Applied Physics Letters, 2008. **93**(12): p. 112904.
17. Yang, S.Y., et al., *Above-bandgap voltages from ferroelectric photovoltaic devices*. Nature Nanotechnology, 2010. **5**(2): p. 143-147.
18. Yao, K., et al., *Large photo-induced voltage in a ferroelectric thin film with in-plane polarization*. Applied Physics Letters, 2005. **87**(21): p. 212906.
19. Dawber, M., K.M. Rabe, and J.F. Scott, *Physics of thin-film ferroelectric oxides*. Reviews of Modern Physics, 2005. **77**(4): p. 1083-1130.
20. Yuan, Y., et al., *Efficiency enhancement in organic solar cells with ferroelectric polymers*. Nature Materials, 2011. **10**: p. 296 - 302.
21. Zhuravlev, M.Y., et al., *Giant Electroresistance in Ferroelectric Tunnel Junctions*. PRL, 2005. **94**: p. 246802.
22. Liu, F., et al., *Ferroelectric-semiconductor photovoltaics: Non-PN junction solar cells*. Appl. Phys. Lett., 2014. **104**: p. 103907.
23. Wang, W., et al., *Field-effect BaTiO₃-Si solar cells*. Appl. Phys. Lett., 2014. **104**: p. 123901.
24. Kozuka, H., et al., *PVP-assisted sol-gel deposition of single layer ferroelectric thin films over submicron or micron in thickness*. Journal of the European Ceramic Society, 2004. **24**(6): p. 1585-1588.
25. Kozuka, H. and M. Kajimura, *Single-step dip coating of crack-free*



- BaTiO₃ films > 1 μm thick: Effect of poly(vinylpyrrolidone) on critical thickness.* Journal of the American Ceramic Society, 2000. **83**(5): p. 1056-1062.
26. Michaelson, H.B., *Work Function of Elements and Its Periodicity*. Journal of Applied Physics, 1977. **48**(11): p. 4729-4733.
27. Ertug, B., *The Overview of The Electrical Properties of Barium Titanate*. American Journal of Engineering Research, 2013. **02**(08): p. 01-07.
28. Tabib-Azar, M., N.S. Shoemaker, and S. Harris, *Non-destructive characterization of materials by evanescent microwaves*. Measurement Science and Technology, 1993. **4**(5): p. 583.
29. Kozuka, H. and A. Higuchi, *Stabilization of poly(vinylpyrrolidone)-containing alkoxide solutions for thick sol-gel barium titanate films*. Journal of the American Ceramic Society, 2003. **86**(1): p. 33-38.
30. Shklyarevskii, I.N. and P.L. Pakhmov, *Separation of the contribution of free and bound electrons into real and imaginary parts of the dielectric constant of gold*. Optika i Spektroskopiya, 1973. **34**(1): p. 163-6.
31. Streetman, B. and S. Banerjee, *Solid State Electronic Devices*. 5th ed. ed. 2000: Prentice Hall.



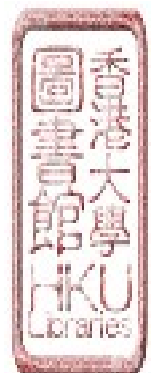
5. Effect of Absorber Layer Thickness and Device Dimension on Non-PN Junction Based Ferroelectric-Semiconductor Solar Cells

In chapter 3 we have studied the concept of the novel non-PN junction based ferroelectric-semiconductor solar cells. The simulation indicated that the device performance can be improved by adjusting dimension parameters. In this chapter, we investigated the factors of semiconductor layer thickness and device dimension for further optimizing the non-PN junction based ferroelectric-semiconductor solar cells design. These approaches are to enhance the charge separation in the absorber layer as well as the device performance.

This part was adapted from a paper under review.

Wentao Wang, Fude Liu,^{a)} Chor Man Lau, Lei Wang, Guandong Yang, Dawei Zheng
Department of Mechanical Engineering, The University of Hong Kong, Hong Kong,
China

*Author to whom correspondence should be addressed. Tel.: (+852) 2859-2631. FAX: 2858-5415. Electronic mail: fordliu@hku.hk. Department of Mechanical Engineering, The University of Hong Kong, Hong Kong, China.



Abstract

We investigated novel non-PN junction BaTiO₃-Si solar cells that utilize the bound surface charges of BaTiO₃ to separate photon generated electron-hole pairs in silicon. The cell structure was optimized through decreasing interdigital electrode space length and silicon thickness to realize manipulation of the polarization induced electric field strength and distribution. In addition, the electrode structure was carefully designed to avoid screening effect. The cells showed switchable diode behavior through controlling polarization direction and exhibited significant improved photovoltaic properties comparing with the previous version, which was attributing to the effective charge carriers separation and collection in silicon drifted by BaTiO₃ polarization. The cells are promising in terms of material selection, device design, and fabrication.

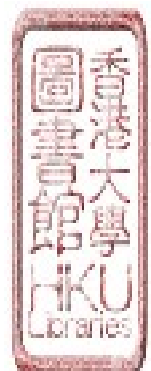
Keywords: Photovoltaics, BaTiO₃, silicon, polarization, solar cells.



5.1 Introduction

Ferroelectric materials have been intensely investigated for photovoltaic (PV) applications [1-5]. Recently we described electronic modulation of a novel type of non-PN junction ferroelectric-semiconductor solar cells [6, 7]. By exploiting asymmetric polarization on ferroelectric film, the light induced charge carrier separation was achieved in the semiconductor layer. We applied BaTiO₃ and silicon to demonstrate this new concept and successfully obtained rectifying behavior and photovoltaic effect. The new cells are unique in that free charge carriers and fixed charge carriers are physically separated from each other. The feature allows us to go beyond traditional junction-based structures and have more freedom in material selection, device design and fabrication.

Nevertheless, the photovoltaic properties haven't optimized yet, which is mainly due to the long electrode space length (1000μm) and large semiconductor thickness (280μm), hence weaken the polarization induced electric field strength and distribution uniformity. Furthermore, the metal electrodes placed in the BaTiO₃/Si interface potentially result in a screening effect. Although this issue can be addressed by using high dielectric constant materials as contacts, such as LMSO, Nb: STO [8]. However, material selection is therefore limited for commercialization. This is demonstrated in the non-PN junction BaTiO₃-Si solar cells with upgraded structure. First of all, we construct the device by incorporating the metal electrodes on the top side of silicon, avoiding the as mentioned screening effect issue. In addition, the cell geometry is optimized through decreasing the interdigital electrode space length and Si thickness, yielding a significant improvement of photovoltaic performance. Fig. 1



schematically shows this device structure and working principle. The central components are the BaTiO₃ ferroelectric layer for generating polarization field and the silicon base to absorb sunlight. Rather than depositing metal electrodes in the BaTiO₃/Si interface [7], Ag anode and Al cathode are placed on the top of silicon surface for charge carriers collection, which avoids the screening effect. The poling electrodes (P-electrodes) are formed on the rear side of BaTiO₃ film for applying external polarization voltage. The P-electrodes patterns are aligned well with those of anode and cathode, respectively. The critical step is to polarize neighboring regions in the BaTiO₃ ferroelectric layer in opposite directions (asymmetric polarization) such that negative and positive bound surface charges are accumulated to different BaTiO₃/Si interface areas in a fashion as shown in the figure. Under such the influence of the electric field due to ferroelectric asymmetric polarizations, photon generated electrons-hole pairs in the silicon absorber separately drift to anode and cathode, respectively, and then complete the external circuit.

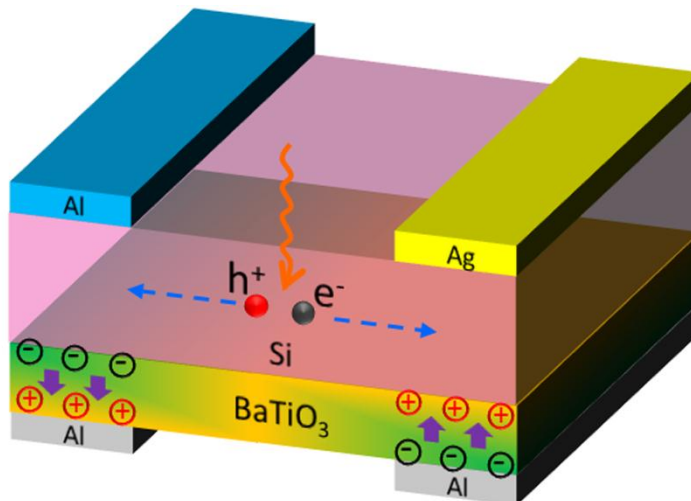
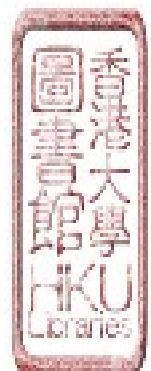
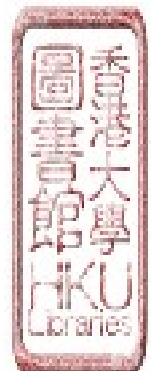


Fig. 1. Schematic of device structure and working principle.



5.2 Experimental

P-type single crystalline Si wafer was etched from thickness of 280 μm to 50 μm by KOH with 50% concentration (wt. %) at 90°C for 5 hours. Then the thin wafer was cut to desired size and cleaned with the RCA (= Radio Corporation of America) clean. BaTiO₃ was then spin coated on Si with the sol-gel method using a precursor solution (0.40 mol/L) based on Ba(CH₃COO)₂, Ti(OC₂H₅)₄, polyvinylpyrrolidone (PVP)-360000, H₂O, CH₃COOH and C₂H₅OH [9]. After each spin coating step, the sample was dried at 350°C for 10 minutes before proceeding to next step; the coating may be repeated several times depending on the film thickness required. Then, the sample was stepwise heated at 300°C and 500°C for 10 minutes, respectively, and finally at 700°C for 15 minutes to achieve full crystallization of BaTiO₃ [10]. Ag and Al were chosen for anode and cathode, respectively, on top of silicon, and P-electrodes of Al were formed on BaTiO₃ surface. All the metal contacts were deposited by thermal evaporation method using a shadow mask. Post annealing at 450°C for 15 minutes was then conducted for co-firing process. Finally, the sample was wired out with Ag paste and metal wire, and was then packaged with epoxy and glass for insulating. The polarization was conducted at 180°C (above BaTiO₃ cure temperature) at first and then at room temperature for 10 minutes, respectively. During the poling process, the P-electrodes were grounded, and +18V was applied on the Al cathode and -18V on the Ag anode simultaneously, which is defined as forward polarization; it is called reverse polarization when the external poling voltage are swapped between anode and cathode. The electrical characterization was carried out with a standard solar simulator (ABET Sun 2000 coupled with Keithley 2602A).

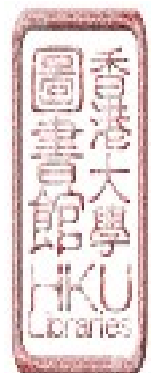


All current density-voltage (J-V) measurements were conducted by sweeping the voltage from the negative to positive.

5.3 Results and discussion

The key of implement effective field-effects in the device is careful control of polarization generated electric field strength and distribution. Our previous theoretical study unveiled the geometry, especially the electrode space length (like the channel length in transistor) and semiconductor thickness, plays a crucial role on the device performance. It was estimated that the device with 50 μm electrode space length and 50 μm silicon thickness would obtain optimized electric field distribution. Nevertheless, the fine electrode space length has high requirements on electrode fabrication and polarization processes, increasing processing complexity as well as product price. We therefore chose 300 μm electrode space length to balance the device performance and fabrication feasibility.

In order to evaluate the native electrostatics situation, we have modeled the device through finite-element method (COMSOL), as indicated in Fig. 2a. We built this model with 150 μm Si to mainly study the correlation between semiconductor thickness and electric field distribution, and therefore to determine the appropriate Si thickness for real cell fabrication. We chose Au as all the contacts to simplify the model. The relative permittivity we applied to Si, BaTiO₃ and Au are 11.9 [11], 290 [12] and 6.9 [13], respectively. To realize BaTiO₃ film polarization condition, the positive and negative bound surface charges were selectively loaded on the specific Si/BaTiO₃ interface fractions as indicated in Fig. 1, with charge density of $\pm 0.1\text{C/cm}^2$



(typical value). The simulated electric field strength distribution in the Si layer is shown in Fig. 2b. Also included is the electric field legend that is color-coded for easy viewing. It is obvious that the induced electric field extends into the Si layer and overall yield a field strength ingredient along the depth direction. In particular, the field is relatively stronger in regions (in green) near the BaTiO₃ layer and is relatively weaker close to the electrodes (in red). We design the device with expectation to obtain uniform electric field distribution with appropriate field strength. Note that within 50 μm depth from the BaTiO₃ surface (above light red zone), the electric field strength is overall over the order of 10³ V/cm, which is comparable to that in a typical PN junction (in the order of 10³ – 10⁴ V/cm) [14]. Consequently, we see that the electric field penetration depth in device is related to the Si thickness. Herein control of the silicon layer thickness is effective factor to make good use of the polarization induced electric field. We then select 50 μm thick silicon wafer for real device study.



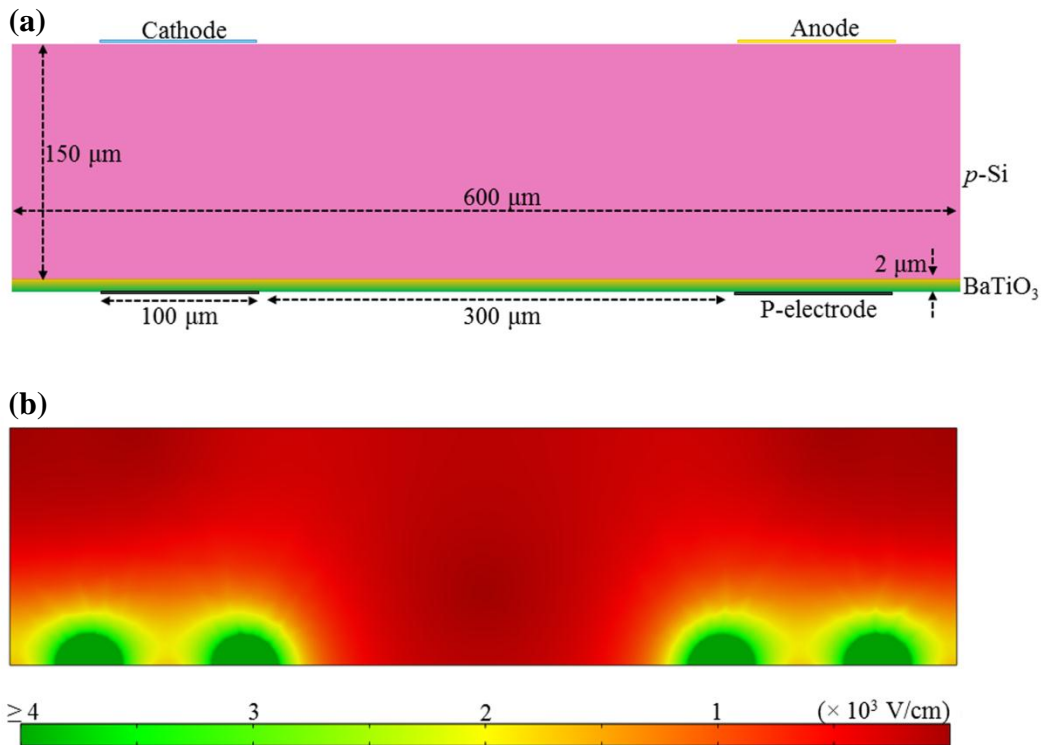


Fig. 2. Simulation of the electric field distribution in the device. (a) Model geometry. (b) Electric field distribution in the device. Also included is the electric field legend that is color coded.

Based on the simulation result, we turn to real devices fabrication and characterization. Fig. 3a depicts the cell current density versus voltage characteristic at before-polarization, forward-polarization and reverse-polarization states, respectively, under dark condition. The device performance strongly depends on the way of poling on the ferroelectric.



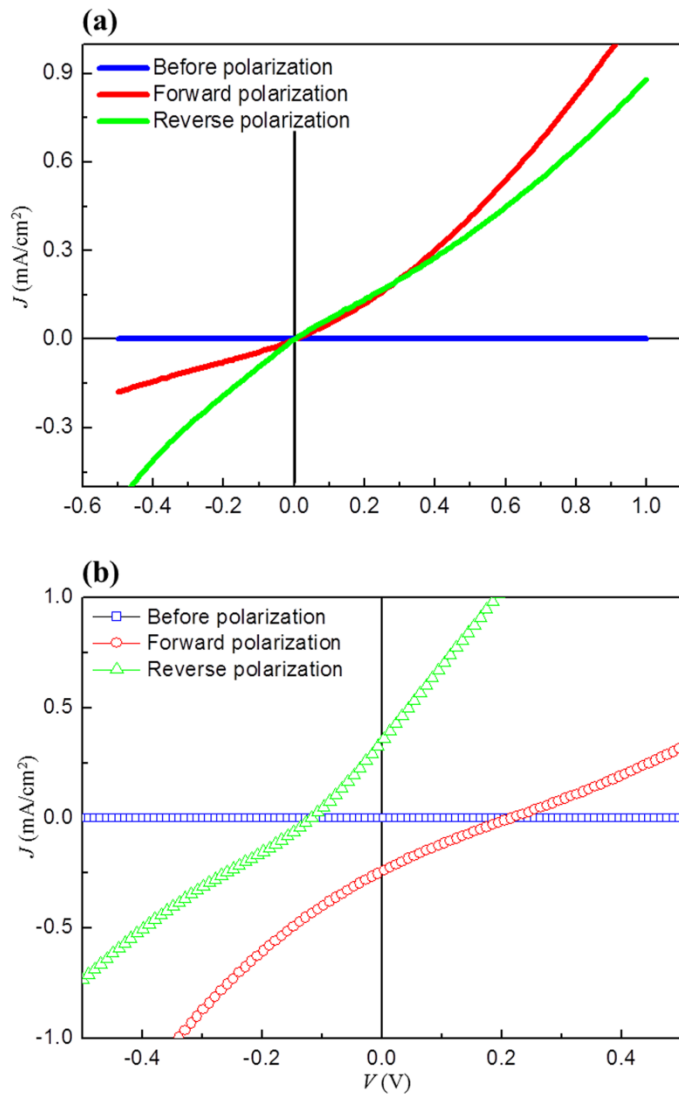
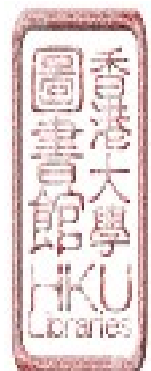


Fig. 3. J-V curves of the device at before-polarization, forward-polarization and reverse-polarization states, respectively. (a) Under dark condition. (b) Under illumination condition.

Before polarization, the J-V curve is a straight line with high resistivity. After forward polarization, the conduction shows a diode like behavior with the rectification ratio of ~ 2.4 at $V = \pm 0.5$ V. While this rectifying J-V curve switch the

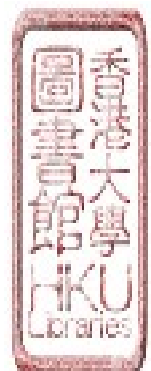


polarity after the reverse polarization, also showing smaller rectification ratio (1.5 at ± 0.5 V). According to the polarity of the J-V characteristic, we infer the net electric field has an overall direction towards from Ag anode to Al cathode after forward polarization, while switch the direction when reverse polarized. It is evidenced that the polarization of BaTiO₃ controls the charge carrier transport properties of Si, which would in principle affect the device photovoltaic properties. Fig. 3b shows illuminated J-V characterization of device under the three polarization conditions (before, forward and reverse polarizations). Before polarization, there isn't photovoltaic output for the as fabricated device, while it shows photovoltaic properties for both forward and reverse polarization states. The forward polarization J-V curve exhibits V_{oc} of 0.215 V, J_{sc} of 0.238 mA/cm², and power conversion efficiency of 0.012%. While the reverse polarized cell generates power output with V_{oc} of 0.117 V, and J_{sc} of 0.359 mA/cm². This result further demonstrates the validity of this new type of non-PN junction solar cell, which is mainly attribute to the effective photo induced charge carrier separation in silicon by ferroelectric BaTiO₃ polarization. Compare with the result of the previous device version [7], this upgraded device shows significant enhanced photovoltaic properties through optimizing the device structure. We also notice that the forward polarized J-V curve shifts downward passing through the forth quadrant, while it shifts upward to the second quadrant after reverse polarization. The switchable electric properties prove that the poling method can determine the photocurrent direction. These negative and positive photo currents directions are consistent with the net polarization induced electric field directions, as indicated by dark J-V characteristic.



In order to understand this phenomenon, we study the effect of the polarization on the energy band diagram of silicon for explanation. For this cell, Ag and Al were selected as the contact electrodes, and the work function are 4.26 and 4.28, respectively [15]. It should be noted Al can actually dope Si to form P+-Si after post annealing process so that the true Al work function is therefore increased. The Fermi level equilibrium of the p type silicon with Al and Ag electrodes generates depletion layers and band bending in the silicon with a net electric field towards from Ag to Al. Therefore Al and Ag work as cathode and anode, respectively, for the as fabricated device. Under illumination, photon absorbed in silicon excites the electron from valence band to conduction band, leaving holes there. Drifted by the net build in potential, the electron-hole pairs separate flowing to the oppositely and collected by Ag/Al electrodes.

After poling the ferroelectric polarization bound surface charge would play the role of dopant, therefore shift the Fermi level. Fig. 4 schematically shows the energy band diagrams of the device under the two diverse polarization conditions. As indicated in Fig. 4a, the ferroelectric forward polarization positively charges the silicon around Ag side and negatively charges the one near Al side. For P-type silicon, $E_i - E_f = k_B T \ln (N_a / n_i)$, where, E_i stands for intrinsic potential energy, E_f Fermi level, N_a doping density, n_i intrinsic carrier density, and $k_B T$ the internal energy [16]. Consequently, the Fermi level shifts upward (downward) in silicon near the Al (Ag) electrode. In order to reach the Fermi level equilibrium state, the conduction band and valence band tilt from Al cathode to Ag anode, which enhance the net build electric field. The photon induced electron- hole pairs would then drift to the opposite



electrodes, and realize the charge separation. Similarly, strong reverse polarization oppositely tilts the band and switch charge carrier flow direction, i.e. the electrons drift to Al while holes move to Ag, as indicated in Fig. 4b.

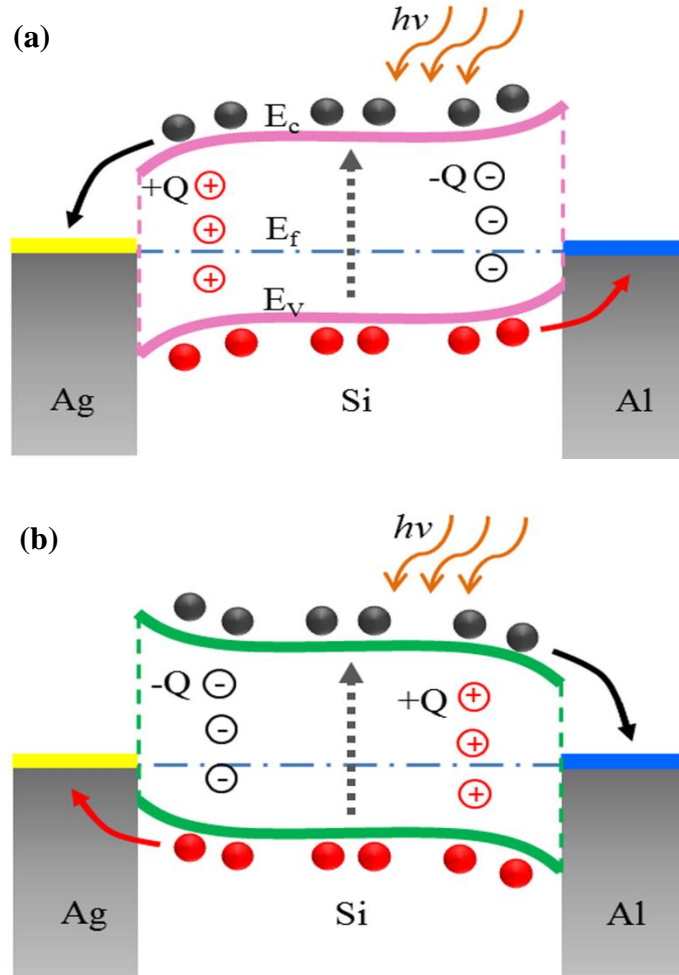
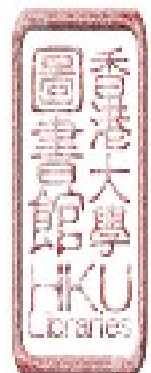


Fig. 4. Schematic of Ag/Si/Al energy band diagrams at different polarization states.

(a) Forward polarization. (b) Reverse polarization.

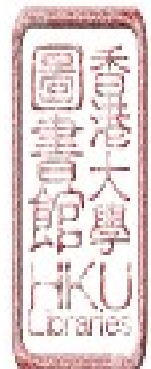
This model mainly focuses on the effect arising from the ferroelectric polarization. Actually, the potential difference result from metal electrodes would



also contribute to the net electric field. We now quantifiably identify the contribution from ferroelectric polarization and work function difference. For the forward polarized photo current density, $J_{\text{forward}} = J_w + J_p$, where, J_w is due to the work function difference, and J_p is attribute to the ferroelectric polarization. The reverse polarized $J_{\text{reverse}} = J_w - J_p$. Then we get $J_w = (J_{\text{forward}} + J_{\text{reverse}}) / 2$, and $J_p = (J_{\text{forward}} - J_{\text{reverse}}) / 2$, which are 0.061 and 0.299 mA/cm², respectively. We see that the ferroelectric polarization plays the major role on photo current, due to the effective charge carrier separation.

5.4 Conclusions

In summary, we investigated the upgraded version of novel non-PN junction BaTiO₃-Si solar cells experimentally and theoretically. The simulation results indicated that decreasing interdigital electrodes space length and silicon thickness were effective to optimize polarization induced electric field strength and distribution. We constructed the device with 300μm electrodes space length and 50μm silicon thickness. In addition, the electrode structure was carefully designed to avoid screening effect. The cells showed switchable diode behavior through controlling polarization direction and exhibited significant enhanced photovoltaic properties comparing with the previous one, which was attributing to the effective photon-generated charge separation in silicon drifted by BaTiO₃ polarization. Although we have focused only on BaTiO₃ and Si, the concept introduced herein may be applied to other material systems because of its flexibility in material selection, device design, and fabrication.



Acknowledgements

The authors acknowledge the financial support of the Seed Funding Programme for Basic Research at HKU (Project Code 201211159091), the HKU Initiative on Clean Energy & Environment (HKU-ICEE), and the University Development Fund (UDF) 2009-2010 (Second Round).



References

1. Zang, Y.Y., et al., *Investigation of the improved performance in a graphene/polycrystalline BiFeO₃/Pt photovoltaic heterojunction: Experiment, modeling, and application*. Journal of Applied Physics, 2012. **112**(5): p. 054103.
2. Li, H., et al., *Ultraviolet photovoltaic effect in BiFeO₃/Nb-SrTiO₃ heterostructure*. Journal of Applied Physics, 2012. **112**(8): p. 083506.
3. Dong, H.F., et al., *Improving the optical absorption of BiFeO₃ for photovoltaic applications via uniaxial compression or biaxial tension*. Applied Physics Letters, 2013. **102**(7): p. 072905.
4. Huang, F. and X.X. Liu, *A ferroelectric-semiconductor-coupled solar cell with tunable photovoltage*. Applied Physics Letters, 2013. **102**(10): p. 103501.
5. Zhang, J.J., et al., *Enlarging photovoltaic effect: combination of classic photoelectric and ferroelectric photovoltaic effects*. Scientific Reports, 2013. **3**: p. 2109.
6. Liu, F.D., et al., *Ferroelectric-semiconductor photovoltaics: Non-PN junction solar cells*. Applied Physics Letters, 2014. **104**(10): p. 103907.
7. Wang, W., et al., *Field-effect BaTiO₃-Si solar cells*. Applied Physics Letters, 2014. **104**(12): p. 123901.
8. Qin, M., K. Yao, and Y.C. Liang, *Photovoltaic mechanisms in ferroelectric thin films with the effects of the electrodes and interfaces*. Applied Physics Letters, 2009. **95**(2): p. 022912.



9. Kozuka, H., et al., *PVP-assisted sol-gel deposition of single layer ferroelectric thin films over submicron or micron in thickness*. Journal of the European Ceramic Society, 2004. **24**(6): p. 1585-1588.
10. Kozuka, H. and M. Kajimura, *Single-step dip coating of crack-free BaTiO₃ films > 1 μm thick: Effect of poly(vinylpyrrolidone) on critical thickness*. Journal of the American Ceramic Society, 2000. **83**(5): p. 1056-1062.
11. Tabib-Azar, M., N.S. Shoemaker, and S. Harris, *Non-destructive characterization of materials by evanescent microwaves*. Measurement Science and Technology, 1993. **4**(5): p. 583.
12. Kozuka, H. and A. Higuchi, *Stabilization of Poly(vinylpyrrolidone)-containing Alkoxide Solutions for Thick Sol-Gel Barium Titanate Films*. Journal of the American Ceramic Society, 2003. **86**(1): p. 33-38.
13. Shklyarevskii, I.N. and P.L. Pakhmov, *Separation of the contribution of free and bound electrons into real and imaginary parts of the dielectric constant of gold*. Optika i Spektroskopiya, 1973. **34**(1): p. 163.
14. Streetman, B. and S. Banerjee, *Solid State Electronic Devices*. 2000: Prentice Hall.
15. Michaelson, H.B., *Work Function of Elements and Its Periodicity*. Journal of Applied Physics, 1977. **48**(11): p. 4729-4733.
16. Nelson, J., *The physics of solar cells*. 2003: Imperial College Press.



6. Preliminary Passivation Study for Non-PN Junction Based Ferroelectric-Semiconductor Solar Cells: Passivating Silicon Grain Boundaries with Small Polar Molecules

In chapter 3-5 we have investigated the concept of ferroelectric-semiconductor solar cells and the effect of key parameters on charge separation. As a crucial component, semiconductor material quality is related to the charge transport properties of cell. Polycrystalline thin film semiconductor materials have great potential for application but are limited to the grain boundary effect. In this chapter, we did preliminary work on grain boundary passivation with small polar molecules. To make things easier, we worked on large grained mc-Si wafers and passivated the grain boundaries with small molecules. The ultimate purpose is to apply these findings to passivate the absorber layer in the ferroelectric-semiconductor solar cells.

This part was adapted from a paper under review.

Wentao Wang ^a, Fude Liu ^{a*}, Lei Wang ^a, Guandong Yang ^a, W.C.H. Choy ^b,
F. Yan^c, S. Johnston^c, M.M. Al-Jassim^c

^aDepartment of Mechanical Engineering, The University of Hong Kong, Hong Kong, China

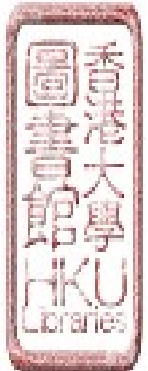
^bDepartment of Electrical and Electronic Engineering, The University of Hong Kong, Hong Kong, China



^cNational Center for Photovoltaics, National Renewable Energy Laboratory,
Golden, CO 80401, USA

^{*}Author to whom correspondence should be addressed. Tel.: (+852) 2859-2631.

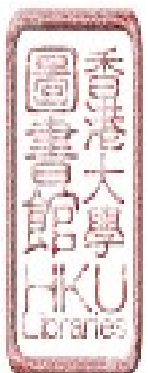
FAX: 2858-5415. Electronic mail: fordliu@hku.hk. Department of Mechanical
Engineering, The University of Hong Kong, Hong Kong, China



Abstract

Grain boundaries (GBs) play a major role in determining the device performance of in particular polycrystalline thin-film solar cells. Hydrogen has traditionally been applied to passivate defects at GBs. However, hydrogenated films are subject to light-induced degradation effects. In this study, we took a novel approach to passivating GBs in multicrystalline silicon (mc-Si) wafers with small polar molecules. We found an excellent correlation between the grain misorientation, electrical resistance across GBs, and passivation effectiveness. In particular, the charge transport across GBs was greatly enhanced after the wafers were properly treated in our polar molecule solutions; the sheet resistance can be reduced by more than one order for large-angle random GBs. The results were explained to be due to the effective charge neutralization and passivation of polar molecules on localized charge states at GBs. These findings may help us achieve high-quality materials at low cost for high-efficiency solar cells by enhancing carrier transport and minimizing carrier recombination.

Keywords: Passivation; Photovoltaics; Polar molecules; Grain boundaries; Silicon



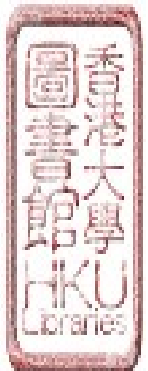
6.1 Introduction

The performance of the novel ferroelectric-semiconductor photovoltaic cell also depends on the charge carrier transport property, which is correlated to the semiconductor quality. Silicon is the workhorse material of the photovoltaics industry, and the multicrystalline and thin-film polycrystalline silicon (*poly-Si*) with grain size in the range of 1 μm to 1 mm is considered a promising candidates because of their potential for low cost among other benefits [1-3]. However, grain boundaries (GBs) are a significant concern because they play a major role in determining the device performance of these polycrystalline thin-film solar cells [4-6]. The high density defects in GBs act as recombination centers to trap the minority flow carriers. To minimize the effect of GBs, the key is to either eliminate them or eliminate their electrical activity [7]. The latter approach of GB passivation is considered to be more feasible and economical. Hydrogen has traditionally been applied to passivate the defects at GBs. It was first studied through introducing hydrogen plasma in bulk *poly-Si* GBs, and effectively reduced GB in-gap states and potential barrier [8]. Extensive studies on hydrogenation technique as well as mechanisms behind were conducted on thin film *poly-Si*, *mc-Si* [5, 9-14]. However, hydrogenated films are subject to the low thermal stability [15, 16]. Furthermore, excessive hydrogenation leads to new defect creation and results in the increase of GB electrical activity in *poly-Si* [17, 18]. Alternative passivation agents are therefore developed. Molecules with polarity such as NH_3 , and H_2O were observed to eliminate the GB trap states in



poly Si [7, 19]. However, the gas diffusion treatment at high temperature is expensive to maintain. A feasible solution can instead by chemical passivation method. For example, immersing hydrogen terminated silicon substrate in quinhydrone-methanol solution can obtain surface passivation effect and higher minority carrier lifetime [20, 21].

In this study, we suggest a novel approach using small polar molecules (methanol, acetonitrile, formic acid, and new ZK-series mixed solutions) by chemical solution process method to passivate GBs in *poly*-Si and multicrystalline silicon (*mc*-Si) wafers. This low temperature passivation method advantages in the operation simplicity and low requirement on process condition. Moreover, different with traditional hydrogen passivation mechanism, we propose to utilize molecule's polarity to eliminate positive and negative charged GBs defect, in principle can widely expended to other polycrystalline thin-film solar cells, including cadmium telluride (CdTe), copper indium gallium selenide (CIGS), and copper zinc tin sulfide (CZTS). In the present experiment investigation, the large-angle random GBs electrical activity can be significantly reduced to more than one order in *mc*-Si. In addition, correlation of GB microstructure with passivation effect was well investigated. *Mc*-Si wafers rather than polycrystalline thin films were chosen because of their large grains, which make it easier to practically study the GB behaviors. We propose this simple polar molecules passivation method can provide effective potential alternative to upgrade photovoltaic device, to achieve the improvement of the energy conversion



efficiency and to reduction of the cost.

6.2 Experimental

Investigation was carried out on *p*-type *mc*-Si wafers (thickness: ~200 um; resistivity: 0.5–3 Ω·cm; grain size: mm–cm). Wafers were first cut into small samples of a few cm. GBs marked lightly with a diamond scribe were examined in detail to see sheet resistance changes before and after passivation. All samples were cleaned using the standard Radio Corporation of America (RCA) clean procedure, followed by etching in 1:50 hydrofluoric acid for 30 seconds, rinsing with deionized water for 1 minute, and then drying with compressed air. The passivation was then conducted by immersing cleaned samples in methanol (CH_3OH), formic acid (HCOOH), acetonitrile (CH_3CN), and our home-made ZK-series polar molecule solutions, respectively, at a fixed temperature (<100 °C) for certain periods of time. The ZK-series polar molecule solutions are mixtures of different polar molecules at different volume ratios. Passivated samples were then taken out, dried with compressed air, and left in air at room temperature for more than 12 hours before measuring the sheet resistance with a four-point probe station (Signatone S-301-4). The resistance measurement was conducted across GBs and on grain bulk, respectively, under both dark and illuminated conditions. The light source was a standard solar simulator (ABET Sun 2000). The resistance across each GB was obtained by averaging several data points acquired along the GB. After finishing the resistance measurement, each sample was first RCA



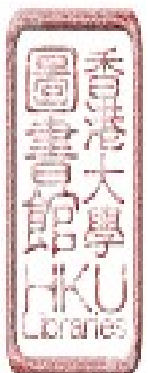
cleaned and then put back in the same chemical solution again for further passivation at an incremental step of 5 hours to study the effect of passivation time on the resistance. In addition, photoluminescence (PL) and electron backscatter diffraction (EBSD) techniques were also applied to study the correlation between the electrical, optical, and structural properties of GBs. For PL imaging, the wafer was illuminated by 810 nm light at an intensity equivalent to one sun, and the data acquisition time was 600 seconds. The plan-view EBSD mapping was carried out with a scanning electron microscope (SEM) (Hitachi S-4300N) at 20 kV, a sample tilt angle of 70°, and a working distance of 15 mm. More details on PL and EBSD can be found elsewhere [22, 23].

6.3 Results and discussion

We first studied the GB passivation with pure polar molecular solutions only. Fig. 1 shows the sheet resistance (R_{sheet}) across GBs *vs.* passivation time on two kinds of GBs — large-angle random and $\Sigma 3$ — under dark (D = dark) and illuminated (L = light) conditions, respectively. The dipole moments of formic acid, methanol, and acetonitrile are 1.41, 1.69, and 3.9 D (D = Debye), respectively [24-26]. As shown in Fig. 1a, methanol is generally more effective in passivating large-angle random GBs than are formic acid and acetonitrile. In particular, after a 10-hour methanol passivation, the dark R_{sheet} and illuminated R_{sheet} values decreased from 5637.2 and 4317.2 Ω/\square to 3711.0 and 3196.5 Ω/\square , respectively (or equivalently, by 34.2% and 26.0%, respectively). The relatively



effective passivation of methanol might be related to its small molecule size of ~0.41 nm [27], which makes it easier to diffuse along GBs for passivation and therefore lowers the energy potential barrier there. However, the R_{sheet} almost returned to its original value when the passivation time was further increased. In contrast, the passivation of acetonitrile and formic acid on large-angle random GBs is not obvious for the entire range of treatment time under both dark and illuminated conditions. For instance, the dark R_{sheet} and illuminated R_{sheet} remained almost constant around 5500 and 4800 Ω/\square , respectively, for large-angle random GBs treated with formic acid. For $\Sigma 3$ GBs (Fig. 1b), R_{sheet} values are usually in the range of 60–180 Ω/\square , which are much smaller than those of large-angle random GBs. We see that the passivation on $\Sigma 3$ GBs did not greatly change the R_{sheet} values, although in general acetonitrile may reduce R_{sheet} , and methanol (or formic acid) may increase R_{sheet} . Overall, we can conclude that with appropriate small polar molecules, the electrical activity of GBs can be modified to a certain extent. However, the passivation effectiveness of pure molecule candidates on large-angle GBs is still limited. We then investigated the passivation performance of our ZK-series polar molecule solutions, whose dipole moments can be varied from 2.2 to 3.4 D.



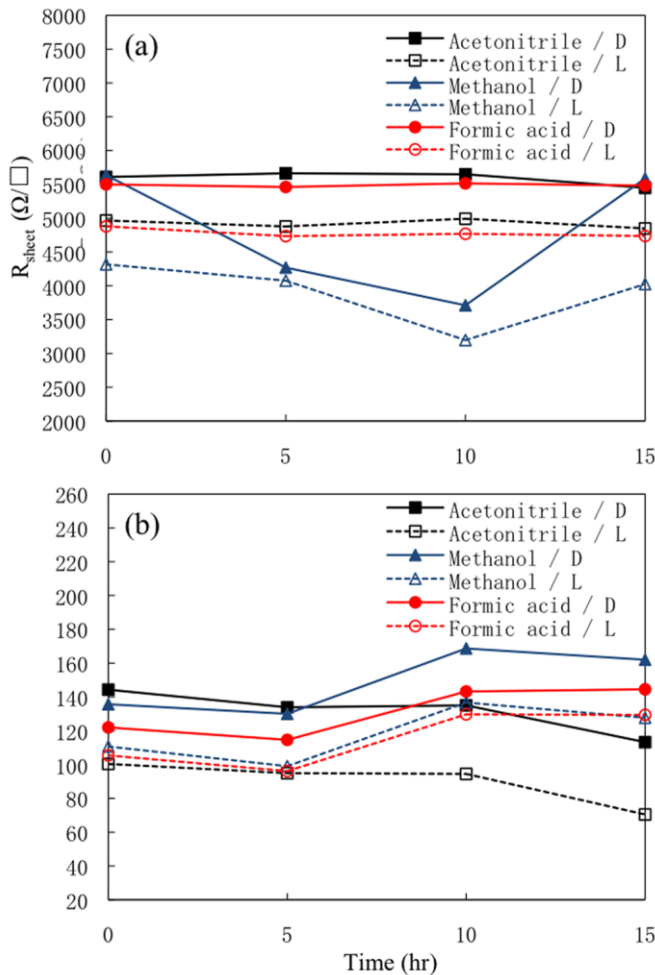
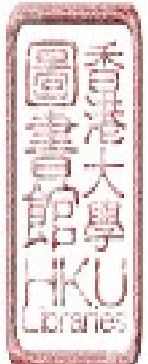
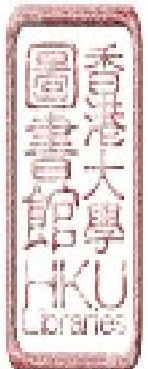


Fig. 1. Sheet resistance (R_{sheet}) across GBs vs. passivation time of acetonitrile, methanol, and formic acid under dark (D) and illuminated (L) conditions, respectively. **(a)** Large-angle random GBs. **(b)** $\Sigma 3$ GBs.

As depicted in Fig. 2a, all three kinds of ZK-series solutions could effectively passivate large-angle random GBs and then greatly reduce their R_{sheet} values. For GBs passivated with ZK-22 solution, the corresponding R_{sheet} decreased dramatically even after the first 5 hours of passivation; the values of R_{sheet} dropped from 5804.9 and 5083.6 Ω/\square to 1144.6 and 848.3 Ω/\square under dark and illuminated conditions, respectively. With further passivation, the R_{sheet}



increased slightly first and then dropped to saturation values of 180.4 and 176.2 Ω/\square , respectively, under dark and illuminated conditions, when the passivation time reached 30 hours. We therefore see that the R_{sheet} across large-angle GBs could be reduced by more than 95% after ZK-22 passivation. Compared to ZK-22 solution, both the ZK-24 and ZK-42 solutions generally followed a similar trend in terms of passivation effectiveness on large-angle GBs. However, for GBs passivated with either the ZK-24 or ZK-42 solution, the corresponding R_{sheet} did not decrease significantly until the passivation reached 10 hours, and after that, the R_{sheet} saturated to low values ($<1000 \Omega/\square$), which makes both the ZK-24 and ZK-42 solutions better passivation candidates as far as the passivation time window is concerned. We also tested the conductivity of ZK-series solutions and found them to be insulating, which rules out the possibility that the resistance reduction after passivation was caused by the conductivity of the polar molecules themselves. We therefore think the improvement of the electrical properties at GBs is due to the interaction between mc-Si GBs and polar molecules. For $\Sigma 3$ GBs passivated with ZK-series solutions, the R_{sheet} was generally not sensitive to the passivation (Fig. 2b), although it fluctuated to some extent, similar to the case of $\Sigma 3$ GBs passivated with pure polar molecules as shown earlier in Fig. 1b. It is reasonable to assume that polar molecules did not have much effect on the electrical activity of $\Sigma 3$ GBs because it is well known that $\Sigma 3$ boundaries are structurally much less defective and thus almost electrically inactive [4, 22]. We observed that all passivated samples showed very stable electrical resistance even



when left in air at room temperature for four weeks. These findings are significant because the R_{sheet} values of defective random GBs can be greatly reduced to be close to the bulk R_{sheet} values (25–150 Ω/\square) through simple passivation with small polar molecules.

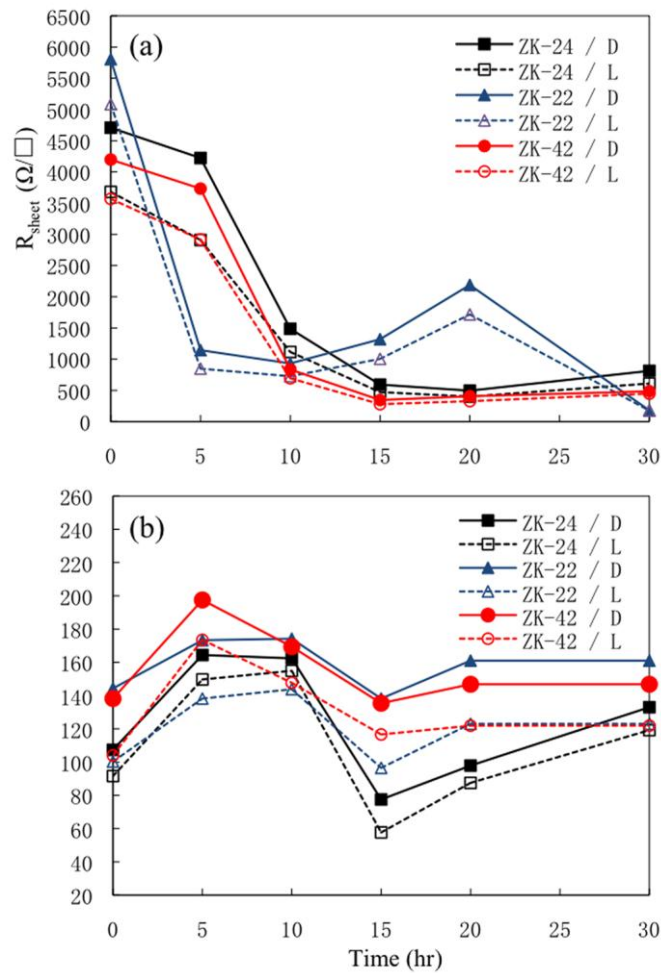


Fig. 2. Sheet resistance (R_{sheet}) across GBs vs. passivation time of ZK-24, ZK-22, and ZK-42 under dark (D) and illuminated (L) conditions, respectively. **(a)** Large-angle random GBs. **(b)** $\Sigma 3$ GB



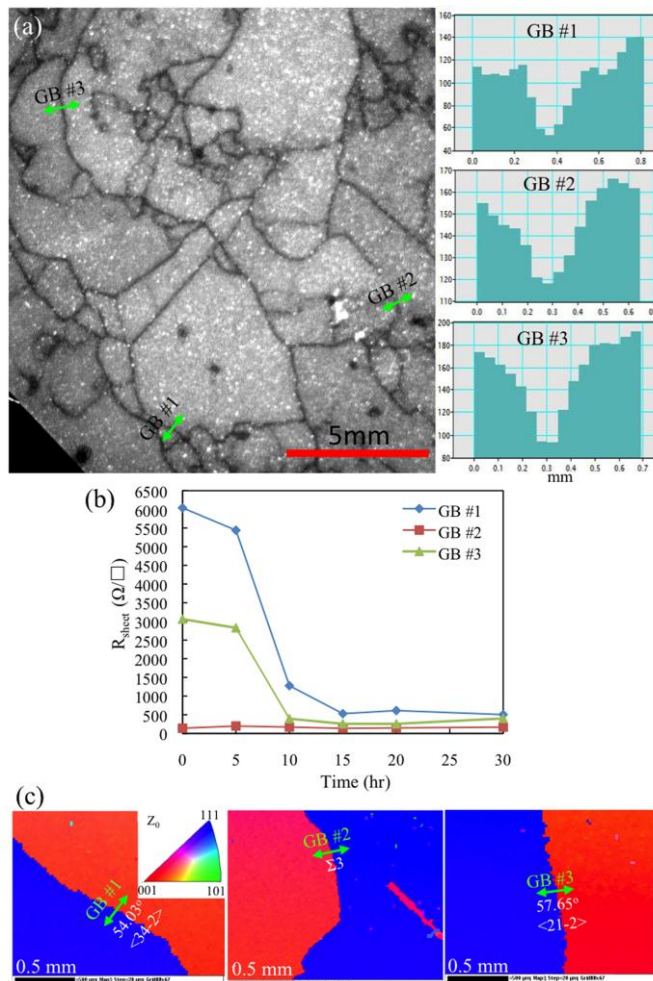
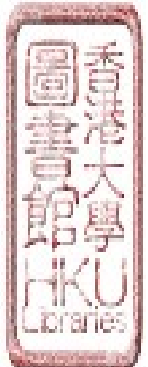


Fig. 3. Sample passivated with ZK-42. **(a)** PL image of a sample passivated for 30 hours. The insets are the corresponding PL intensity profiles across GBs #1–3. **(b)** Sheet resistance (R_{sheet}) across GBs #1–3 vs. passivation time under dark condition. **(c)** Plan-view EBSD maps at GBs #1–3. EBSD maps are color-coded with the IPF coloring in the sample normal direction Z_0 . The inset is the color-coding legend.

To further investigate the passivation effectiveness of ZK-series solutions, we worked specifically on samples passivated with ZK-42 solution with EBSD and PL. The PL image of a sample passivated with ZK-42 for 30 hours is shown



in Fig. 3a. The contrast in a PL image is closely related to the defect density and lifetime in association with the material purity [28]. We can clearly see the GBs in the PL image due to their strong contrast with adjacent grain bulk. Also shown are the corresponding PL intensity profiles across GBs #1–3 indicated by arrows. The darkness of the three GBs follows the order GB #1 > GB #3 > GB #2 as far as the intensity counts are concerned: 55, 118, and 82 for GB #1, GB #2 and GB #3, respectively. In fact, we selected the three typical GBs #1–3 according to their different R_{sheet} values before passivation (6040.8, 138.2, and 3060.7 Ω/\square for GBs #1–3, respectively). We then measured the R_{sheet} under dark conditions at different passivation times (Fig. 3b). We see that the R_{sheet} values across GBs #1 and #3 decreased greatly after passivation for 10 hours and then became almost saturated with increasing passivation time, whereas the R_{sheet} across GB #2 was insensitive to passivation. After passivation for 30 hours, the R_{sheet} values across GBs #1–3 are 503.7, 168.3, and 400.9 Ω/\square , respectively, which is consistent with the aforementioned intensity profile counts. To explain these findings, we further investigated the same GBs with plan-view EBSD mapping to observe the grain misorientation between two adjacent grains. Fig. 3c shows EBSD maps at GBs #1–3, respectively. The maps are color-coded with the inverse pole figure (IPF) coloring in the sample normal direction Z_0 . Also shown is the grain misorientation (angle and axis of rotation) between adjacent grains. It indicates that GBs #1 and #3 are large-angle random GBs whereas GB #2 is a $\Sigma 3$ coincidence site lattice (CSL) boundary. We therefore confirmed that our ZK-series solutions are very



effective in passivating large-angle random GBs in *mc*-Si and do not passivate $\Sigma 3$ GBs or deteriorate their electrical properties. These findings are consistent with those reported on GBs passivated with hydrogen [5]. In our recent study on upgraded metallurgical-grade silicon (UMG-Si) wafers, we also found a similar correlation between the optical response and different GBs passivated with a methanol–iodine solution [22]. However, we observed that methanol–iodine passivated *mc*-Si samples showed a wider range of PL imaging contrast for different GBs than ZK-series solution passivated ones, which further verified that our ZK-series solutions can effectively passivate random GBs.

To explain the passivation-enhanced conductivity of random GBs, we refer to a typical random GB model for *p*-type Si before passivation (Fig. 4a) [29]. As mentioned above, large-angle random GBs show high resistance for carriers to cross over, because high defects and impurity densities exist there [22]. These defects introduce extra electronic states localized within the band gap and act as trap states at GBs. When Fermi levels line up as a result of charge transfer to reach equilibrium, a potential barrier and interfacial polarization will be formed along the GB; the barrier will oppose the immigration of charge carriers. It is therefore reasonable that random GBs, in particular large-angle ones, show large R_{sheet} values. Tsurekawa *et al.* [30] showed that random boundaries possess barrier heights almost twice as high as those of coincidence boundaries. After passivation with ZK-series solutions, it is expected that the electric dipole moments of proper polar molecules in solutions and the interfacial dipole moments at the GB cancel



each other out so that the GB potential barrier can be greatly lowered (Fig. 4b) and the corresponding R_{sheet} can be greatly reduced. Small molecules with high polarity was also applied in organic solar cells acting as both electron donor and acceptor to adjust interfacial energy barrier [31]. However, for pure solutions such as methanol, formic acid, and acetonitrile, we believe the molecular dipoles may not match with the interfacial dipoles at the GB, which leads to poor charge neutralization and passivation of polar molecules on localized charge states at GBs. It should be pointed out that the actual situation could be more complicated than the brief picture presented here. Therefore, more research work is needed to further clarify what actually happens at GBs during passivation; for instance, how deep small polar molecules can diffuse into GBs and how long they can stay there.

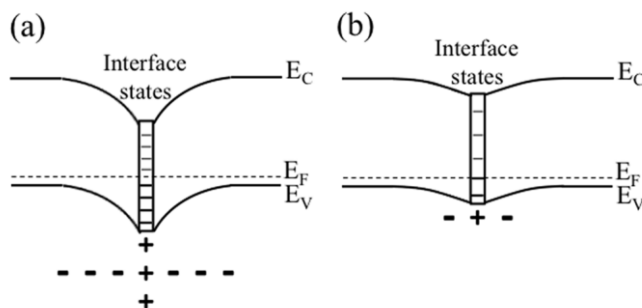


Fig. 4. Random GB model. **(a)** Before passivation. **(b)** After passivation.

6.4 Conclusions

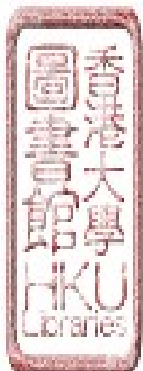
In summary, four-point probe, PL, and EBSD techniques were employed to study the passivation effect of small polar molecules on GBs in mc-Si wafers, including methanol, acetonitrile, formic acid, and new ZK-series mixed solutions.



It was shown that the ZK-series polar molecule solutions have a much stronger passivation effect than a single type of polar molecule solution. The R_{sheet} across large-angle GBs could be reduced by up to more than one order to be close to the bulk R_{sheet} ($25\text{--}150 \Omega/\square$) through simple passivation with ZK-series mixed solutions. In addition, we found an excellent correlation between the grain misorientation and passivation effectiveness. The results were explained with a GB model to be due to the effective charge neutralization and passivation of polar molecules on localized charge states at GBs. These findings are important because we believe that using non-hydrogen based approaches to passivation may help us achieve high-quality, economical semiconductor materials for photovoltaics and other solid-state devices such as thin-film transistors.

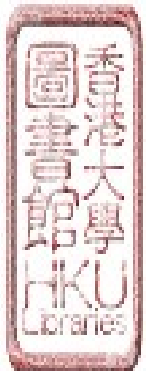
Acknowledgements

F. Liu acknowledges the financial support from the Seed Funding Programme for Basic Research at HKU (Project Codes 200910159016 and 201211159091), the University Development Fund (UDF) 2009-2010 (Second Round), and the HKU Initiative on Clean Energy & Environment (HKU-ICEE). W.C.H. Choy is grateful for the financial support of the General Research Fund (Grant Codes: HKU712010E and HKU711612E) from the Research Grants Council of Hong Kong Special Administrative Region, China. The authors also thank Yanfa Yan from the University of Toledo for stimulating discussion.

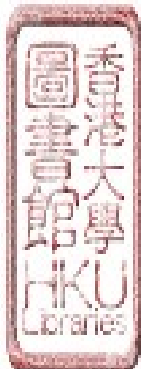


References

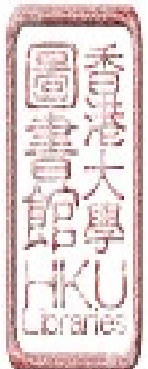
1. Schropp, R.E.I., R. Carius, and G. Beaucarne, *Amorphous silicon, microcrystalline silicon, and thin-film polycrystalline silicon solar cells.* MRS Bulletin, 2007. **32**(3): p. 219-224.
2. Beaucarne, G., *Silicon Thin-Film Solar Cells.* Advances in OptoElectronics, 2007. **2007**: p. Article ID 36970.
3. Green, M.A., *Crystalline and thin-film silicon solar cells: state of the art and future potential.* Solar Energy, 2003. **74**(3): p. 181-192.
4. Chen, J., et al., *Recombination activity of $\Sigma 3$ boundaries in boron-doped multicrystalline silicon: Influence of iron contamination.* Journal of Applied Physics, 2005. **97**(3): p. 033701.
5. Bertoni, M.I., et al., *Influence of defect type on hydrogen passivation efficacy in multicrystalline silicon solar cells.* Progress in Photovoltaics: Research and Applications, 2011. **19**(2): p. 187-191.
6. Dimassi, W., et al., *Two-dimensional LBIC and Internal-Quantum-Efficiency investigations of grooved grain boundaries in multicrystalline silicon solar cells.* Solar Energy, 2011. **85**(2): p. 350-355.
7. Honda, S., et al., *Microscopic study of the H₂O vapor treatment of the silicon grain boundaries.* Journal of Non-Crystalline Solids, 2008. **354**(19–25): p. 2310-2313.
8. Seager, C.H. and D.S. Ginley, *Passivation of grain boundaries in*



- polycrystalline silicon.* Applied Physics Letters, 1979. **34**(5): p. 337-340.
9. Carnel, L., et al., *Defect passivation in chemical vapour deposited fine-grained polycrystalline silicon by plasma hydrogenation.* Thin Solid Films, 2005. **487**(1-2): p. 147-151.
10. Dekkers, H.F.W., L. Carnel, and G. Beaucarne, *Carrier trap passivation in multicrystalline Si solar cells by hydrogen from SiN:H layers.* Applied Physics Letters, 2006. **89**(1): p. 013508-013508-3.
11. Darwiche, S., et al., *Effects of hydrogen plasma on passivation and generation of defects in multicrystalline silicon.* Solar Energy Materials and Solar Cells, 2007. **91**(2-3): p. 195-200.
12. Nickel, N.H., A. Yin, and S.J. Fonash, *Influence of hydrogen and oxygen plasma treatments on grain boundary defects in polycrystalline silicon.* Applied Physics Letters, 1994. **65**(24): p. 3099-3101.
13. Rajesh, C., et al., *Reduction in surface recombination through hydrogen and 1-heptene passivated silicon nanocrystals film on silicon solar cells.* Solar Energy, 2012. **86**(1): p. 489-495.
14. Bousbih, R., et al., *Silicon lifetime enhancement by SiNx:H anti-reflective coating deposited by PECVD using SiH4 and N2 reactive gas.* Solar Energy, 2012. **86**(5): p. 1300-1305.
15. Banerjee, S., et al., *Hot-electron degradation of n-channel polysilicon MOSFETs.* Electron Devices, IEEE Transactions on, 1988. **35**(2): p. 152-157.



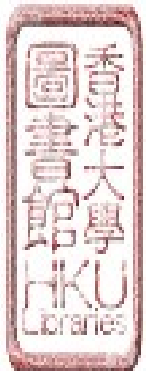
16. Nickel, N.H., W.B. Jackson, and N.M. Johnson, *Light-induced creation of metastable paramagnetic defects in hydrogenated polycrystalline silicon*. Physical Review Letters, 1993. **71**(17): p. 2733-2736.
17. Saad, A., et al., *Influence of low-energy ion-beam treatment by hydrogen on electrical activity of grain boundaries in polycrystalline silicon*. Vacuum, 2005. **78**(2–4): p. 269-272.
18. Honda, S., et al., *Defects generation by hydrogen passivation of polycrystalline silicon thin films*. Solar Energy, 2006. **80**(6): p. 653-657.
19. Huang-Chung, C., W. Fang-Shing, and C.-Y. Huang, *Effects of NH₃ plasma passivation on N-channel polycrystalline silicon thin-film transistors*. Electron Devices, IEEE Transactions on, 1997. **44**(1): p. 64-68.
20. Chhabra, B., et al., *High effective minority carrier lifetime on silicon substrates using quinhydrone-methanol passivation*. Applied Physics Letters, 2010. **96**(6): p. 063502.
21. Chhabra, B., et al., *Surface characterization of quinhydrone-methanol and iodine-methanol passivated silicon substrates using X-ray photoelectron spectroscopy*. physica status solidi (a), 2011. **208**(1): p. 86-90.
22. Liu, F.D., et al., *Optical response of grain boundaries in upgraded metallurgical-grade silicon for photovoltaics*. Solar Energy Materials and Solar Cells, 2011. **95**(8): p. 2497-2501.
23. Regan, W., et al., *Screening-Engineered Field-Effect Solar Cells*. Nano



- Letters, 2012. **12**(8): p. 4300-4304.
24. Zecca, A., et al., *Positron scattering from formic acid*. Physical Review A, 2008. **78**(4): p. 042707.
25. Kebarle, P., R.M. Haynes, and J.G. Collins, *Competitive solvation of the hydrogen ion by water and methanol molecules studied in the gas phase*. Journal of the American Chemical Society, 1967. **89**(23): p. 5753-5757.
26. Wright, D., R. Caldwell, and M.S. El-Shall, *Vapor phase homogeneous nucleation of acetonitrile: the effect of dipole--dipole interaction*. Chemical Physics Letters, 1991. **176**(1): p. 46-54.
27. Bhattacharyya, D., et al., *Pervaporation of alcohol-water and dimethylformamide-water mixtures using hydrophilic zeolite NaA membranes: mechanisms and experimental results*. Journal of Membrane Science, 2000. **179**(1-2): p. 185-205.
28. Schroder, D.K., *Semiconductor Material and Device Characterization*. 2nd ed. 1998: Wiley.
29. Nelson, J., *The Physics of Solar Cells*. 2002: Imperial College Press.
30. Tsurekawa, S., K. Kido, and T. Watanabe, *Interfacial state and potential barrier height associated with grain boundaries in polycrystalline silicon*. Materials Science and Engineering a-Structural Materials Properties Microstructure and Processing, 2007. **462**(1-2): p. 61-67.
31. Choi, J.W., et al., *Solution-processed bulk heterojunction organic solar cells with high polarity small molecule sensitizer*. Solar Energy Materials



and Solar Cells, 2011. **95**(8): p. 2069-2076.



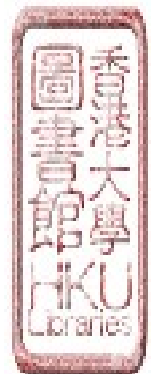
7. Conclusions

Novel ferroelectric-semiconductor photovoltaic devices were investigated in detail with experimental results and theoretical simulation. This type of solar cell is fundamentally different with traditional PN junction based solar cells, utilizing ferroelectric polarization for charge separation in semiconductor layer. Systematical works have been conducted on: (1) device working principle and mechanism study; (2) effect of electrode; (3) influence of device key dimension parameters. Furthermore, in order to improve the semiconductor layer transport for the novel ferroelectric-semiconductor photovoltaics, multicrystalline was selected for study. A polar molecules system was developed to play the role in grain boundaries passivation. The small polar molecule composition and solution passivation process were carried out to optimize the passivation effect.

The key findings are summarized as follows.

The novel ferroelectric-semiconductor photovoltaic devices:

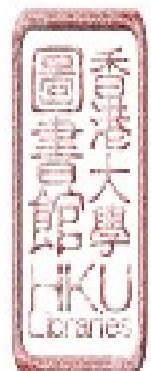
- The novel ferroelectric semiconductor non PN junction system is effective for photovoltaic device application. Real solar cells showed the rectifying behavior and photovoltaic effect after specific asymmetric polarization.
- Theoretical simulation indicated that the induced electric field due to the BaTiO₃ polarization could extend into the Si layer and then photon-generated carries in Si could be separated and collected for electricity generation. The polarization induced electric field strength can be comparable to the typical PN



junction by control of the device dimension.

- Deposition of electrodes on the semiconductor surface only, rather than at the ferroelectric/semiconductor interface, can avoid the screening effect issue, and therefore improve the open circuit voltage and short circuit current density.
- Electrodes materials play an important role on cell performance. The device with Au/Ti , and Al/Ti electrodes both showed enhanced photovoltaic effect than that with Al/Al contacts.
- Improving the ferroelectric quality with high polarization charge density can enhance the polarization effect as well as the device performance.
- Adjusting the interdigital electrode space length and semiconductor thickness can optimize polarization induced electric field strength and distribution. Through decreasing electrodes space length to 300 μ m and silicon thickness to 50 μ m, the device showed significant enhanced photovoltaic properties comparing with the previous one, which was attributing to the effective photon-generated charge separation in silicon drifted by BaTiO₃ polarization.
- The cell electric and photovoltaic properties are related to the polarization direction. Forward and reverse polarization methods can switch the direction of photocurrent and diode behavior.
- The novel ferroelectric-semiconductor non PN junction solar cell can be applied to other ferroelectric semiconductor material systems, not only limited to BaTiO₃ and silicon materials.

Passivating silicon grain boundaries with small polar molecules for



ferroelectric-semiconductor photovoltaics:

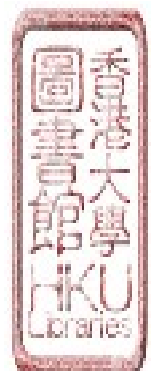
- the ZK-series polar molecule solutions have a much stronger passivation effect than a single type of polar molecule solution, such as methanol, acetonitrile, and formic acid. The R_{sheet} across large-angle GBs could be reduced by up to more than one order to be close to the bulk R_{sheet} ($25\text{--}150 \Omega/\square$) through simple passivation with ZK-series mixed solutions.
- The correlation between the grain misorientation and passivation effectiveness was built up. The ZK-series solutions are very effective in passivating large-angle random GBs in *mc*-Si and do not passivate $\Sigma 3$ GBs or deteriorate their electrical properties. The results were explained with a GB model to be due to the effective charge neutralization and passivation of polar molecules on localized charge states at GBs.

In the future, research work with the purpose of boosting up the novel ferroelectric semiconductor photovoltaic device efficiency can be conducted. It includes electrodes fabrication improvement, surface passivation and interface buffer layer incorporation, various ferroelectric and semiconductor materials adaption, and device structure design upgrade. As to the grain boundaries passivation technique, it is planned to evaluate the effect on the ferroelectric-semiconductor photovoltaic device performance.

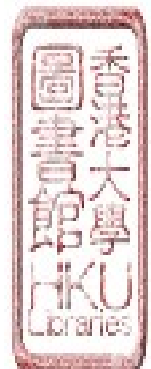


Overall References

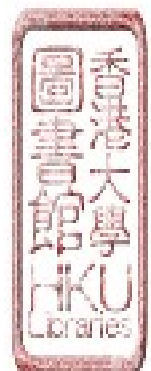
- Banerjee, S., et al., Hot-electron degradation of n-channel polysilicon MOSFETs., IEEE Transactions on Electron Devices, 1988. 35(2): p. 152-157.
- Beaucarne, G., Silicon Thin-Film Solar Cells. Advances in OptoElectronics, 2007. 2007: p. Article ID 36970.
- Bertoni, M. I., et al., Influence of defect type on hydrogen passivation efficacy in multicrystalline silicon solar cells. Progress in Photovoltaics: Research and Applications, 2011. 19(2): p. 187-191.
- Bhattacharyya, D., et al., Pervaporation of alcohol-water and dimethylformamide-water mixtures using hydrophilic zeolite NaA membranes: mechanisms and experimental results. Journal of Membrane Science, 2000. 179(1-2): p. 185-205.
- Bousbih, R., et al., Silicon lifetime enhancement by SiNx:H anti-reflective coating deposited by PECVD using SiH4 and N₂ reactive gas. Solar Energy, 2012. 86(5): p. 1300-1305.
- Cao, D. W., et al., Understanding the nature of remnant polarization enhancement, coercive voltage offset and time-dependent photocurrent in ferroelectric films irradiated by ultraviolet light. Journal of Materials Chemistry, 2012. 22(25): p. 12592-12598.
- Cao, D. W., et al., Polarization effect on the photocurrent of Pt sandwiched multi-crystalline ferroelectric films. Materials Chemistry and Physics, 2011. 129(3): p. 783-786.
- Cao, D. W., et al., High-Efficiency Ferroelectric-Film Solar Cells with an n-type



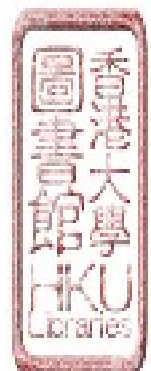
- Cu₂O Cathode Buffer Layer. *Nano Letters*, 2012. 12(6): p. 2803-2809.
- Cao, D. W., et al., Interface layer thickness effect on the photocurrent of Pt sandwiched polycrystalline ferroelectric Pb(Zr, Ti)O₃ films. *Applied Physics Letters*, 2010. 97(10): p. 102104.
- Cao, D. W., et al., Interface effect on the photocurrent: A comparative study on Pt sandwiched (Bi_{3.7}Nd_{0.3})Ti₃O₁₂ and Pb(Zr_{0.2}Ti_{0.8})O₃ films. *Applied Physics Letters*, 2010. 96(19): p. 192101.
- Carnel, L., et al., Defect passivation in chemical vapour deposited fine-grained polycrystalline silicon by plasma hydrogenation. *Thin Solid Films*, 2005. 487(1–2): p. 147-151.
- Chen, J., et al., Recombination activity of Σ3 boundaries in boron-doped multicrystalline silicon: Influence of iron contamination. *Journal of Applied Physics*, 2005. 97(3): p. 033701.
- Chhabra, B., et al., High effective minority carrier lifetime on silicon substrates using quinhydrone-methanol passivation. *Applied Physics Letters*, 2010. 96(6): p. 063502.
- Chhabra, B., et al., Surface characterization of quinhydrone–methanol and iodine–methanol passivated silicon substrates using X-ray photoelectron spectroscopy. *physica status solidi (a)*, 2011. 208(1): p. 86-90.
- Choi, J. W., et al., Solution-processed bulk heterojunction organic solar cells with high polarity small molecule sensitizer. *Solar Energy Materials and Solar Cells*, 2011. 95(8): p. 2069-2076.
- Choi, T., et al., Switchable Ferroelectric Diode and Photovoltaic Effect in BiFeO₃.



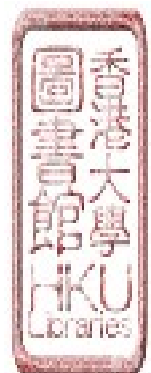
- Science, 2009. 324(5923): p. 63-66.
- Darwiche, S., et al., Effects of hydrogen plasma on passivation and generation of defects in multicrystalline silicon. Solar Energy Materials and Solar Cells, 2007. 91(2-3): p. 195-200.
- Dawber, M., K.M. Rabe, and J.F. Scott, Physics of thin-film ferroelectric oxides. Reviews of Modern Physics, 2005. 77(4): p. 1083-1130.
- Dekkers, H. F. W., L. Carnel, and G. Beaucarne, Carrier trap passivation in multicrystalline Si solar cells by hydrogen from SiN:H layers. Applied Physics Letters, 2006. 89(1): p. 013508.
- Diaz, M.B., et al., Resistivity topography: a grain boundary characterisation method. Solar Energy Materials and Solar Cells, 2002. 72(1-4): p. 473-486.
- Dimassi, W., et al., Two-dimensional LBIC and Internal-Quantum-Efficiency investigations of grooved grain boundaries in multicrystalline silicon solar cells. Solar Energy, 2011. 85(2): p. 350-355.
- Dong, W., et al., Enhanced Photovoltaic Effect in BiVO₄ Semiconductor by Incorporation with an Ultrathin BiFeO₃ Ferroelectric Layer. Acs Applied Materials & Interfaces, 2013. 5(15): p. 6925-6929.
- Dong, H. F., et al., Improving the optical absorption of BiFeO₃ for photovoltaic applications via uniaxial compression or biaxial tension. Applied Physics Letters, 2013. 102(7): p. 072905.
- Ertug̃, B., The Overview of The Electrical Properties of Barium Titanate. American Journal of Engineering Research, 2013. 02(08): p. 01-07.
- Fridkin, V. M., Bulk photovoltaic effect in noncentrosymmetric crystals.



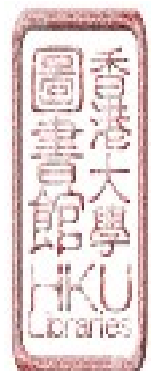
- Crystallography Reports, 2001. 46(4): p. 654-658.
- Gabrielyan, V. T., et al., Influence of K, Mg and Fe impurities on the composition, absorption spectra and photovoltaic properties of LiNbO_3 crystals. Ferroelectrics, 2002. 281: p. 151-161.
- Glass, A. M. and D. Vonderlinde, Photovoltaic, Photoconductive and Excited-State Dipole Mechanisms for Optical Storage in Pyroelectrics. Ferroelectrics, 1976. 10(1-4): p. 163-166.
- Green, M. A., Crystalline and thin-film silicon solar cells: state of the art and future potential. Solar Energy, 2003. 74(3): p. 181-192.
- Harshan, V. N. and S. Kotru, Influence of work-function of top electrodes on the photovoltaic characteristics of $\text{Pb}_{0.95}\text{La}_{0.05}\text{Zr}_{0.54}\text{Ti}_{0.46}\text{O}_3$ thin film capacitors. Applied Physics Letters, 2012. 100(17): p. 173901.
- Honda, S., et al., Defects generation by hydrogen passivation of polycrystalline silicon thin films. Solar Energy, 2006. 80(6): p. 653-657.
- Huang, X. L. M., Su Lyn, Ferroelectrics New Research: Electrical Engineering Developments. 2012: NOVA.
- Huang, F. and X.X. Liu, A ferroelectric-semiconductor-coupled solar cell with tunable photovoltage. Applied Physics Letters, 2013. 102(10): p. 103501.
- Huang-Chung, C., W. Fang-Shing, and C.-Y. Huang, Effects of NH_3 plasma passivation on N-channel polycrystalline silicon thin-film transistors. Electron Devices, IEEE Transactions on, 1997. 44(1): p. 64-68.
- Honda, S., et al., Hydrogenation of polycrystalline silicon thin films. Thin Solid Films, 2006. 501(1-2): p. 144-148.



- Honda, S., et al., Microscopic study of the H₂O vapor treatment of the silicon grain boundaries. *Journal of Non-Crystalline Solids*, 2008. 354(19-25): p. 2310-2313.
- Honda, S., et al., Annealing in water vapor as a new method for improvement of silicon thin film properties. *Journal of Non-Crystalline Solids*, 2006. 352(9-20): p. 955-958.
- Ionov, P.V., Photosensitivity of Ferroelectric Niobates. *Fizika Tverdogo Tela*, 1973. 15(9): p. 2827-2828.
- Ji, W., K. Yao, and Y.C. Liang, Evidence of bulk photovoltaic effect and large tensor coefficient in ferroelectric BiFeO₃ thin films. *Physical Review B*, 2011. 84(9): p. 094115.
- Ji, W., K. Yao, and Y.C. Liang, Bulk Photovoltaic Effect at Visible Wavelength in Epitaxial Ferroelectric BiFeO₃ Thin Films. *Advanced Materials*, 2010. 22(15): p. 1763-1766.
- Johnson, N.M., D.K. Biegelsen, and M.D. Moyer, Deuterium Passivation of Grain-Boundary Dangling Bonds in Silicon Thin-Films. *Applied Physics Letters*, 1982. 40(10): p. 882-884.
- Kamalasanan, M.N., et al., Structural and Optical-Properties of Sol-Gel-Processed BaTiO₃ Ferroelectric Thin-Films. *Applied Physics Letters*, 1991. 59(27): p. 3547-3549.
- Kebarle, P., R.M. Haynes, and J.G. Collins, Competitive solvation of the hydrogen ion by water and methanol molecules studied in the gas phase. *Journal of the American Chemical Society*, 1967. 89(23): p. 5753-5757.
- Kozuka, H., et al., PVP-assisted sol-gel deposition of single layer ferroelectric thin



- films over submicron or micron in thickness. Journal of the European Ceramic Society, 2004. 24(6): p. 1585-1588.
- Kozuka, H. and M. Kajimura, Single-step dip coating of crack-free BaTiO₃ films > 1 μm thick: Effect of poly(vinylpyrrolidone) on critical thickness. Journal of the American Ceramic Society, 2000. 83(5): p. 1056-1062.
- Kozuka, H. and A. Higuchi, Stabilization of Poly(vinylpyrrolidone)-containing Alkoxide Solutions for Thick Sol-Gel Barium Titanate Films. Journal of the American Ceramic Society, 2003. 86(1): p. 33-38.
- Li, H., et al., Ultraviolet photovoltaic effect in BiFeO₃/Nb-SrTiO₃ heterostructure. Journal of Applied Physics, 2012. 112(8): p. 083506.
- Liu, F., et al., Working principles of solar and other energy conversion cells. Nanomaterials and Energy, 2012. 2(1): p. 3-10.
- Liu, F., et al., Ferroelectric-semiconductor photovoltaics: Non-PN junction solar cells. Appl. Phys. Lett., 2014. 104: p. 103907.
- Liu, F., et al., Optical response of grain boundaries in upgraded metallurgical-grade silicon for photovoltaics. Solar Energy Materials and Solar Cells, 2011. 95(8): p. 2497-2501.
- Liu, Q., et al., Improved photovoltaic performance of crystalline-Si/organic Schottky junction solar cells using ferroelectric polymers. Applied Physics Letters, 2013. 103(16): p. 163503.
- Luque, A.H., Steven, Handbook of Photovoltaic Science and Engineering. 2003: Wiley.
- Mataré, H.F., Defect Electronics in Semiconductors. 1971, New York: Wiley.



interscience.

Micheron, F., Sensitivity of Photorefractive Processes. *Ferroelectrics*, 1978. 18(1-3): p. 153-159.

Michaelson, H.B., Work Function of Elements and Its Periodicity. *Journal of Applied Physics*, 1977. 48(11): p. 4729-4733.

Nelson, J., *The physics of solar cells*. 2003: Imperial College Press.

Nickel, N.H., W.B. Jackson, and N.M. Johnson, Light-induced creation of metastable paramagnetic defects in hydrogenated polycrystalline silicon. *Physical Review Letters*, 1993. 71(17): p. 2733-2736.

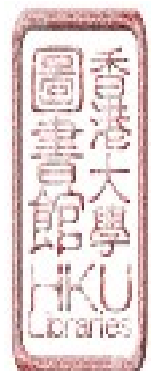
Nickel, N.H., N.M. Johnson, and W.B. Jackson, Hydrogen Passivation of Grain-Boundary Defects in Polycrystalline Silicon Thin-Films. *Applied Physics Letters*, 1993. 62(25): p. 3285-3287.

Nickel, N.H., A. Yin, and S.J. Fonash, Influence of hydrogen and oxygen plasma treatments on grain boundary defects in polycrystalline silicon. *Applied Physics Letters*, 1994. 65(24): p. 3099-3101.

Qin, M., K. Yao, and Y. Liang, High efficiency photovoltaics in nanoscaled ferroelectric thin films. *Applied Physics Letters*, 2008. 93: p. 122904.

Qin, M., K. Yao, and Y.C. Liang, Photovoltaic characteristics in polycrystalline and epitaxial $(\text{Pb}_{0.97}\text{La}_{0.03})(\text{Zr}_{0.52}\text{Ti}_{0.48})\text{O}_3$ ferroelectric thin films sandwiched between different top and bottom electrodes. *Journal of Applied Physics*, 2009. 105(6): p. 061624.

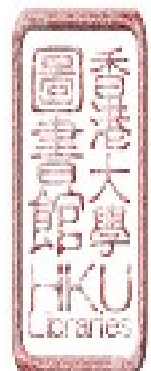
Qin, M., et al., Thickness effects on photoinduced current in ferroelectric $(\text{Pb}_{0.97}\text{La}_{0.03})(\text{Zr}_{0.52}\text{Ti}_{0.48})\text{O}_3$ thin films. *Journal of Applied Physics*, 2009.



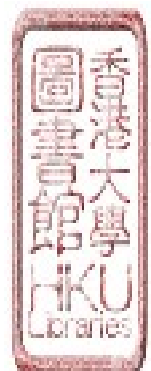
- 105(12): p. 014104.
- Qin, M., K. Yao, and Y.C. Liang, Photovoltaic mechanisms in ferroelectric thin films with the effects of the electrodes and interfaces. *Applied Physics Letters*, 2009. 95(2): p. 022912.
- Qu, T.L., et al., Resistance switching and white-light photovoltaic effects in BiFeO₃/Nb-SrTiO₃ heterojunctions. *Applied Physics Letters*, 2011. 98(17): p. 173507.
- Rajesh, C., et al., Reduction in surface recombination through hydrogen and 1-heptene passivated silicon nanocrystals film on silicon solar cells. *Solar Energy*, 2012. 86(1): p. 489-495.
- Regan, W., et al., Screening-Engineered Field-Effect Solar Cells. *Nano Letters*, 2012. 12(8): p. 4300-4304.
- Saad, A., et al., Influence of low-energy ion-beam treatment by hydrogen on electrical activity of grain boundaries in polycrystalline silicon. *Vacuum*, 2005. 78(2-4): p. 269-272.
- Seager, C.H. and D.S. Ginley, Studies of the Hydrogen Passivation of Silicon Grain-Boundaries. *Journal of Applied Physics*, 1981. 52(2): p. 1050-1055.
- Seager, C.H. and D.S. Ginley, Passivation of Grain-Boundaries in Polycrystalline Silicon. *Applied Physics Letters*, 1979. 34(5): p. 337-340.
- Schroder, D.K., *Semiconductor Material and Device Characterization*. 2nd ed. 1998: Wiley.
- Schropp, R.E.I., R. Carius, and G. Beaucarne, Amorphous silicon, microcrystalline silicon, and thin-film polycrystalline silicon solar cells. *MRS Bulletin*, 2007.



- 32(3): p. 219-224.
- Shklyarevskii, I.N. and P.L. Pakhmov, Separation of the contribution of free and bound electrons into real and imaginary parts of the dielectric constant of gold. Optika i Spektroskopiya, 1973. 34(1): p. 163-6.
- Streetman, B. and S. Banerjee, Solid State Electronic Devices. 2000: Prentice Hall.
- Tabib-Azar, M., N.S. Shoemaker, and S. Harris, Non-destructive characterization of materials by evanescent microwaves. Measurement Science and Technology, 1993. 4(5): p. 583.
- Tsurekawa, S., K. Kido, and T. Watanabe, Interfacial state and potential barrier height associated with grain boundaries in polycrystalline silicon. Materials Science and Engineering a-Structural Materials Properties Microstructure and Processing, 2007. 462(1-2): p. 61-67.
- Uchino, K., Ferroelectric devices, ed. second. 2010: CRC Press.
- Volk, T. R., et al., Effect of Illumination on Domain-Structure and Curie Temperature in BaTiO₃. Fizika Tverdogo Tela, 1972. 14(11): p. 3214.
- Wadhwa, P., et al., Electronic Junction Control in a Nanotube-Semiconductor Schottky Junction Solar Cell. Nano Letters, 2010. 10(12): p. 5001-5005.
- Wadhwa, P., et al., Electrolyte-Induced Inversion Layer Schottky Junction Solar Cells. Nano Letters, 2011. 11(6): p. 2419-2423.
- Wang, W., et al., Field-effect BaTiO₃-Si solar cells. Appl. Phys. Lett., 2014. 104: p. 123901.
- Wright, D., R. Caldwell, and M.S. El-Shall, Vapor phase homogeneous nucleation of acetonitrile: the effect of dipole--dipole interaction. Chemical Physics Letters, 1993. 217(1-2): p. 11-16.



1991. 176(1): p. 46-54.
- Würfel, P., Physics of Solar Cells: From Basic Principles to Advanced Concepts. 2 ed. 2009: Wiley-VCH.
- Xiao, Z.G., et al., Synthesis and Application of Ferroelectric P(VDF-TrFE) Nanoparticles in Organic Photovoltaic Devices for High Efficiency. *Advanced Energy Materials*, 2013. 3(12): p. 1581-1588.
- Xing, J., et al., Photovoltaic effects and its oxygen content dependence in $\text{BaTiO}_{(3-\delta)}$ /Si heterojunctions. *Applied Physics Letters*, 2008. 92(7): p. 071113.
- Xu, J., et al., Space charge effect on the photocurrent of Pt-sandwiched $\text{Pb}(\text{Zr}_{0.20}\text{Ti}_{0.80})\text{O}_3$ film capacitors. *Journal of Applied Physics*, 2009. 106(11): p. 113705.
- Yang, S.Y., et al., Above-bandgap voltages from ferroelectric photovoltaic devices. *Nature Nanotechnology*, 2010. 5(2): p. 143-147.
- Yang, B., et al., Tuning the Energy Level Offset between Donor and Acceptor with Ferroelectric Dipole Layers for Increased Efficiency in Bilayer Organic Photovoltaic Cells. *Advanced Materials*, 2012. 24(11): p. 1455-1460.
- Yang, X.L., et al., Enhancement of Photocurrent in Ferroelectric Films Via the Incorporation of Narrow Bandgap Nanoparticles. *Advanced Materials*, 2012. 24(9): p. 1202-1208.
- Yao, K., et al., Large photo-induced voltage in a ferroelectric thin film with in-plane polarization. *Applied Physics Letters*, 2005. 87(21): p. 212906.
- Yi, H.T., et al., Mechanism of the Switchable Photovoltaic Effect in Ferroelectric BiFeO_3 . *Advanced Materials*, 2011. 23(30): p. 3403-3407.



Yuan, Y. B., et al., Efficiency enhancement in organic solar cells with ferroelectric polymers. *Nature Materials*, 2011. 10(4): p. 296-302.

Yuan, Y. B., et al., Understanding the effect of ferroelectric polarization on power conversion efficiency of organic photovoltaic devices. *Energy & Environmental Science*, 2012. 5(9): p. 8558-8563.

Zang, Y. Y., et al., Enhanced photovoltaic properties in graphene/polycrystalline BiFeO₃/Pt heterojunction structure. *Applied Physics Letters*, 2011. 99(13): p. 132904.

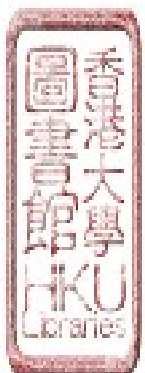
Zhang, J. J., et al., Enlarging photovoltaic effect: combination of classic photoelectric and ferroelectric photovoltaic effects. *Scientific Reports*, 2013. 3: p. 2109.

Zhang, P., et al., Enhanced photocurrent in Pb(Zr_{0.2}Ti_{0.8})O₃ ferroelectric film by artificially introducing asymmetrical interface Schottky barriers. *Materials Chemistry and Physics*, 2012. 135(2-3): p. 304-308.

Zecca, A., et al., Positron scattering from formic acid. *Physical Review A*, 2008. 78(4): p. 042707.

Zheng, F., et al., Separation of the Schottky barrier and polarization effects on the photocurrent of Pt sandwiched Pb(Zr_{0.2}Ti_{0.8})O₃ films. *Applied Physics Letters*, 2008. 93(17): p. 172101.

Zhuravlev, M.Y., et al., Giant Electroresistance in Ferroelectric Tunnel Junctions. *PRL*, 2005. 94: p. 246802.



Appendix

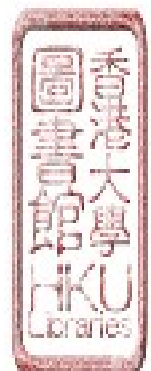
BaTiO₃ Preparation Through Sol-Gel Method

BaTiO₃ (BTO) thin film was selected to fabricate the novel non-PN junction ferroelectric-semiconductor solar cells. The BTO film quality plays a key role on deciding device performance. Consequently, a uniform, condensed and crack-free BTO thin film is required for new cell application. We chose sol-gel method to prepare BTO due to the advantages of easier composition control and low process condition requirement [1].

To synthesize BTO solution, barium acetate ($\text{Ba}(\text{CH}_3\text{COO})_2$), titanium isopropoxide ($\text{Ti}(\text{OC}_3\text{H}_7)_4$), acetic acid (CH_3COOH), and deionized water (H_2O) were used as starting materials. Two grams barium acetate was dissolved in 5ml acetic acid and 5 ml water mixed solvent at room temperature with constant stirring for 1 hour. Titanium isopropoxide was then added to the barium acetate solution, and stirred for 1 hour until got clear precursor solution.

For obtaining BTO thin film, the resulting BTO solution was spin coated on silicon substrate at 3000 rpm for 30 seconds. The drying step was conducted at 100°C for 30 minutes in ambient air. Finally, the film was annealed in tube furnace at 800°C for 2 hours with heating rate of 10°C/minute to crystallize the BTO, followed by cooling to room temperature slowly.

Fig. 1 shows the SEM image of obtained poly-crystalline BTO thin film. However, serious crack can be observed in the film. This may due to the condensation



reaction during the heat treatment. The film densification would result in a very high residual stress, which is the origin for film crack formation. The organic polymer poly(vinylpyrrolidone) (PVP) is effective for prevention crack formation in BTO sol-gel preparation [2, 3]. This is possibly due to that the hydrogen bonds between the C=O groups of PVP and the O-H groups of the metalloxane polymers would suppress the film condensation reaction and promote the residual stress relaxation [2]. Furthermore, hydrolysis speed and viscosities should be well controlled to improve BTO film quality.

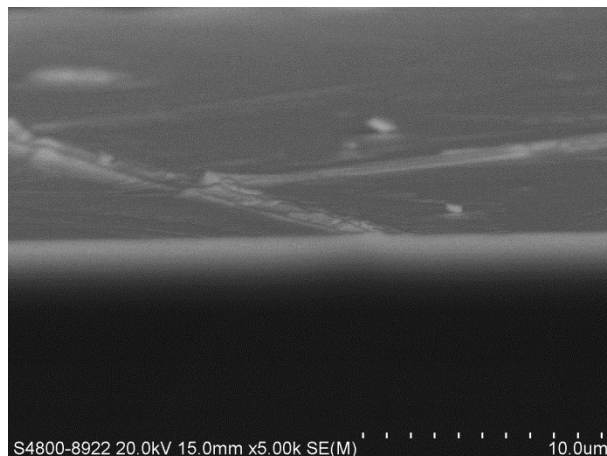


Fig. 1. SEM image of BaTiO₃ film prepared by sol-gel method.

We then developed new approach with the purpose of getting crack-free BTO thin film. Firstly, PVP with 55000 molecule weight was applied to the new method. Furthermore, the precursor solution concentration was reduced to 0.45mol/L adjusting by C₂H₅OH, H₂O, and CH₃COOH solvents. In addition, stepwise heat treatment was conducted. The time for heat treatment at 300°C, 500°C and 800°C are for 30 minutes, 30 minutes and 60 minutes, respectively.

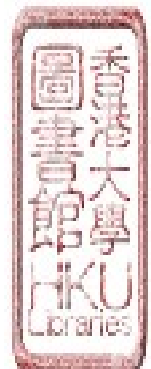


Fig. 2 shows the SEM top down view images of the BTO thin film prepared with PVP addition. Crack-free BTO thin film was successfully achieved. This film can uniformly cover the whole silicon surface area, significantly addressing the film crack issue. However, the resulting film is full of pore with diameters of hundred nanometers, which is harmful for ferroelectric properties.

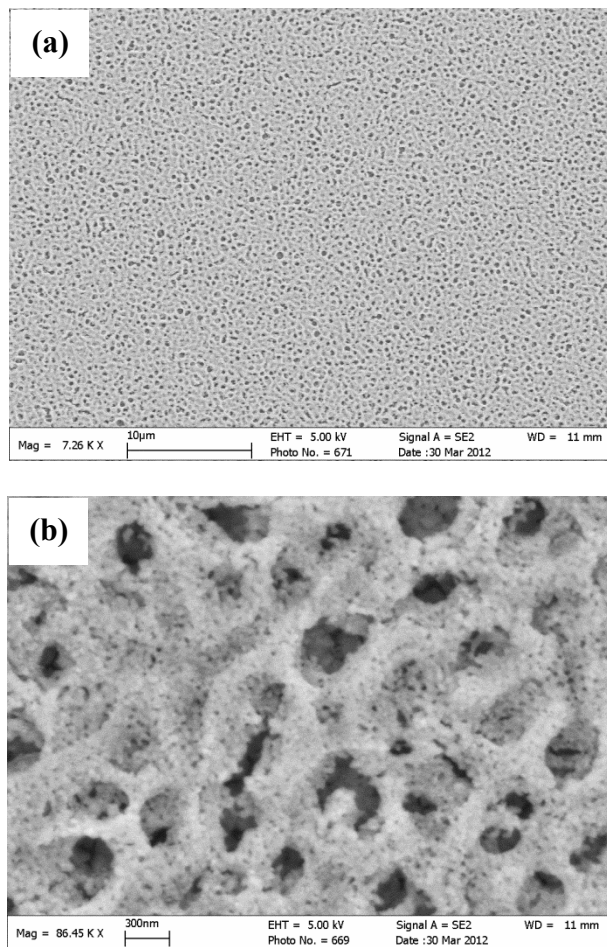


Fig. 2. SEM images of BaTiO₃ film prepared with PVP.

(a) Top-down view. (b) Zoom-in top-down view.



We then used $\text{Ti}(\text{OC}_2\text{H}_5)_4$ instead of $\text{Ti}(\text{OC}_3\text{H}_7)_4$ for precursor preparation [4]. In addition, PVP with 360000 molecule weight was added. Furthermore, stepwise annealing time is shortening to control the crystallization process. The time for heat treatment at 300°C, 500°C and 700°C are for 10 minutes, 10 minutes and 15 minutes, respectively. The obtained BTO film quality is shown in Fig. 3. A relative dense microstructure, with 50-100 nm grain size was observed.

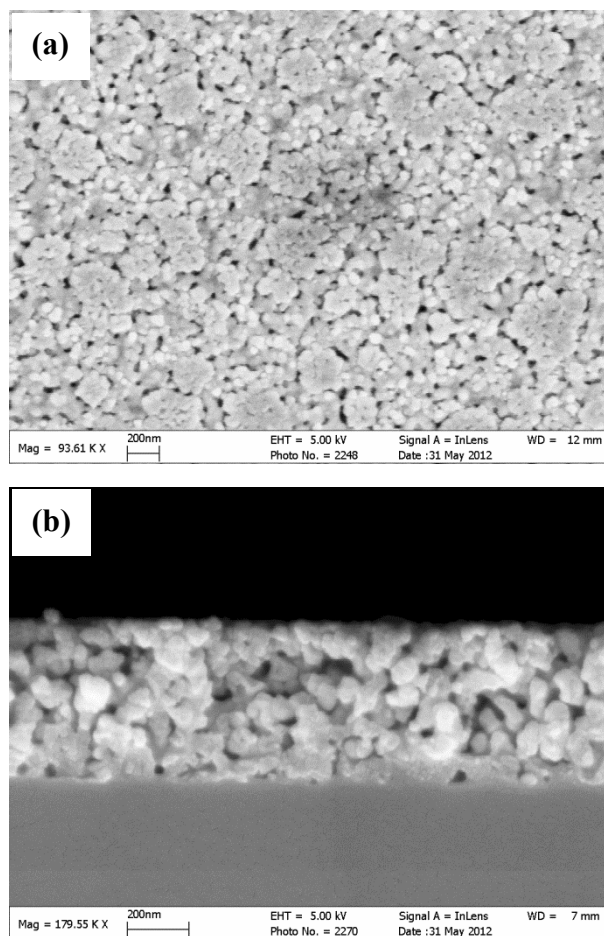


Fig. 2. SEM images of BaTiO_3 film prepared with new approach.

(a) Top-down view. (b) Cross-section view.



We finally obtained crack-free and condensed BTO thin film by sol-gel method thorough control of the precursor solution composition and annealing process. This BTO film was applied on our novel non-PN junction ferroelectric-semiconductor solar cells for systematical study.



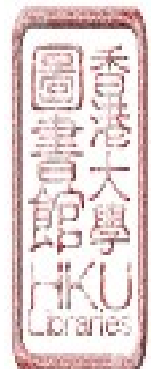
References

1. Kamalasan, M.N., et al., *Structural and Optical-Properties of Sol-Gel-Processed BaTiO₃ Ferroelectric Thin-Films*. Applied Physics Letters, 1991. **59**(27): p. 3547-3549.
2. Kozuka, H. and M. Kajimura, *Single-step dip coating of crack-free BaTiO₃ films > 1 μm thick: Effect of poly(vinylpyrrolidone) on critical thickness*. Journal of the American Ceramic Society, 2000. **83**(5): p. 1056-1062.
3. Kozuka, H., et al., *PVP-assisted sol-gel deposition of single layer ferroelectric thin films over submicron or micron in thickness*. Journal of the European Ceramic Society, 2004. **24**(6): p. 1585-1588.
4. Kozuka, H. and A. Higuchi, *Stabilization of poly(vinylpyrrolidone)-containing alkoxide solutions for thick sol-gel barium titanate films*. Journal of the American Ceramic Society, 2003. **86**(1): p. 33-38.



Publications

1. Wang W., Liu F., Lau C., Wang L., Yang G., Zheng D., Li Z., *Field effect BaTiO₃-Si solar cells*. Applied Physics Letters, 2014.104: p. 123901.
2. Wang W., Wang L., Yang G., Liu F., *Control of charge separation and collection in silicon solar cells with BaTiO₃ ferroelectric layers*. Scientific reports, under review.
3. Wang W., Wang L., Yang G., Liu F., *Enhance of charge separation and collection in 50μm thickness silicon solar cells with BaTiO₃ ferroelectric layer*. To be submitted.
4. Wang W., Wang L., Liu F., Choy W.C.H., Yan F., Johnston S., Al-Jassim M.M., *Passivating silicon grain boundaries with small polar molecules for photovoltaics*. Journal of Photovoltaics, under review.
5. Wang W., Wang L., Liu F., Yan F., Johnston S., Al-Jassim M.M., *Silicon grain boundary passivation for photovoltaics: A novel approach with small polar molecules*. 38th IEEE PVSC, Austin, 2012.
6. Wang W., Wang L., Liu F., *Grain boundary passivation with small polar molecules for photovoltaics*, 37th IEEE PVSC, Seattle, 2011.
7. Liu F., Wang W., Wang L., Yang G., *Ferroelectric-semiconductor photovoltaics: Non PN junction solar cells*. Applied Physics Letters, 2014. 104: p. 103907.
8. Liu F., Wang W., Wang L., Yang G., *Working principles of solar and other energy conversion cells*. Nanomaterials and Energy, 2012. 2: p. 3.



9. Wang L., Wang W., Yang G., Leung K., Liu F., *A high-capacity aluminum/air electrochemical power source*. RSC Advances, 2014. DOI: 10.1039/C4RA05222F.
10. Wang L., Wang W., Liu D., Yang G., Xuan J., Wang H., Leung K., Liu F., *A hybrid aluminum/hydrogen/air cell system*. International Journal of Hydrogen Energy, 2013. 38: p. 14801.
11. Wang L., Wang W., Leung K., Liu F., *Aluminum/hydrogen/air tandem fuel cell with tri-electrodes*, ES Fuel Cell 2013, 2013, Minneapolis, USA.
12. Liu F., Wang L., Yang G., Wang W., *Rapid melt crystallization of amorphous-silicon thin films*. Applied Physics Letters, 2013. 102: p. 082109.
13. Wang L., Liu F., Wang W., Wang H., Leung K., *A passive aluminum hydrogen air tandem cell*. Micro and Nanosystems, 2013.
14. Yang G., Wang L., Wang W., Liu F., *Diamond-like carbon deposition at low electrical field with photocatalytic reactions on light emission diodes*. Advanced Functional Materials, under review.

